INVESTIGATIONS INTO THE SPATIAL DISTRIBUTION OF γH2AX AROUND A DNA DOUBLE-STRAND BREAK AND THE ANALYSIS OF DOUBLE-STRAND BREAK MOBILITY

TOMISIN OLUKOGA

Thesis submitted for the degree of Doctor of Philosophy

University of Sussex

January 2018

Declaration

I hereby declare that this thesis has not been and will not be submitted in whole, or in part, to another University for the award of any other degree.

Signature……

Acknowledgements

The last four years have truly been an adventure. Like with any good adventure story there have been extreme highs and sobering lows along the way. I feel blessed to have had a support system that has been able to get me through to the end of this PhD. So, I'd like to start by saying thank you to my supervisor Dr Velibor Savic for his early guidance and giving me the opportunity to start this work. Thanks to past members of the Sweet lab with whom I have had both a close working and personal relationship.

Thank you to Professor Keith Caldecott for welcoming me in to his lab full of stars and helping me to feel part of the team. Thanks to the Caldecott lab for all the scientific insights, help, advice, encouragement, drive, empathy and laughs. They have been incredible and played a big part in my push for the finish line.

Thanks to everyone in the GDSC for creating such a community-like collaborative environment to learn and work in. There have been so many people that have made an impact and I don't have the space to thank them all, but I hope they've got as much from me as I from them

Last, but most definitely not least of all, my family and friends! People who have been there throughout it all. THANK YOU!

UNIVERSITY OF SUSSEX

Tomisin Olukoga

A thesis submitted for the degree of Doctor of Philosophy

INVESTIGATIONS INTO THE SPATIAL DISTRIBUTION OF γH2AX AROUND A DOUBLE-STRAND BREAK AND THE ANALYSIS OF DOUBLE-STRAND BREAK MOBILITY

Summary

A hallmark of the cellular response to DNA double-strand breaks (DSBs) is histone H2AX phosphorylation by the protein kinase ATM. H2AX is unevenly distributed throughout chromatin and is rapidly phosphorylated to form γH2AX up to 2 megabases either side of DSBs. Studies in yeast systems have shown that while γH2A can spread in *cis* surrounding the break site, it can also spread in *trans* onto unbroken chromosomes located in close spatial proximity. Although the majority of data in the current literature presents the well characterised *in cis* spread of γH2AX, there are strong indications that it can also occur *in trans* in mammalian systems; analogous to the findings shown in yeast. This thesis lays out the steps taken to develop a novel system to address the spatial distribution of γH2AX around a nascent DSB.

Since the first published live imaging experiments of the dynamics of chromatin by in vivo single particle tracking there has been extensive investigation into the regulation and biological function of movement of damaged DNA. In yeast, a relative consensus exists that DSB induction increases the movement of a DSB. In contrast to yeast however, data published of DSB movement in higher eukaryotes has been controversial, caused by conflicting results. Here, I developed a cell-based system, and utilised time-lapse live cell imaging to show that a chromosomal locus containing a single endonuclease-induced DSB shows confined movement in comparison to an undamaged locus. Furthermore, this confined movement of a damaged locus is compounded by treatment with an ATM kinase inhibitor but not a DNA-PKcs kinase inhibitor, suggesting that the kinase activity of ATM and not the kinase activity of DNA-PKcs plays a significant role in the dynamics of DSBs.

Table of Contents

List of Abbreviations

53BP1	p53 binding protein 1
ALT	Alternative lengthening of telomeres
Alt-NHEJ	Alternative NHEJ
APLF	Aprataxin and PNK-like factor
ATM	Ataxia telangiectasia mutated
ATP	Adenosine tri-phosphate
ATR	Ataxia telangiectasia and Rad3 related
BARD1	BRCA1-associated RING domain protein 1
BER	Base excision repair
BLM	Bloom syndrome RecQ like helicase
BRCT	BRCA1 C-terminal domain
ChIP	Chromatin immunoprecipitation
CK2	Casein kinase 2
DDR	DNA damage response
DNA	Deoxyribonucleic acid
DNA-PK	DNA-dependent protein kinase
DNA-PKcs	DNA-dependent protein kinase catalytic subunit
DSB	Double-strand break
EXO1	Exonuclease 1
FA	Fanconi anaemia
FANCD2	Fanconi anaemia group D2 protein
FANCI	Fanconi anaemia complementation group I

FHA	Forkhead-associated domain
γH2AX	Histone H2AX pSer139
GFP	Green fluorescent protein
HP1	Heterochromatin protein 1
HR	Homologous recombination
IR	Ionising radiation
KAP-1	Kruppel associated box domain protein 1
LET	Linear energy transfer
LINC	Linker of nucleoskeleton and cytoskeleton complex
MDC1	Mediator of DNA damage checkpoint protein 1
MMEJ	Microhomology-mediated end joining
MMR	Mismatch repair
MRN	Mre11-Rad50-Nbs1
MRX	Mre11-Rad50-Xrs2
MSD	Mean square displacement
NER	Nucleotide excision repair
NHEJ	Non-homologous end joining
PAR	Poly(ADP-ribose)
PARG	Poly(ADP-ribose) glycohydrolase
PARP1	Poly(ADP-ribose) polymerase 1
PARP2	Poly(ADP-ribose) polymerase 2
PHD	Plant homeodomain
PIKK	Phosphatidylinositol 3-kinase-related kinase

PKNP	Polynucleotide kinase/phosphatase
PML	Promyelocytic leukaemia nuclear body
PRC1	Polycomb repressive complex 1
PTM	Post-translational modification
RAG1/2	Recombination activating gene 1/2
RFP	Red fluorescent protein
RNA	Ribonucleic acid
RNF168	Ring finger protein 168
RNF8	Ring finger protein 8
RPA	Replication protein A
SCID	Severe combined immunodeficiency
SiR-DNA	Silicon-rhodamine DNA
SSA	Single-strand annealing
SSB	Single-strand break
SSBR	Single-strand break repair
SUMO	Small ubiquitin-like modifier
TA	Triamcinolone acetonide
TAD	Topologically associating domain
TDP1	Tyrosyl-DNA phosphodiesterase 1
TDP2	Tyrosyl-DNA phosphodiesterase 2
TOP1	DNA topoisomerase 1
TOP2	DNA topoisomerase 2
UV	Ultraviolet

XLF	XRCC4-like factor
XRCC4	X-ray cross complementing group 4

List of Figures

CHAPTER 1

1 Introduction

Cells are constantly exposed to a number of DNA damaging factors that challenge genomic integrity by causing DNA lesions; many thousands of which arise in human cells every day (LINDAHL and BARNES, 2000). The majority of these lesions occur as intrinsic by-products of typical cell metabolism or DNA replication, and can be present as programmed DNA lesions that form as intermediates during developmentally regulated genome rearrangements in lymphocytes and germ cells (Jackson and Bartek, 2009). DNA lesions can also be caused by extrinsic factors such as ionising radiation (IR), ultraviolet radiation (UV), toxic environmental chemicals and chemotherapeutic drugs. DNA has been estimated to experience close to 10^5 lesions per cell per day (Lindahl, 1993) and is the only biological molecule that accumulates damage over a lifetime and relies solely on repair mechanisms to be kept intact. Proper repair of lesions is critical for maintaining cellular viability, genomic integrity, and in multicellular organisms, for the suppression of neoplastic transformation. Eukaryotic cells have thus evolved specialised and lesion-specific molecular repair mechanisms to detect and repair many types of specific lesions.

1.1 DNA Damage Repair

Small alterations of DNA bases that do not distort the DNA helix are repaired by base excision repair (BER), initiated by spontaneous hydrolysis or cleavage of a chemically altered base by DNA glycosylases, (Krokan *et al.*, 2000). Correction of mismatch of bases in DNA that have evaded the 3' to 5' exonuclease proofreading activity of DNA polymerase is made by the mismatch repair (MMR) mechanism, (Jiricny, 2006). More

complex bulky lesions, such as pyrimidine dimers are processed by nucleotide excision repair (NER), an extremely versatile and complex pathway, through the removal of short 24-32 nucleotide lengths of single stranded DNA (ssDNA). Intrastrand crosslinks (ICLs) can also be readily removed by NER (O'Donovan *et al.*, 1994), in this case via recombination-dependent or recombination-independent pathways. A single strand break (SSB) in DNA is repaired by single strand break repair (SSBR). The most common type of DNA damage, SSBs can occur directly by disintegration of oxidised sugars or indirectly through the DNA base excision repair (BER) of oxidised bases and abasic sites (Demple and DeMott, 2002). Additionally, SSBs can arise from an abortive activity of the enzyme DNA topoisomerase 1 (TOP1). One of the most deleterious of lesions that can occur in the genome of eukaryotic cells, double strand breaks (DSBs) are processed by two main pathways; non-homologous end joining (NHEJ) or homologous recombination (HR). While NHEJ promotes the potentially inaccurate re-ligation of DSBs, HR restores the genomic sequence of broken ends precisely by utilising sister chromatids as templates for repair.

1.2 Double-Strand Breaks

DNA DSBs arise when the sugar-phosphate backbone of both strands of the two complementary DNA strands are broken simultaneously, resulting in the liberation of two DNA ends. Because liberated ends can physically separate from each other, DSBs are considered one of the most severe lesions. In dividing primary mammalian fibroblasts, it is estimated that there are approximately 10 DSBs per day per cell, based on metaphase chromosome and chromatid breaks (Martin *et al.*, 1985). DSBs develop in all stages of the cell cycle as a result of both exogenous factors and endogenous

factors. One class of agents causing exogenous DNA damage resulting in DSBs are topoisomerase inhibitors such as etoposide, which act by inhibiting the action of topoisomerase 2 (TOP2), an enzyme that induces transient DSBs. Typically, Top2 re-ligates the break and dissociates from DNA (Berger *et al.*, 1996). Etoposide specifically inhibits this re-ligation step and traps covalently linked topoisomerase-DNA cleavage complexes (Burden and Osheroff, 1998) Ionising radiation causes extensive base damage and additionally gives rise to SSBs by producing radiolysis radicals that attack the sugar-phosphate backbone in the form of strand nicks (Thompson, 2012). At high doses of irradiation two such nicks are present within one helical turn, leading to a DSB (Milligan *et al.*, 1995) IR generates DSBs with non-ligatable 'dirty ends' consisting of phosphoglycolates or 3'-terminal phosphates (Weinfeld and Soderlind, 1991), in contrast to DSBs generated by endonucleases which possess 'clean ends' with canonical 3'-hydroxyl and 5'-phosphate terminal nucleotides.

Even in the absence of exogenous factors, spontaneous DSBs can occur during an unperturbed cell cycle during replication. Progression of replication forks can be impeded by secondary DNA structures, DNA bound proteins or collisions with the transcription machinery (Prado and Aguilera, 2005), leading to stalled replication forks and the potential for formation of a DSB. A growing body of evidence has also implicated transcription as a cause of DSBs. R-loops, consisting of an RNA:DNA hybrid in which the nascent RNA displaces the non-transcribed DNA strand (Sollier and Cimprich, 2015) are a potential source of genomic instability and collisions between replication and transcription machineries can result in DSBs. Recent reports in *S. pombe* have shown that DNA:RNA hybrids can occur in a DSB-dependent manner, associated with PolII recruitment to the DSB region (Ohle *et al.*, 2016).

Even though DSBs are so potentially threatening, a number of physiologically and developmentally important processes require the generation of programmed site-specific DSBs and their subsequent repair pathways. The development of germ cells and lymphocytes are two cellular examples of the endogenous induction of DSBs. During the meiotic cell cycle, DSBs are programmed in early prophase I by the evolutionarily conserved topoisomerase-like enzyme, Spo11 (Lam and Keeney, 2015), and are processed by HR during the first nuclear division. The distribution of these meiotic DSBs is not random and is subject to control at multiple levels (Cooper, Garcia and Neale, 2016). These mechanisms operate together to actively regulate the number of DSBs forming per cell and to ensure that they are distributed evenly across all chromatids (Cooper *et al.*, 2014). In developing lymphocytes V(D)J recombination establishes antigen receptor diversity.

The lymphocyte-specific RAG1/RAG2 (RAG) endonuclease initiates V(D)J combination by introducing DSBs adjacent to V,D and J gene segments (Schatz and Swanson, 2011). DSB repair proteins process and join RAG-liberated ends to from V(D)J rearrangements upstream of the constant (C) region exons, thus giving rise to immunoglobin (Ig) genes in B lymphocytes and T cell receptor genes in T lymphocytes. These rearrangements proceed through DSB intermediates that are subsequently repaired by NHEJ to generate a large number of diverse antigen receptors (reviewed in Rooney et al. 2004). So, DNA DSB formation can be deleterious, but can also be a beneficial intermediate in cellular processes. Their repair is thus of utmost importance in maintaining the evolutionary development and survival of all living organisms. To this end eukaryotes are equipped with several different but related DSB repair mechanisms.

1.3 DSB repair

Cells rely on an intricate network of multiple DNA repair pathways to repair DSBs. The two predominant pathways, non-homologous end joining (NHEJ) and homologous recombination (HR) are mechanistically distinct but complementary, and operate optimally under different circumstances. NHEJ and HR may either compete or cooperate to process DSBs depending on the context in which the break is encountered (Takata *et al.*, 1998). Cooperation between the two pathways has been indicated due to evidence showing that mice carrying null mutations in both NHEJ and HR have very low viability and high radiation sensitivity. NHEJ can operate throughout the cell cycle and ligates two ends of a DSB independently of homology. Depending on the specific sequences and chemical modifications generated at DSBs NHEJ may be precise or mutagenic (Lieber *et al.*, 2003).

Another distinct pathway that is related to NHEJ is micro-homology-mediated end joining (MMEJ), also known as alternative NHEJ (alt-NHEJ). Conversely, repair by HR can be error-free but requires the presence of a homologous template, usually a sister chromatid which allows accurate repair of post-replicative DSBs in the S and G2 phases of the cell cycle (Pâques and Haber, 1999). DSBs can be repaired by a number of different HR pathways of which single strand annealing (SSA) is the simplest mechanism. SSA allows the formation of a deletion between homologous sequences flanking a DSB. One of the main factors that influences repair pathway choice is the extent to which DNA end processing needs to take place. Classical NHEJ does not require end resection and precise joining of 3' overhangs requires the Ku70 and Ku80 proteins as well as DNA ligase IV. In MMEJ repair however, bigger deletions with longer micro-homologies are Ku

independent, and in mammals, DNA ligase IV independent (Decottignies, 2013). HR and SSA are also dependent on DSB resection although consisting of a more extensive end resection process.

1.3.1 Non-homologous end joining (NHEJ)

An efficient DSB repair pathway in multicellular eukaryotes, NHEJ provides a mechanism for the repair of DSBs throughout the cell cycle but is particularly important during G0, G1 and early S-phase. As those genes responsible for DSB repair in human cells were elucidated, it became clear that the most radiosensitive mutants were defective in NHEJ. In this context, NHEJ in mammalian cells is often referred to as the major pathway in DSB repair. (**Fig. 1.1**). The first protein to bind a DSB is Ku as there are approximately 400,000 molecules per cell, and with a K_D of approximately 1nM it binds tighter to duplex DNA ends than any other protein in the cell (Falzon, Fewell and Kuff, 1993). Ku is a heterodimer and consists of Ku70 and Ku80, forming a shape that resembles a torus, with a hole large enough to allow duplex DNA to pass through (Walker, Corpina and Goldberg, 2001). Ku loads DNA only at termini, binds to the sugar backbone of DNA although makes no contact with DNA bases, and fits sterically to major and minor groove contours so as to position the DNA helix in a defined path through the protein ring (de Vries *et al.*, 1989). Ku has no validated enzymatic function and its primary function is considered to be to improve stability of NHEJ enzymes at DNA termini.

Once Ku is bound, it serves as a scaffold to recruit other NHEJ factors to the break. In classical NHEJ, Ku recruits the DNA-dependent protein kinase catalytic subunit (DNA-PKcs) to form the DNA-PK holoenzyme (Gottlieb and Jackson, 1993). The

interaction between the two requires the presence of DNA (Gottlieb and Jackson 1993) and upon binding of DNA-PKcs to the DNA-Ku

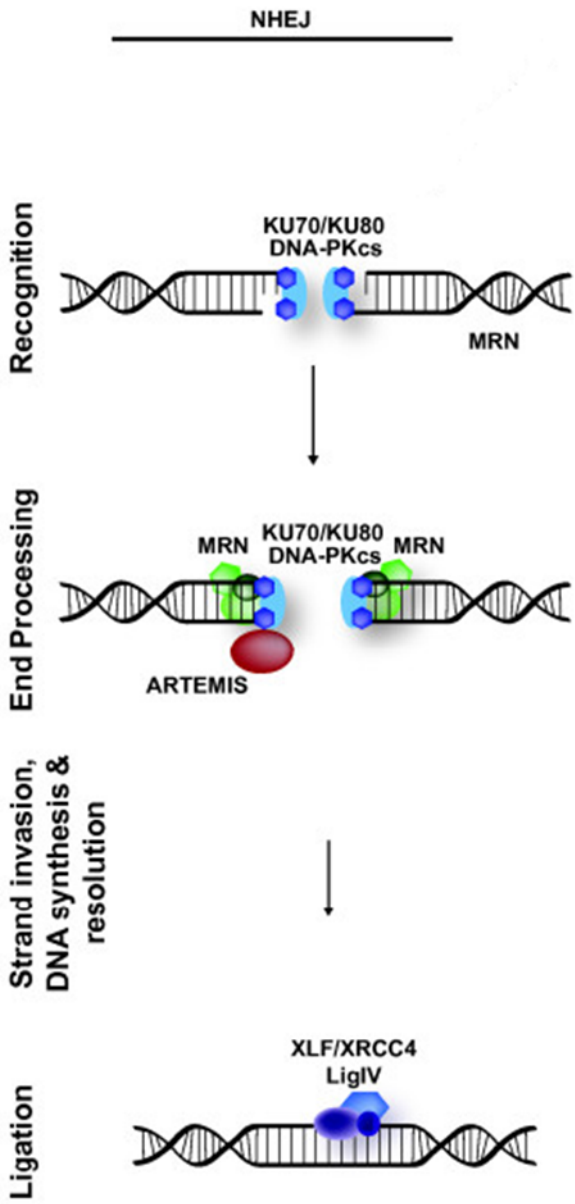

Figure 1.1. Non-homologous end joining repair pathway

Adapted from Lans et al, 2012. In NHEJ, broken DNA ends are bound by the KU70/KU80 heterodimer, which orchestrates the activity of other repair factors and recruits DNA-PKcs. Autophosphorylation of DNA-PKcs induces remodelling at the DSB end, which exposes the damaged DNA termini for end processing. DNA ends refractory to direct ligation are processed by the ARTEMIS endonuclease. DNA ends are joined by the activity of polymerases and theXRCC4, XLF, Ligase 4 ligase complex.

complex, an inward translocation of Ku on double stranded DNA (dsDNA) ultimately results in activation of the serine/threonine kinase activity of DNA-PKcs. DNA-PKcs is able to phosphorylate itself which subsequently influences its conformation and dynamics, relieving the blockage of the broken DNA ends to allow further processing (Weterings *et al.*, 2003).

DNA termini must be transformed to 5’ phosphorylated ligatable ends in order for repair to be completed. The nuclease Artemis is recruited to the break, likely through interaction with DNA-PKcs (Ma *et al.*, 2002) and processes DNA ends through a DNA-PKcs-independent 5’-to-3’ exonuclease activity and a DNA-PKcs-dependent endonuclease activity (Ma *et al.*, 2002). Other factors implicated as important for end processing by removing blocking end groups include: polynucleotide phosphatase (PNKP) (Bernstein *et al.*, 2005), aprataxin (Ahel *et al.*, 2006), aprataxin and PNKP like factor (APLF) (Kanno *et al.*, 2007), and tyrosyl-DNA-phosphodiesterases 1 and 2 (TDP1 and TDP2) (Pommier *et al.*, 2014). PNKP is a DNA kinase and a DNA phosphatase in which the 5’-kinase domain is responsible for adding phosphate to a 5’-hydroxyl termini and a 3’-phosphatase domain for removing 3’-phosphate groups. Aprataxin is a member of the histidine family of nucleotide hydrolases and transferases which catalyse the removal of adenylate groups covalently linked to 5’ phosphate termini.

The final step in repair is the ligation of broken ends by the X-ray cross-complementing-4 –XRCC4-like-DNA ligase IV (XRCC4-XLF-ligase IV) complex. DNA ligase IV has activity alone but is stabilised by XRCC4, which stimulates the ligase activity of ligase IV by promoting its adenylation (Grawunder *et al.*, 1997). XLF stimulates the

activity of ligase IV towards mismatched and non-cohesive ends (Ahnesorg, Smith and Jackson, 2006). On completion of repair, Ku must be removed from the ligated DNA ends. Human cell data has implicated the E3 ubiquitin ligase RNF8 in dissociation of Ku from DNA ends (Feng and Chen, 2012). Depletion of RNF8 resulted in prolonged retention of Ku80 at laser generated DSBs. Also, reports indicate that the phosphorylation status of DNA-PKcs mediates its dissociation from DSBs. Inhibition of phosphorylation of serine 2056 and threonine 2609 altered the dynamic of DNA-PKcs at DSB sites, resulting in a rigid binding to DNA ends *in vivo*, thus interfering with the NHEJ process (Uematsu *et al.*, 2007).

The model of classical NHEJ is a sequential stepwise recruitment of each component or complex to the break site starting with the recruitment of Ku to the DSB, followed by DNA-PKcs. However DNA-PKcs is not necessarily the next factor recruited, and in fact is not required for recruitment of the other NHEJ factors to a DSB as evidenced by the localisation of XRCC4, DNA ligase IV and XLF to DSBs independently of DNA-PKcs (Mari *et al.*, 2006) and (Yano and Chen, 2008). The order of recruitment of factors after initial binding of Ku is flexible and depends on the complexity of the DSB (Reynolds *et al.*, 2012). Therefore, less complex DSBs may be repaired rapidly, involving Ku, XRCC4, Ligase IV and XLF only, while more complex DSBs require DNA-PKcs.

1.3.2 Homologous recombination (HR)

HR is a relatively slow process compared to NHEJ. An early determinant of DSB repair pathway choice is the process of DSB resection. Required for HR but not NHEJ, resection is comprised of the 5’ to 3’ nucleolytic processing of DNA ends at a DSB. (**Fig. 1.2**). In the

early response to a DSB, the Mre11-Rad50-Nbs1 (Nijmegen breakage syndrome 1) (MRN) complex binds DNA ends via Rad50 homo-dimerization to connect the DNA ends

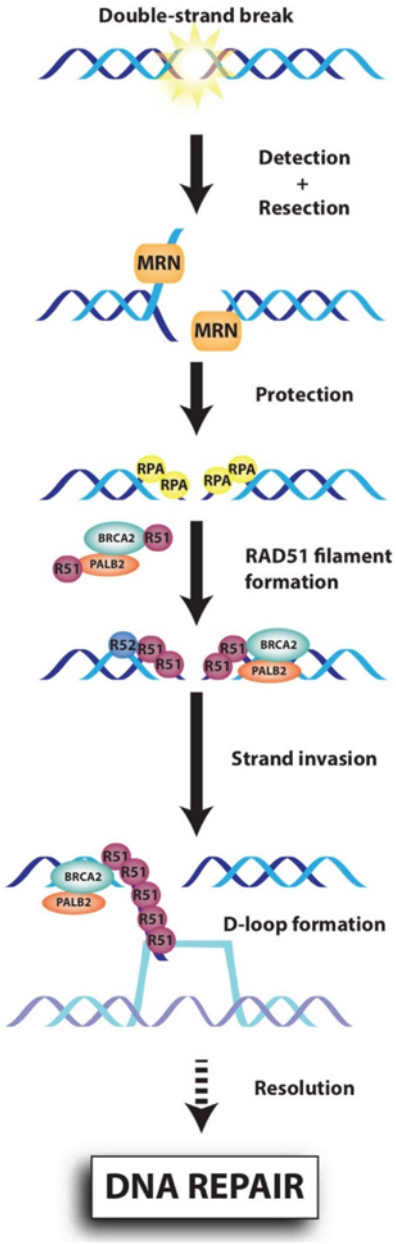

Figure 1.2. The homologous recombination repair pathway

Adapted from (Velic *et al.*, 2015). Schematic representation of DNA repair by homologous recombination. The MRN complex competes with Ku in binding to the DSB end which initiates resection (together with EXO1, CtIP and BLM) and generates 3'-ssDNA that is coated with RPA. The BRCA1-PALB2-BRCA2 complex then mediates the replacement of RPA by RAD51. The RAD51 nucleoprotein filament, invades the complementary DNA template leading to the formation of the D-loop structure. Following branch migration and resolution, faithful DNA repair occurs.

prior to repair (Hopfner *et al.*, 2002). MRN also possesses exo- and endo-nuclease activities and in conjunction with auxiliary factors including CtIP, RECQ helicases, and the nucleases Exo1 and Dna2, performs an initial incision, removing about 100 bp of DNA (Sartori *et al.*, 2007) and (Mimitou and Symington, 2009). The resulting ssDNA containing a 3'-hydroxyl overhang is rapidly coated by the ssDNA-binding protein replication protein A (RPA), which melts the DNA's secondary structure (Sung and Klein, 2006). The DNA strand invasion and homology search steps require formation of a nucleoprotein filament composed of multimers of the Rad51 recombinase bound to ssDNA. RPA effectively competes with Rad51 ass RPA binds more readily to ssDNA. So much so that a complex of mediator proteins including breast cancer type 1 susceptibility protein (BRCA1)/ BRCA1-associated RING domain 1(BARD1)and breast cancer type 2 susceptibility protein (BRCA2) are necessary to displace RPA to promote Rad51 binding. Although each of these proteins is required for formation of IR-induced Rad51 nuclear foci (Sugawara et al. 2003), the direct loading function is provided by BRCA2 (Sharan *et al.*, 1997; Pellegrini *et al.*, 2002). Disruption of either BRCA2 or Rad51 leads to an increased incidence of SSA and reduces HR (Moynahan, Pierce and Jasin, 2001). Therefore, formation of Rad51 filament directs the pathway of repair towards HR and suppresses the potentially mutagenic pathway of SSA.

Following its formation, the Rad51 nucleoprotein filament mediates homology search in the sister chromatid. Bacterial studies using Rad51 orthologue RecA, have indicated that homology search likely occurs through random collisions between the nucleoprotein filament and DNA, testing segments of dsDNA in a repetitive fashion until homology is found (Bianco, Tracy and Kowalczykowski, 1998). Strand invasion into a homologous sequence in the sister chromatid forms a D-loop intermediate and the 3'

end of the invading strand is extended by a DNA polymerase. It has been posited that a D-loop captures the second end of the break after ligation of the invading strand, leading to the formation of double Holliday junctions. Although originally postulated to be resolved as either a crossover or non-crossover, reports have shown double Holliday junction resolution leans towards the formation of crossovers (Allers and Lichten, 2001). Once a Holliday junction has been formed it is able to undergo branch migration along the DNA, giving rise to increasing or decreasing lengths of heteroduplex DNA. Double Holliday junctions can be dissolved by the branch migration and topoisomerase activity of the Bloom's syndrome protein and topoisomerase III alpha, forming non-crossover products (Wu and Hickson, 2003). Intermediates that escape this action of the Bloom's syndrome protein can be processed by the MUS81-EME1 complex which cleaves Holliday junctions form crossover products.

1.4 Signalling Response to DSBs

In eukaryotes, the cellular response to DNA damage is coordinated and regulated by the cellular DNA damage response (DDR); a network of signalling pathways that interact together. In response to unrepaired DNA damage and ultimately to prevent duplication and segregation of damaged DNA, these pathways are able to suspend or stop the cell cycle at critical stages before or during DNA replication at the G1/S and intra-S checkpoints, and before mitosis at the G2/M checkpoint. Similar to classical signal transduction pathways, the DDR uses signal 'sensors', 'transducers' and 'effectors' to detect lesions, signal their presence and promote their repair, respectively (Harper and Elledge, 2007).

DDR sensors of DSBs are proteins that directly recognise and interact with the break. Sensors initiate a signalling cascade that has an impact on a wide variety of cellular processes, by activating the upstream DDR protein kinases. A protein kinase cascade caused by transducers of the DDR facilitate downstream phosphorylation events. While the effectors of the signalling network are substrates of these protein kinases and participate in a broad spectrum of cellular processes that are paramount for genomic stability, such as DNA replication, repair and cell-cycle control.

In response to unrepaired DSBs, Mre11-Rad50-Nbs1 (MRN) is one of the first factors recruited to the break and displays direct binding to DNA ends *in vitro* (de Jager *et al.*, 2001). The MRN complex binds DSBs via a globular head region comprised of Mre11 and Rad50 ATPase domains. Mre11 dimerisation ensures stable DNA binding, and Rad50 dimerisation tethers DNA ends together (de Jager *et al.*, 2001; Williams *et al.*, 2008). As could be anticipated when considering factors binding similar DNA structures, Ku competes with the budding yeast MRX complex for binding (Clerici *et al.*, 2008). MRN is required for the rapid localisation of ATM to DSBs and is involved in the activation of ATM in a DSB-dependent manner. (Uziel *et al.*, 2003; Lee and Paull, 2005). Poly (ADP-ribose) polymerase 1 (PARP1) is also activated by DSBs and catalyses the addition of poly (ADP-ribose) chains on proteins that recruit DDR factors to chromatin at DSBs. PARP1 has been proposed to mediate the initial accumulation of MRN at DSBs (Haince *et al.*, 2008).

In mammalian cells, the ATM, ATM and Rad3-related (ATR) and DNA-PKcs kinases are the most upstream DDR kinases. Whereas ATM and DNA-PKcs are primarily involved in the processing of DSBs, ATR responds to different types of DNA damage,

including DSBs. They belong to the phosphatidylinositol-3-kinase-like kinase (PIKK) family and are large serine/threonine kinases. A plethora of proteins are phosphoporylated at Ser/Thr-Glu motifs and additional sites in an ATM- or ATR-dependent manner, while DNAPK-cs regulates a smaller number of targets (Matsuoka *et al.*, 2007). Recruitment of ATM by MRN and PARP1 could contribute to the stabilisation of DDR factors at a DSB through the activation of γH2AX complexes.

A large number of downstream targets regulated by ATM and ATR have been identified through unbiased screens for ATM and ATR substrate (Matsuoka *et al.*, 2007). These studies revealed a strong enrichment for proteins involved in DNA replication, DNA polymerase complexes and factors known to be directly involved in DNA repair (Branzei & Foiani 2007). These findings point to a much broader role for the DDR in cellular physiology beyond its role in controlling the cell cycle.

1.5 Histone H2AX and the DSB Signalling Cascade

The eukaryotic genome is maintained as a nucleoprotein superstructure known as chromatin which is composed of DNA and its associated proteins. Chromatin confers an organization that is important for both resolving problems of spatial accommodation and for functional utilization of the DNA. The basic building module of chromatin is the nucleosome which consists of 146bp of DNA wrapped around a histone octamer containing two copies each of core histones H2A, H2B, H3 and H4(Clark & Felsenfeld 1971). The histone linker protein, histone H1, further compacts DNA by 'locking' the DNA at the entry and exit points from the nucleosome. Each core histone in the nucleosome contains a globular domain, which is necessary for histone-histone and histone-DNA

contacts, as well as a dynamic tail motif in both COOH and NH2-terminal regions, which are targets of post translational modifications. The tight packaging of eukaryotic DNA into chromatin allows the accommodation of an enormous length of DNA in such a small nuclear space.

The incorporation of histone variants rather than canonical histones (Talbert and Henikoff, 2010), is one mechanism evolved by cells to influence chromatin complexity by creating specialized nucleosomes. H2AX is a member of the H2A family of histones which is comprised of thirteen family members. Histone H2A variants mostly differ in their C-termini with regards to length and sequence of amino acids. Histone variant H2AX was first described in 1980 (Talbert and Henikoff, 2010) and constitutes between 2 and 25% of the total H2A pool (Rogakou *et al.*, 1998; Hatimy *et al.*, 2015) and is unevenly distributed throughout chromatin (Bewersdorf, Bennett and Knight, 2006).

One of the earliest events of the DDR, in response to a DSB, is the localized phosphorylation of H2AX at serine 139 of its C-terminal tail by ATM and DNA-PKcs (Rogakou *et al.*, 1998). Serine 139 phosphorylated H2AX, termed γH2AX, forms locally on chromatin within seconds (Marková, Schultz and Belyaev, 2007) and forms discrete nuclear foci that are visually detectable by immunofluorescence. γH2AX can form foci linearly covering chromatin up to and beyond 1 Mb away from both sides of the break site (Marková, Schultz and Belyaev, 2007). In *Saccharomyces cerevisiae*, γH2AX is present in a 40-50 kb region around an unrepairable DSB, and the greatest enrichment of γH2AX occurred 3-5 kb on either side of the break, with γH2AX absent in sequences 1-2 kb on both sides of the DSB (Shroff *et al.*, 2004). Work in mammalian cells studied the extent to which γH2AX spreads in primary thymocytes and immortalized *bcr-abl*

expressing pre-B cells induced to undergo V(D)J recombination in G1. This study reported mapping of the γH2AX domain over several hundred kilobases (Savic *et al.*, 2009). Intriguingly, H2AX appears to be the primordial form of histone H2A. Despite only accounting for less than 10% of all H2A species in mammalian cells, the two histone genes present in *S. cerevisiae* both encode proteins with an H2AX-like C-terminal tail, and like H2AX, these species are also subject to C-terminal phosphorylation in response to a DSB (Jackson, Downs and Lowndes, 2000a).

1.5.1 H2AX dosage dependence

H2AX can be considered as a dosage-dependent genomic caretaker and tumour suppressor as various studies have shown $H2AX^{-/-}$ cells exhibit increased sensitivity to radiation (Bassing *et al.*, 2002), elevated levels of genomic instability (Celeste *et al.*, 2002), defective chromosomal DSB repair (Franco *et al.*, 2006) and an impaired G2/M checkpoint (Fernandez-Capetillo *et al.*, 2002). $H2AX^{+/-}$ murine cells express H2AX in chromatin at 50% of the level of $H2AX^{+/+}$ cells yet exhibit phenotypes similar to those observed in $H2AX^{-/-}$ cells (Bassing *et al.*, 2003), indicating that expression of both alleles of H2AX is required for a fully effective DDR. In addition, $H2AX^{+/-}$ mice are not tumour prone (Celeste, Difilippantonio, *et al.*, 2003), but $H2AX^{-/-}$ mice exhibit an increased predisposition to thymic lymphomas (Bassing *et al.*, 2003). Furthermore, $H2AX^{+/-}$ and $H2AX^{-/-}$ mice in p53 null backgrounds develop lymphomas solid tumours with clonal translocations (Bassing *et al.*, 2003; Celeste, Difilippantonio, *et al.*, 2003). Given that H2AX suppresses genomic instability in murine cells, it is notable that the human H2AX gene (H2AFX) maps to a cytogenetic region (11q23) that is often altered in a large

number of cancers (Celeste, Difilippantonio, *et al.*, 2003), suggesting possible similar dosage-dependent functions of H2AX in humans.

1.5.2 γH2AX signalling cascade

The formation of γH2AX serves as a binding site for DDR protein factors. These DDR factors can be recruited to DSBs in a γH2AX-independent manner, but the formation of γH2AX is essential for the retention of these factors in chromatin around DSBs (Celeste, Fernandez-Capetillo, *et al.*, 2003). γH2AX is bound by the large nuclear protein mediator of DNA damage checkpoint 1 (MDC1) via its tandem C-terminal BRCT repeat, and appears to orchestrate most γH2AX functions (Stucki *et al.*, 2005). MDC1 recruits and interacts constitutively with the MRN complex, through direct interaction of casein kinase-phosphorylated target sites with the FHA domain of Nbs1 (Chapman and Jackson, 2008), consequently recruiting and activating ATM (Lee and Paull, 2004). ATM, the major kinase responsible for phosphorylation of H2AX forms additional γH2AX molecules further away from the break. γH2AX/MDC1 acts as the binding platform to which a number of proteins implicated in HR and NHEJ assemble. These include BRCA1 with its heterodimeric interacting partner BARD1 and 53BP1.

RNF8 and RNF168, a set of E3 ubiquitin ligases, are required for recruitment of 53BP1 and BRCA1 to γH2AX/MDC1 chromatin (Huen *et al.*, 2007; Kolas *et al.*, 2007). RNF8 binds directly to MDC1 through a phospho-dependent interaction between the RNF8 forkhead-associated domain (FHA) and motifs in MDC1 that are phosphorylated by ATM. Once bound, RNF8 ubiquitylates various chromatin elements at the break site, including histone H2A, by adding K63 linked ubiquitin chains (Kolas *et al.*, 2007). RNF8 recruits RNF168, the RNF8-associated E3 ubiquitin ligase which acts biochemically

upstream of RNF8 by monoubiquitylating histone H2A on K13-K15 residues (Mattiroli *et al.*, 2012). Monoubiquitylation of H2A or H2AX K13-15 by RNF168 with the ubiquitin-conjugating E2 enzyme UBCH5, acts as a priming mark for amplification of RNF8 and E2 UBC13 dependent ubiquitylation of H2A/H2AX (Panier *et al.*, 2012).

RNF168-mediated H2AK15Ub, along with a number of additional factors, is then able to recruit 53BP1 (Baldeyron *et al.*, 2011). Histone H2AX is dispensable for the recruitment of 53BP1 as long as the H2AK15Ub mark is established, as observed in the case of spontaneous 53BP1 focus formation around replication stress-induced lesions (covered in more detail below) (Lukas *et al.*, 2011). The mechanism of BRCA1 recruitment to γH2AX/MDC1 chromatin has been shown to be driven by a physical interaction with ubiquitylated chromatin components, mediated by the interaction of BRCA1 with the ubiquitin binding protein RAP80 (Sobhian *et al.*, 2007). So, the MDC1/RN8/RNF168 response produces a specific set of ubiquitylated chromatin marks that lay a foundation for specific recognition of DDR factors containing ubiquitin binding domains.

1.6 Spatial Three-Dimensional Spread of γH2AX in Yeast

Unlike mammals, in yeast *Saccharomyces cerevisiae* the predominant histone H2A can itself be phosphorylated on S129. Yeast H2A is phosphorylated locally in chromatin upon DSB formation (forming γH2A) with a comparable distribution pattern to mammalian systems, although spreading occurs over a reduced distance (Shroff *et al.*, 2004). Interestingly, reports in yeast systems have shown that while γH2A can exhibit

discontinuous intra-chromosomal distribution, it can also exhibit inter-chromosomal distribution (Renkawitz et al. 2013; Lee et al. 2014). Renkawitz et al. 2013 showed that upon generation of a single I-SceI-induced DSB break, γH2A ChIP signals almost perfectly matched the Rad51 profile in homology search and like Rad51, occurred on the broken chromosome but also spread *in trans* onto unbroken chromosomes. In addition, using a strain bearing an I-SceI cleavage site in the centromeric region of chromosome IV, small but significant γH2A ChIP signals were observed specifically at centromeres and surrounding sequences of all other unbroken chromosomes. An analogous result was shown by (Lee et al. 2014) in which two yeast strains were created that carried a single HO cleavage site on chromosome 2. One strain contained the cleavage site positioned 14 kb from *CEN2* and the other strain contained the cleavage site 387 kb from *CEN2*. In the strain carrying the single HO site close to the centromere, there was a marked enrichment of γ-H2A at pericentromeric regions of all others chromosomes; however, this *trans* spreading was not present in the strain carrying the DSB far from the centromere. In yeast, chromosome centromeres tend to be clustered and in close proximity, thus the results published by both groups suggest that yeast γH2A phosphorylation can spread in *trans* to unbroken DNA in close proximity.

1.7 Spatial Three-Dimensional Spread of γH2AX in Mammalian Cells

One attempt to answer the question of spatial effect of a DSB on chromatin was made by (Iacovoni *et al.*, 2010). Through ChIP-Seq analysis in a human cell line, the authors reported no apparent spatial spread of γH2AX, based on the observation that no detectable γH2AX accumulated at any non-linear chromosomal location devoid of

an *Asi*SI DSB site. Thus, they concluded that γH2AX mainly spreads in *cis* around DSBs. The underlying problem with this conclusion is that it is based on the premise that chromatin is static and that identical distal inter- or intra-chromosomal interactions between the break site and chromatin would occur in every cell in a population. There is a large body of evidence showing that the position and interaction of chromatin regions is stochastic, and in most cases there are only moderate tendencies to associate with a specific partner on a population level (Gilbert et al. 2004). These interactions would be far below the requirements needed to support the conclusion made by the authors. Further reducing the chance of inter-chromosomal interactions being uniform throughout the population, the nuclear position of a genomic locus is not fixed and the locus can move over time within a confined space (Dion and Gasser, 2013), potentially leading to stochastic interactions with neighbouring chromatin. Also, there have been reports published suggesting that the presence of a DSB in chromatin increases its mobility (Krawczyk *et al.*, 2012). Because inter-chromosomal chromatin interactions with the break site are not uniform from cell to cell in a population, the ChIP-Seq signal observed *in trans* would not be strong enough to reach the detection threshold. In the same vein, spatial non-linear distribution of γH2AX could spread stochastically, in accordance with the likelihood of association with different chromatin regions and the break site, thus resulting in a change in the ChIP-Seq signal that would be well below the measurable level.

1.8 Protein Modifications in Response to a DSB

DSB-induced chromatin responses are driven by various protein post-translational modifications (PTMs) that promote the recruitment and dissociation of DDR factors or regulate the residence times of these factors around the break. These PTMs include: poly(ADP-ribosyl)ation (PARylation), phosphorylation, ubiquitylation, sumoylation, methylation and acetylation.

1.8.1 PARylation

PARylation is one of the earliest detected modifications at sites of DNA damage (Polo and Jackson, 2011) and is quickly removed by PAR glycohydrolase (PARG). PARylation is catalysed by PARP1 and PARP2 enzymes in response to DNA breaks in mammalian cells (Krishnakumar and Kraus, 2010). PARP1 is able to sense DSBs and act to promote MMEJ. Upon detecting a DSB, PARP1 is thought to mediate the initial accumulation of the MRN complex in a γH2AX- and MDC1-independent manner (Haince *et al.*, 2008). PARP1 has been shown to play an initial role in the DDR by facilitating ATM activation, as evidenced by delayed phosphorylation of ATM substrates observed in the absence of PARP1 following treatment with DNA damaging agents (Haince *et al.*, 2007). Current models predict the PAR-dependent events could then contribute to the activation of the γH2AX cascade and stabilization of DDR factors at DSBs and ultimately facilitate repair. Upon DSB induction, it has been observed in multiple studies that chromatin undergoes a transient PARP-1-dependent and H2AX/ATM-independent relaxation immediately after DSB induction (Luijsterburg *et al.*, 2016)s. In all of the cases put forward, specific

domains and/or motifs on DDR factors mediate their binding to PAR (Karras *et al.*, 2005; Isogai *et al.*, 2010).

1.8.2 Phosphorylation

A prevalent PTM for regulating protein function, phosphorylation only occurs on the side chain of the Serine, Threonine and Tyrosine amino acids in eukaryotic cells. Phosphorylation and dephosphorylation reactions in the DDR have been well characterized, as hundreds of phosphorylated targets have been identified by mass spectrometry based screens (Matsuoka *et al.*, 2007). The action of phosphorylations in the DDR can be considered to be three-fold: regulation of the structure of DDR proteins, regulation of the activity of DDR proteins and provision of a regulated docking site for other DDR factors. As such, DDR proteins frequently display phospho-binding motifs such as breast cancer C-terminal (BRCT) or forkhead associated (FHA) domains (Callebaut and Mornon, 1997; Mohammad and Yaffe, 2009), that are of central importance in mediating the phospho-dependent assembly of DDR protein complexes. The classic example of phosphorylation of a substrate is the formation of γH2AX through phosphorylation of Ser 139 by ATM, ATR and DNA-PKcs, which directs the assembly of downstream DDR components including checkpoint mediators and chromatin-modifying complexes. This event is accompanied by the de-phosphorylation of the neighbouring Tyrosine 142 (Tyr 142), a residue constitutively phosphorylated in the absence of damage (Xiao *et al.*, 2009). De-phosphorylation of Tyr 142 is required for recognition of γH2AX by MDC1.

In some cases, phosphorylation can promote the dissociation of proteins from sites of damage; a phenomenon first characterised by the demonstration that DNA-PKcs autophosphorylation results in its to dissociation from Ku (Chan and Lees-Miller, 1996). Another example of a phospho-dependent dissociation mechanism is the release of the transcriptional co-factor KAP1 from chromatin, which depends on its phosphorylation by ATM (Aaron A. Goodarzi *et al.*, 2008). In addition, de-localisation of the heterochromatin component HP1 from damage sites has been reported to take place following casein kinase 2-(CK2)dependent phosphorylation within the chromodomain of HP1.

1.8.3 Ubiquitylation

Ubiquitylation is the process by which ubiquitin, a 76 amino acid polypeptide, is covalently attached to other proteins. E1, E2, and E3 ubiquitin ligases can create monoubiquitin or polyubiquitin chains (Pickart, 2001). Ubiquitylation plays an essential role in the orchestration of the assembly of DDR proteins at DSB sites in vertebrate cells (Al-Hakim *et al.*, 2010). Various protein-ubiquitin conjugates have been detected at DSBs (Morris and Solomon, 2004; Stewart *et al.*, 2009) that serve as docking platforms for focal DDR protein assembly. Consequently, ubiquitin ligases including: BRCA1 (Scully *et al.*, 1997), RNF8, RNF168 (Doil *et al.*, 2009a), RAD18 (Watanabe *et al.*, 2009), HERC2 (Bekker-Jensen *et al.*, 2010) and Polycomb repressive complex (PRC1) (Chou *et al.*, 2010) have been demonstrated to accumulate at DSBs. Similar to protein phosphorylation (see above), ubiquitin chains can be recognized by specific protein domains termed ubiquitin binding domains (UBDs). In addition to the mechanism of ubiquitylation at damage sites

causing recruitment of DDR components, the direct ubiquitylation of DDR factors can serve to target the factor to damage sites. For example, the Fanconi Anaemia (FA) core complex monoubiquitylates the FA proteins FANCD2 and FANCI at replication-associated DNA breaks, resulting in their localization to HR foci (Alpi and Patel, 2009).

1.8.4 SUMOylation

Small ubiquitin-like modifier (SUMO) has emerged as a key player in the DDR (Jackson and Durocher, 2013). Like ubiquitin, SUMO is conjugated to lysine residues in target proteins through an enzymatic cascade involving E1, E2 and E3 enzymes, and SUMOylation can be removed by SUMO-specific proteases. Post translational modification by SUMO occurs through non-covalent interaction with target proteins via SUMO interaction motifs (SIMs), and through multiple interactions between SUMOs and SIMs within different subunits of protein complexes. Human BLM (Eladad *et al.*, 2005), XRCC4 (Yurchenko, Xue and Sadofsky, 2006), and RPA (Dou *et al.*, 2010), have all been identified as SUMOylation targets. It has been established that SUMO conjugation at DSBs promotes protein ubiquitylation and DDR focus formation; specifically that SUMOylation of BRCA1 and 53BP1 by the PIAS1 and PIAS4 SUMO E3 ligases promote BRCA1/BARD1 ubiquitin E3 ligase activity and increases residence time of 53BP1 and BRCA1 at the break site (Galanty *et al.*, 2009).

1.8.5 Methylation

It has been well established that histone methylation is required for the focal recruitment of 53BP1 to DNA breaks via recognition of methylated histone residues by

its tandem Tudor domain (Huyen *et al.*, 2004). Histone methylations H3K79me3 and H4K20me are associated with the retention of 53BP1 on chromatin, however, both of these modifications are constitutive (Huyen *et al.*, 2004). This is in contrast to the DNA damage-dependent H2AX phosphorylation and histone ubiquitylation. It has been suggested that these methylation marks are not usually readily accessible, but become exposed upon DNA damage-induced repositioning of nucleosomes as a result of histone ubiquitylation (Huen and Chen, 2010).

Tudor domains, chromodomains and PHD finger domains all bind methylated lysine residues and target DDR factors to break sites. An example is the binding of H3K4me3 by the RAG2 recombinase PHD finger at antigen receptor genes, which is necessary for effective V(D)J recombination(Liu *et al.*, 2007). Methylation of DDR factors themselves can also regulate their focal recruitment to DNA breaks. In the case of Mre11 and 53BP1, methylation on their glycine-arginine-rich (GAR) motifs promotes their focal accumulation by regulating their DNA binding activities (Dery *et al.*, 2008).

1.8.6 Acetylation

The significance of histone acetylation in response to DSBs is underlined by the recruitment of the TIP60 acetyltransferase and a number of histone deactylases (HDACs) in mammalian cells (Polo and Jackson, 2011). TIP60 acetylates histone H4 at I-SceI-induced DSBs, stimulating the loading of 53BP1 and BRCA1 at the break site (Murr *et al.*, 2006). TIP60 has also been shown to acetylate H2AX, promoting eviction of the histone variant from damaged chromatin (Ikura *et al.*, 2007). It has been suggested that TIP60

mediated acetylation could contribute to local chromatin relaxation around a DSB and also enhance ATM activity, thus generating a positive feedback loop to further stimulate DNA damage-induced protein phosphorylation (Xu and Price, 2011). DSB-dependent acetylation has been demonstrated in the males absent on the first (MOF)-dependent acetylation of H4K16 following IR. IR induces focus formation of MDC1, 53BP1 and BRCA1 in mammalian cells, possibly through interactions between the histone H4 tail and H2AX stimulating the binding of MDC1 to γH2AX.

1.9 53BP1 Focal Accumulation at a DSB

53BP1 was first described as a binding partner of the tumour suppressor protein p53 (Iwabuchi *et al.*, 1994), and as already intimated in this chapter, plays a role as a key regulator in the signalling of DSBs. A large protein consisting of 1972 amino acids, 53BP1 has no apparent enzymatic activity but contains binding surfaces for numerous DDR proteins that respond to DSBs. 53BP1 plays multiple roles in the DDR, recruiting additional DDR factors to the site of damage, promoting ATM-dependent checkpoint signalling and mediating DSB repair pathway choice (Panier and Boulton, 2014). Following induction of a DSB and activation of ATM, 53BP1 forms microscopically visible nuclear foci (Schultz *et al.*, 2000). Key structural elements of 53BP1 include the tandem Tudor domain, the ubiquitylation-dependent recruitment (UDR) motif and BRCT repeats.

In response to a DSB break 53BP1 is able to recognise the H4K20me2 histone mark on chromatin via binding of its tandem Tudor domain, and this interaction is vital for its recruitment to DSBs (Botuyan *et al.*, 2006). Multiple studies have shown that the majority of H4K20me2 is formed independently of DNA damage, with one study in particular showing that H4K20me2 is a highly abundant histone mark present in over 80% of nucleosomes (Pesavento *et al.*, 2008). Therefore, for such an abundant epigenetic mark to be capable of promoting the specific focal recruitment of 53BP1 to DSBs, 53BP1 binding at DSB sites is regulated at various levels including crosstalk with the ubiquitylation machineries**.** As such, 53BP1 only binds to nucleosomes that are both methylated at H4K20 and ubiquitylated at H2AK15.

Binding of the 53BP1 tandem Tudor domain to H4K20me2 has been shown to be necessary but not sufficient for efficient focal recruitment (Zgheib *et al.*, 2009), thus reinforcing the fact that there is additional regulation of 53BP1 recruitment to the break site. 53BP1 binds H2AK15ub via a direct and highly selective interaction with its UDR motif, which is essential for RNF8-RNF168-dependent recruitment of 53BP1. Point mutations in the UDR motif impair 53BP1 focus formation and abolish the binding of 53BP1 to H2AK15ub but not H4K20me2, indicating that binding of 53BP1 to H4K20me2 occurs independently of RNF168-mediated histone ubiquitylation (Fradet-Turcotte *et al.*, 2013). 53BP1 only binds to nucleosomes that contain both H4K20me2 and H2AK15ub. The bivalent recognition of these histone marks echoes the mechanism of the DSB-dependent accumulation of the 53BP1 fission yeast orthologue, Crb2. Crb2 also binds two distinct histone marks and binds H4K20me2 via tandem Tudor domains (Sanders *et al.*, 2004). In addition Crb2 focus formation relies on the interaction of its C-terminal BRCT domains with γH2AX, (Sanders, Arida and Phan, 2010; Sofueva *et al.*,

2010) and only the combined binding of methylated and phosphorylated histone residues enables Crb2 to accumulate efficiently (Du, Nakamura and Russell, 2006).

The C-terminal BRCT repeats of 53BP1 are dispensable for its focal recruitment to DSBs (Joo *et al.*, 2007), nonetheless the role of the BRCT domain remained controversial and a role for the domain in the DDR was for the most part discounted for some time (Callen *et al.*, 2013). A recent report by (Baldock *et al.*, 2015) however, evidenced that the $BRCT_2$ domain had a clear specificity for γH2AX and in isolation from other parts of 53BP1, was sufficient for localization to sites of γH2AX-associated DNA damage, thus adding a third independent histone mark 53BP1 can bind.

The γH2AX-independent recruitment of 53BP1 in response to DNA damage also occurs in the case of spontaneous 53BP1 focus formation at incompletely replicated DNA structures transmitted through mitosis from the previous cell cycle. (Harrigan *et al.*, 2011). Mild forms of replication stress have been shown to be sufficient to elicit chromosomal stress that manifests as 53BP1 nuclear bodies (Lukas *et al.*, 2011). Originally described as Oct1/PTF/transcription (OPT) domains (Pombo *et al.*, 1998), these now established 53BP1 nuclear bodies (53BP1 NBs) are largely confined to the G1 phase of the cell cycle. Lukas et al. 2011 showed that after co-immunostaining cells with antibodies against 53BP1 and cyclin A, a marker of S and G2 phases, 53BP1 nuclear bodies rarely overlapped with cyclin-A-positive nuclei. In addition, using time-lapse microscopy of cells expressing GFP-tagged 53BP1, the authors found that while G2 cells did not contain 53BP1 foci, they rapidly appeared shortly after the same cells divided and entered G1. Evidence has been presented that 53BP1 nuclear bodies contain DNA lesions that are sequestered into large chromatin domains enriched in 53BP1 and other

markers associated with the DDR (Harrigan *et al.*, 2011; Fernandez-Vidal, Vignard and Mirey, 2017).

1.10 Impact of Chromatin on the DDR and DSB Repair

1.10.1 Chromatin architecture and the activation of the DDR

When studying the DDR in its cellular context it is important to consider that the physiological substrate for the DDR machinery in the cell nucleus is chromatin. It has been well established that the action of chromatin remodelling complexes that are recruited to DSB sites play an important role in the DDR and the repair of lesions (Wurtele and Verreault, 2006). What isn't fully understood however, is the link between the generation of a DSB leading to architectural changes in chromatin, and the activation of ATM. Evidence has been shown implying that the initial detection of a DSB is triggered by an alteration in chromatin structure, rather than by DDR sensor proteins binding to DNA ends (e.g. MRN complex and Ku). Electron microscopy studies have revealed that generation of DSBs leads to a rapid ATP-dependent local decondensation of chromatin that occurs in the absence of ATM activation (Kruhlak *et al.*, 2006), suggesting that changes in chromatin structure are involved in the activation of DDR signalling through the activation of ATM (Bakkenist and Kastan, 2003). In addition, one study has shown the nucleosome-binding protein HGMN1 modulates the interaction of ATM with chromatin before and after DSB generation, thereby optimising ATM activation (Kim *et al.*, 2009).

1.10.2 DDR in the context of heterochromatin

The range of various types of chromatin compaction challenges the repair of DNA, a process that has to be equally efficient in all chromatin contexts. Heterochromatin has been proposed to constitute a barrier to DDR signalling and DSB repair (Goodarzi and Jeggo, 2012). One of the first studies showing that heterochromatin is refractory to γH2AX modification was made in budding yeast, and demonstrated that γH2AX spreading from an endonuclease-induced DSB into the *HML* and *HMR* loci, which are mainly de-acetylated and heterochromatic, does not occur, in contrast to efficient γH2AX spreading into euchromatic sequences (Kim *et al.*, 2007). This finding was corroborated in another study in which ChIP was used to detect γH2AX and found γH2AX expansion was reduced in heterochromatic sequence (Karagiannis *et al.*, 2007). Jakob et al. 2011 used high linear energy transfer (LET) radiation to generate linear ion tracks traversing heterochromatic regions in both human and murine cells, and found that the linear path of DSBs, marked by γH2AX, bent around heterochromatic regions.

DNA repair in heterochromatin compartments has been associated with DSB movement. In *Drosophila,* DSBs induced in the heterochromatic domain of cells rapidly accumulate the early markers of the DDR, activate the early steps of HR and are then re-localised outside of the domain (Chiolo *et al.*, 2011). An analogous relocation of DSBs was observed upon break induction by linear ion tracks in chromocentres of murine cells. In contrast to these studies, (Lemaître *et al.*, 2014) showed that a DSB induced at the nuclear lamina, which is considered a heterochromatic compartment, did not relocate outside of the compartment in human cells.

1.11 DSBs in the formation of Chromosomal Translocations

1.11.1 Chromosomal translocations

Chromosomal translocations have been linked to a number of disorders, including mental retardation, infertility and cancer. In karyotyping, translocations are manifested as a change in the length or banding pattern of a chromosome arm. Two types of chromosomal translocations are non-reciprocal and reciprocal. Non-reciprocal translocations are one way translocations in which a chromosomal segment is transferred to a nonhomologous chromosome. In contrast, reciprocal translocations involve the exchange of segments from two nonhomologous chromosomes. In both cases, if no genetic material is lost during the exchange the translocation is considered to be a balanced translocation. Another category of translocation are Robertsonian translocations in which the q arms of two acrocentric chromosomes fuse at a single centromere. Chromosome p arms are lost during Robertsonian translocations, but as a result of very short p arms that are repetitive on acrocentric chromosomes, Robertsonian translocations present no phenotypic consequences.

Depending on the chromosome breakpoint, a translocation can result in the disruption or mis-regulation of normal gene function. Analyses of DNA sequences surrounding a translocation has provided valuable mechanistic insights into cancer. The first consistent specific translocation identified was t(9;22)(q34;q11), resulting in the ‘Philadelphia chromosome’ in chronic myeloid leukaemia (CML) (NOWELL, 1962). This translocation fuses the coding sequence of the BCR gene on chromosome 22 with the coding sequence of the ABL gene on chromosome 9. The resulting BCR-ABL fusion

protein encoded by the chimeric gene is a protein tyrosine kinase that constitutively activates signalling pathways involved in cell growth and proliferation (Epstein *et al.*, 1988). Other translocations, such as those that place the coding sequence of one gene in proximity to the regulatory sequence for a different gene have been described; the first of which was the translocation involving chromosomes 8 and 14 in patients with Burkitt's lymphoma. The most common translocation associated with Burkitt's lymphoma is t(8;14)(q24;q32) (approx 80% of all cases) (Hecht and Aster, 2000) which places the c-myc proto-oncogene from chromosome 8 under the control of the immunoglobin heavy chain gene (IGH) promoter on chromosome 14. The MYC protein normally signals for cell proliferation, and the translocation causes high levels of MYC overexpression in lymphoid cells, where the IGH promoter is normally active. The advent of molecular cytogenetic techniques, such as fluorescence in situ hybridization (FISH), multicolour FISH and array-based comparative genomic hybridization has opened the way for precise mapping of structural rearrangements within genes (Kearney and Horsley, 2005; Pinkel and Albertson, 2005).

The molecular characterisation of the Philadelphia chromosome and the Burkitt's lymphoma translocation have dramatically increased the understanding of the pathogenic significance of chromosomal translocations and gene fusions in the origin of human cancers (Rowley, 2001). Evidence of chromosomal translocations and their possible role in cancer was first put forward by Theodor Boveri in 1914 (Boveri, 1914). Although characterised in many cancers, the mechanism by which chromosomal translocations form are poorly understood. What is clear is that chromosomal translocations are induced by DSBs. A combination of several events is required for a translocation to take place. These include: errors in DSB repair, spatial proximity of

translocation partners and the capacity of damaged loci to re-localise within the nuclear space. Ligation of broken DNA ends cannot occur without catalysis by DDR proteins, implying that translocations are actively generated by the DDR machinery.

1.11.2 DSB mobility in the formation of chromosomal translocations

DSBs are the most deleterious form of DNA damage and a failure to re-join DSBs can ultimately lead to cell death, while mis-repair of DSBs can specifically lead to chromosomal breaks and translocations. Multiple DSBs are particularly dangerous to a cell since they may lead to translocations. However even isolated DSBs can cause substantial damage, potentially killing a cell, if it leads to the inactivation of an essential gene, or more commonly, triggers apoptosis. (Rich, Allen and Wyllie, 2000)**.** In the last decade, there have been many studies into the mobility of DSBs, fuelled by their tumorigenic potential. DSBs are powerful inducers of mutations and there is experimental evidence showing a causal link between the induction of mutations and chromosomal translocations. (Richardson and Jasin, 2000)**.** Indeed, it is generally accepted that such chromosomal translocations must have arisen through the generation of one or more DSBs that were erroneously repaired. A combination of several events is required for a translocation to take place. These include: errors in DSB repair, spatial proximity of translocation partners and the capability of damaged loci to re-localise within the nuclear space.

Two hypotheses have been put forward to describe the proximity of broken loci resulting in translocation events. The ‘contact first’ hypothesis postulates that broken loci are proximal within the nucleus and are largely immobile or have reduced mobility,

thus leading to an increased probability of translocation of neighbouring loci. An alternative 'breakage first' hypothesis proposes that broken chromosomes ends on different chromosomes are able to freely move within the nuclear space and upon contact may lead to a translocation. In this case, the probability of translocation of broken loci may increase with the scale of movement of DSBs. Intriguingly, (Vassilis Roukos *et al.*, 2013) concluded that the vast majority of translocations they observed in their system were formed from pre-positioned proximal DSBs. However, they also observed a small subset of translocations generated by DSBs that underwent long range motion, consequently unifying the 'contact first' and 'breakage first' models.

1.12 DSB Mobility in Yeast and Higher Eukaryotes

In yeast, a relative consensus exists that DSB induction increases both the movement of undamaged chromosomes and of the DSB itself (Dion *et al.*, 2012). Large scale movement of damaged loci is specific to persistent DSBs, and persistently unrepairable DSBs move towards the nuclear periphery via association with Mps3, telomerase and proteins of the nuclear core complex (Oza and Peterson, 2010). In addition, DSBs in sub-telomeric regions are also sequestered to the nuclear periphery (Taddei *et al.*, 2006; Therizols *et al.*, 2006). Increased mobility of DSBs in yeast is mediated by key repair enzymes RAD51, Sae2, RAD54, Mec1, and RAD9 (Oza *et al.*, 2009; Dion *et al.*, 2012; Miné-Hattab and Rothstein, 2012).

In contrast to yeast however, data published of DSB mobility in higher eukaryotes has been controversial, caused by conflicting results. Mobility of DSBs

induced by X-ray or γ-irradiation did not differ from intact loci (Nelms *et al.*, 1998; Falk *et al.*, 2007; Jakob *et al.*, 2009)**,** with (Khrulak et al. 2006) showing similar results in cells irradiated with an argon laser in which DSBs were immobile and did not form clusters. In cells in which a single DSB was induced by I-SceI, broken ends were positionally stable and unable to roam the cell nucleus (Soutoglou, Jonas F. Dorn, *et al.*, 2007). Conversely, by using α-radiation to create DSBs along a confined linear track, (Jacob A Aten *et al.*, 2004) found that breaks were redistributed into clusters giving rise to MRE11 dependent 'repair centres' that were mostly predominant in the G1 phase of the cell cycle. Likewise, DSBs generated by γ-rays or etoposide, induced movement of damaged chromatin greater than two-fold over that of undamaged loci (Krawczyk *et al.*, 2012). Reports of evidence for repair centres has also shown IR induced 53BP1-GFP foci between 1 and 2 µm apart can rapidly gather into larger clusters (Neumaier *et al.*, 2012)**.** More recently, through the use of a high throughput capture Hi-C assay, (Aymard *et al.*, 2017) demonstrated that DSBs cluster primarily during the G1 cell-cycle phase, and only when they were induced within transcriptionally active genes. Loss of ATM reduced mobility of DSBs created by γ-rays and charged nuclei (Becker *et al.*, 2014a) and at nuclease-induced breaks (Caron *et al.*, 2015).

A well-defined context in which DSB movement has been established in mammalian cells, is at de-protected and damaged telomeres. Dysfunctional telomeres activate the DSB response through a depletion of shelterin and telomeres are joined by NHEJ to cause telomere fusions (Doksani and de Lange, 2014). Loss of 53BP1 reduced the mobility of telomere ends and resulted in almost complete loss of telomeric fusions (Dimitrova *et al.*, 2008). Another example of DSB mobility occurring at telomeres is the directed movement of telomere ends into clusters referred to as ALT-associated PML

bodies (APBs). Tang et al. 2013 generated DSBs specifically in telomeres to elicit a DSB repair response, observing a directed movement in ALT but not telomerase positive cells.

Thesis Objectives

The phosphorylation of histone H2AX to form γH2AX in the vicinity of a DSB is a key component in DDR signalling at DSBs in eukaryotes, and the generation of γH2AX plays an important role in the repair of DNA. However, the spatial organisation of γH2AX around a DSB in mammals is yet to be fully uncovered. Whilst the *in cis* formation of γH2AX has been well characterised, and initial reports have pointed to some sort of spatial regulation of the DDR, the question of whether γH2AX accumulates *in trans* in a non-linear fashion is still yet to be answered. The first part of this thesis lays out the steps taken investigate the spatial distribution of γH2AX around a nascent DSB.

In yeast, a relative consensus exists that DSB induction increases the movement of a DSB. In contrast, conflicting data of the movement of DSBs in higher eukaryotes has been published. The second part of this thesis aims to give clearer insights into the dynamics of a single DSB in vivo in human cells

Chapter 2

2 Materials and Methods

2.1 Cloning and sub-cloning

2.1.1 Bacterial transformation

MAX efficiency® Stbl2™ competent *E. coli* (Invitrogen) or homemade calcium competent DH5α *E. coli* were thawed on wet ice. The required number of microcentrifuge tubes were placed on ice. DNA was added to the cells, moving the pipette through the cells whilst dispensing. After incubating the cells on ice for 30 minutes they were heat-shocked for 25 seconds in a 42°C water bath and placed on ice for a further 2 minutes. 200 µl of room temperature S.O.C. medium (Invitrogen) was added to the mixture, which in turn was shaken with a speed of 225 rpm at 30°C for 90 minutes (tubes containing ligation reaction) or 37°C for 60 minutes (tubes containing plasmid DNA). The entire mixture was plated as necessary on LA (lysogeny broth agar) plates supplemented with either kanamycin or ampicillin antibiotic and left to incubate overnight at 37°C.

2.1.2 Plasmid DNA purification

Competent cells that had been transformed with plasmids or a ligation were picked using a pipette tip, placed in 3 ml of LB (lysogeny broth) supplemented with antibiotic and grown overnight at 30°C. Plasmid DNA was then extracted according to the protocol provided with the Macherey Nagel plasmid DNA purification kit.

2.1.3 DNA gel extraction/PCR cleanup

The Nucleospin® Gel and PCR Clean-up (Macherey Nagel) kit was used to purify DNA fragments from enzymatic reactions, such as PCR, and from agarose gels. In the case of

excised gel bands, the sample was heated in NTI buffer (Macherey Nagel) at 50 °C for 10 mins to dissolve the agarose. Resulting steps taken to purify the DNA were identical for both gel extraction and PCR cleanup samples. In brief, in the presence of chaotropic salt, the DNA is bound to the silica membrane of NucleoSpin® Gel and PCR Clean-up column. Washing steps are conducted with ethanolic Wash Buffer NT3 in order to remove any contaminants. Pure DNA is then eluted under low salt conditions with double distilled H_2O.

2.1.4 Genomic DNA extraction

Genomic DNA was extracted and prepared from human U2OS cells with the NucleoSpin® Tissue kit from Macherey Nagel. Lysis of cells was achieved by incubation of sample material in a proteinase K/SDS solution. In order to create the appropriate conditions for DNA binding to the silica membrane in the NucleoSpin® Tissue Columns, chaotropic salts and ethanol are added to the lysate. This binding process can be reversed and is specific to nucleic acids. Contaminations are removed by washing with two different buffers. Pure genomic DNA is eluted under low ionic strength conditions in double distilled H_2O.

2.1.5 DNA Ligations

Ligations were performed on amplified DNA from PCR (plasmid or genomic DNA) or DNA digested by restriction enzymes. All ligations were performed using the Rapid DNA Ligation kit (Thermo Scientific). Varying insert:vector ratios were used in order to attain a successful ligation and the amount of insert DNA to be added per reaction was calculated using the following formula:

{(ng of vector) x (kb size of insert) / (kb size of vector)} x {insert:vector ratio)

2.1.6 Restriction endonuclease digestions

All restriction digestions were performed with restriction enzymes provided by NEB and FastDigest restriction enzymes provided by Thermo Scientific.

2.1.7 Polymerase chain reaction

Phusion polymerases (Thermo Scientific, NEB) were used for all PCR reactions conducted. PCR reaction and cycling conditions were optimised and adapted in order to achieve amplification of target DNA.

2.1.8 DNA sequencing

Sanger sequencing was conducted by Eurofins Genomics using their custom DNA sequencing service.

2.1.9 Agarose gel electrophoresis

DNA was separated by electrophoresis using gels, ranging from 0.8 % - 2% agarose, prepared in 1x TBE buffer. Images of bands were captured using the InGenius LHR gel imaging UV Transilluminator from Syngene, and analysed using GeneTools anaylysis software (Syngene).

2.2 Mammalian cell culture

2.2.1 Cell line maintenance

Human osteosarcoma U2OS cells were cultured at 37°C/5% CO_2 in Gibco® Dulbecco's Modified Eagle's Medium (DMEM) supplemented with 10% foetal calf serum (FCS) (PAN Biotech) or 10% charcoal stripped foetal bovine serum (FBS), 2mM L-Glutamine (Gibco®) and 1% Penicillin-Streptomycin solution (Corning). U2OS cells were also cultured in CO_2 Independent Medium (Gibco®) when necessary**.**

2.2.2 Transfections

Transfection of plasmid DNA was performed in U2OS cells according to the supplier's protocol for each transfection reagent used (both liposomal and non-liposomal).

2.2.3 Stable cell line generation

To generate stable cell lines, U2OS cells were transfected with plasmid constructs using Fugene HD (Promega) transfection reagent according to the protocol provided by the manufacturer. All constructs were linearised with a specific restriction enzyme prior to transfection and either co-expressed with an antibiotic selection marker on the same construct or on a second, co-transfected vector. 48 hours after non targeted transfection of U2OS cells in a 6 well dish, the desired concentration and type of antibiotic was added and cells left under selection pressure for approximately 2 weeks. A change of medium containing fresh antibiotic was made every 3 days to compensate for loss of selection pressure. Under selective conditions, resistant cells outgrew non-resistant cells resulting in a heterogeneous population of cells that were likely to have

incorporated the transfected construct into their genome. To generate a clonal cell line, cells were trypsinised and plated in a 96 well dish in such a way that approximately 1 cell per well was plated. Those wells that had only one population of cells (monoclonal) were marked and taken for testing and analysis. This procedure of single cell cloning was repeated a second time to obtain 100% clonal purity.

2.2.4 Determination of antibiotic concentration

Cells were split into 24-well plates containing culture medium without any antiobiotic. The following day the culture medium was aspirated from the wells and replaced with fresh medium containing increasing concentrations of the desired anitobitic titrated within a range specific to that of the antibiotic. Cells were fed every 3 days with fresh selection medium and cell death observed after 7 days by light microscopy. The working concentration was chosen as the mimimum concentration that showed complete cell death in a well.

2.2.5 Electroporation

U2OS-tetO-lacO-I-SceI cells were transfected by electroporation using the Amaxa Nucleofector™ 2b Device. Optimal conditions for electroporation were achieved through use of Cell Line Nucleofector® Kit V, and a U2OS specific protocol. In brief, cells were harvested by trypsinization and an aliquot of $8x10^5$ cells was centrifuged. The

resulting cell pellet was resuspended carefully in 100 µl of room temperature Nucleofector® Solution (82 µl Nucleofector® Solution plus 18 µl supplement) and mixed with a total of 2 µg DNA, before being transferred into a certified cuvette. Nucleofector® Program X-001 was selected and applied to the cell/DNA suspension, after which, 500 µl of pre-warmed culture media was added and the entire suspension transferred to a prepared 35 mm glass bottom dish (MatTek)

2.3 Induction of DNA damage

2.3.1 Inducible double-strand break

A single targeted double strand break was introduced into U2OS cell line U2OS-tetO-lacO-I-SceI cells cultured in DMEM supplemented in 10% charcoal stripped FCS on addition of the hormone Triamcinolone Acetonide (TA). TA was added at a concentration of 10^{-5}M.

2.3.1 X-Ray Irradiation

All experiments were performed by irradiating cycling U2OS cells with a dose of 0.5Gy using 250kV x-rays at a dose rate of 0.5Gy/minute.

2.4 2-D Fluorescence in situ hybridisation (FISH)

2.4.1 Preparation of probe and sample

Dual colour FISH was performed with probes specific for pLAU44i-pCI Puro (tetO-ISceI) and pLAU43 (lacO) plasmid DNA. tetO-ISceI and lacO plasmids were digested with specific restriction enzymes. The resulting linearized DNA was mixed in a reaction

mixture for direct enzymatic labelling of DNA in a nick translation labelling assay, using a Nick Translation Kit (Jena Bioscience) to create fluorescently labelled probes. A typical reaction mixture used in the assay is tabled below.

PCR-grade water	Fill up to 20 µl
10x NT labelling buffer	2 µl
ATT0 488/550 NT labelling mix	2 µl
Linearised plasmid DNA	1-1.5 µg
Enzyme mix	2 µl
Total	**20 µl**

U2OS cells were then plated and grown on coverslips placed in a 24-well dish. Cells were fixed with Carnoy's fixative; a 3:1 mix of Methanol:Acetic acid.

2.4.2 Co-denaturation, hybridisation and washing steps

Labelled probes were mixed together with human Cot1-DNA (ThermoFisher) to block nonspecific hybridisation and resuspended in hybridisation buffer. Fixed cell samples on coverslips in a 24 well plate were washed with 500 µl 2x SSC for 5 mins. Cell samples on coverslips were then dehydrated through a 70% (v/v), 90% (v/v) and 100% (v/v) alcohol series before being placed faced down on clean slides with labelled probes in

hybridisation buiffer pipetted on them. Co-denaturation and co-hybridisation of cell samples and labelled probes was performed on a heatblock at 80°C for 5 mins and the sample left to incubate overnight a 37°C in a humid environment.

Washing steps consisted of washing the sample in room temperature 2x SSC for 5 minutes followed by further washing in 0.1x SSC at 65°C for 40 minutes. The sample was washed once more with 2x SSC before being staining for 5 minutes with 4',6-Diamidino-2-Phenylindole, Dihydrochloride (DAPI) and preserved for fluorescence microscopy imaging in DAPI-free mounting media (Vectashield). Imaging was done on the ScanR inverted microscope (Olympus).

2.5 Immunofluorescence microscopy

Cells were harvested, plated and grown on glass coverslips in a 24-well dish and were then fixed in 4% (w/v) paraformaldehyde in PBS for 10 minutes. Phosphate buffer solution (PBS) was used to wash the cells three times before permeabilisation for 10 minutes using 0.5% (v/v) Triton X-100 (Sigma Aldrich). Cells were immunolabelled at room temperature using specific primary and secondary anitbodies diluted in DMEM culture media supplemented with 10% FCS. Primary antibody at the desired concentration was incubated with cells for 30 minutes. Primary antibody was then aspirated and the cells washed 3 times with 0.1% PBS—Tween® 20 (Sigma Aldrich) before incubation for 30 minutes with a secondary antibody conjugated to a fluorescent dye. All secondary antibodies used in this study were conjugated to Alexa Fluor® dyes (Life Technologies). Secondary antibody was aspirated and cells washed 3 times with 0.1% (v/v) PBS—Tween® 20. Following this, cells were washed once with 0.1% (v/v)

NP40 in PBS, incubated for 5 mins in 4',6-Diamidino-2-Phenylindole, Dihydrochloride (DAPI) diluted in PBS before being mounted on slides with DAPI-free mounting medium (Vectashield).

2.6 Metaphase spread FISH

100 µl of 10 µg/ml Gibco KaryoMAX® Colcemid solution in PBS was added to U2OS cells cultured in 10 ml of DMEM in a 10 cm dish (Corning) and incubated at 37°C for 90 minutes. After incubation, the cells were trypsinised (without a PBS wash prior) using Trypsin-EDTA and spun down at room temperature to leave a pellet. 7 ml of hypotonic solution (0.8% Sodium Citrate) was added dropwise to the sample whilst gently tapping the tube to mix. The sample was left to incubate at room temperature for 10 minutes and spun down. Most of the supernatant was aspirated but approximately 500 µl was left. Following this, 7 ml of Carnoy's fixative was slowly added to the sample which was then incubated for 10 mins and spun down. The final pellet was resuspended in 300 µl Carnoy's fixative.

2.6.1 Slide preparation

A wet paper towel was placed on the benchtop and two glass 5 ml pipettes running parallel to each other were placed on the paper towel. The required number of slides was rested so to lie perpendicularly on the two pipettes. A droplet of cells was dropped from a height onto the laid out slides. Slides were then left to dry and mature for at least

24 hours before performing the co-denaturation, hybridisation and washing steps as described in the 2D FISH protocol.

2.7 Immuno-FISH

Cells were plated on circular glass coverslips and fixed the following day in ice cold 4% (v/v) PFA in PBS for 20 minutes. Cells were washed with ice cold PBS three times before permeabilisation with 0.5% Triton X-100 in PBS for 20 minutes, and then washed in the same way again. Coverslips with fixed cells were placed cell side up on a slide and sealed with rubber cement (Marabu Fixogum). Pre-denaturation of samples was then performed in a fume hood by placing slides in a Coplin jar filled with a denaturing solution of 70% Formamide, 2x SSC and 0.1 mM EDTA at 70°C for 5 minutes. Samples were then dehydrated in an alcohol series of 70%, 85%, 100% ethanol for 1 minute each. 5 µl of FISH probe (prepared as in 2-D FISH protocol) was pipetted onto pre-warmed (37°C) slides, samples placed cell side down and sealed with rubber cement. Samples and FISH probe were co-denatured at 95°C on a heat block for 5 minutes and left to hyrbidise overnight at 37°C in a humid environment.

The following day sample coverslips were placed cell side up on fresh slides and immersed in 2X SSC for 5 minutes. Each slide was then immersed in 0.5X SSC in Coplin Jars in a water bath set to 65°C. Following this, coverslips were removed from slides, placed in a 24-well dish and washed with PBS. They were then incubated with primary antibody for 30 minutes and washed three times in 0.1 % PBS-T before incubation with secondary antibody for 30 minutes. Finally samples were washed three times with PBS,

washed once with 0.1% NP-40 stained with DAPI for 5 minutes and mounted on to slides with mounting medium.

2.8 γH2AX Chromatin immunoprecipitation – qPCR

2.8.1 ChIP

Cells were treated as needed for the experiment, trypsinised and spun down in a centrifuge. The resulting cell pellet was re-suspended in 1 ml PBS at room temperature followed by addition of Formaldehyde to the total concentration of 1%. This mixture was incubated on a rotating wheel for 9 minutes. Glycine was then added to a final concentration of 0.125M to quench formaldehyde reactivity. The mixture was centrifuged at 2000g for 2 minutes and the resulting pellet re-suspended in 300 µl SDS lysis buffer (1% SDS, 10 mM EDTA, 50mM Tris-HCl [pH7.5]) containing protease inhibitor (Pierce Protease Inhibitor Mini Tablets, EDTA-free ThermoFisher) and 50 mM phosphate inhibitor. The cell seuspemsion was left for 10 minutes on ice to fully lyse cells and was sonicated (Diagenode Bioruptor) to 300-500 bp average DNA fragment size at 4°C for 15 minutes (30 seconds on/30 seconds off) at high amplitude. Debris was removed by centrifugation at 13,200 x g at 4°Cfor 20 minurtes and the supernatant diluted 10-fold in ice cold immmunoprecipitation buffer (300 mM NaCl, 10 mM Tris-HCl [pH7.5], 2 mM EDTA, 0.3% NP-40, protease inhibitors and phosphate inhibitors) and incubated overnight with 5 µg of γH2AX antibody (clone JBW103, Merck Millipore)

with rotation at 4°C. The following day 10 µg of rabbit anti-mouse antibody was added for 1 hr with rotation at 4°C. 0.25 mg of pre-washed protein G magnetic beads (Pierce, ThermoFisher) were added to the antigen sample/antibody mixture and left to incubate

with rotation for 1 hour. The beads were collected with a magnetic stand (DynaMag2, ThermoFisher) and washed and pelleted six times for 10 minutes at room temperature in wash buffer (IP buffer + 0.1% SDS). Crosslinked protein-DNA complexes were eluted for 15 minutes at room temperature with elution buffer (100 mM $NaHCO_3$, 1% SDS) and incubated in NaCl at 100 mM concentration overnight at 65°C to reverse crosslinks. DNA was purified using Nucleospin® Gel and PCR Clean-up (Macherey Nagel) kit and used as template for q-PCR quantification.

2.8.2 qPCR

Real time PCR was performed in 96 well PCR microplates (Star Lab) using the LightCycler® 480 Instrument II System (Roche). DNA samples were prepared as per the ChIP protocol, specific primers were designed to amplify target regions of interest and 2x SYBR Green qPCR Master Mix (Biotool) was used to perform SYBR Green I based quantitative PCR (qPCR). 5 µl (approximately 200ng/reaction) of total input genomic DNA or immunoprecipitated genomic DNA was pipetted in wells in a 96 well plate and the plate centrifuged in order to sediment the DNA at the bottom of wells. The reaction master mix was prepared as shown below, mixed thoroughly by pipetting up and down and dispensed in appropriate volumes into the 96 well plate. Reactions were mixed gently in wells in the 96-well plate taking care not to create any bubbles and the plate placed in a thermal cycler which was programmed appropriately**.**

Component	Amount per reaction (µl)	Final Concentration
2x Biotool SYBR Green Master Mix	7.5	1x
Forward Primer	0.45	300 nM

Reverse Primer	0.45	300 nM
Nuclease-free Water	1.6	-
Total Reaction Volume	**10**	**-**

Step	Temperature	Time	Cycle
Initial Denaturation	95°C	10 mins	1 cycle
Denaturation	95°C	15 secs	40 cycles
Annealing/Extension	58°C	1 mins	
Melting Curve	95°C 60°C 95°C	15 secs 1 mins 15 secs	1 cycle
Total Reaction Volume	15 ul		

2.9 SDS-PAGE and western blotting

2.9.1 Sample preparation

Cells were treated as necessary, harvested, resuspended in PBS and subjected to lysis in SDS lysis buffer (20mM Tris-HCl [pH 7.5], 150 mM NaCl, 2 mM EDTA, 0.5% SDS). The sample was placed on ice for 10 minutes before sonication (Diagenode Bioruptor) at 4°C

for 3 minutes (30 seconds on/30 seconds off) at high amplitude and denatured in LDS protein loading buffer (Bolt LDS sample buffer) at 95°C for 5 minutes before loading.

2.9.2 SDS-PAGE and WB

Proteins were resolved via Sodium Dodecyl Sulphate Polyacrylamide Gel Electrophoresis (SDS-PAGE), in a Novex™ Bolt™ Mini Gel Tank, using precast 4-12% Bolt Bis-Tris gradient gels (Novex, Life Technologies). Gels were run at 165 V in 1X Bolt™ MES SDS running buffer (Novex, Life Technologies). Following separation of proteins on the gel, the gel was transferred to a nitrocellulose membrane (iBlot® Gel Transfer Stack, Life Technologies) using the iBlot® Gel Transfer Device to perform dry blotting of proteins to the membrane. The desired program is set on the transfer device and the membrane transferred for 8 minutes. Membranes were then blocked for 1 hour with 5% (w/v) non-fat dried milk (Marvel) dissolved in 0.1% (v/v) PBS-T supplemented with sodium azide. Membranes were incubated on a shaker for 1 hour at room temperature with primary antibody diluted in fresh milk dissolved in 0.1% PBS-T at a dilution of 1:1000. The primary antibody solution was removed after incubation and the mebrane washed three times in 0.1% (v/v) PBS-T. Horseradish peroxidase (HRP)-conjugated secondary antibody diluted (1:1000) in blocking buffer was then added for incubation with the membrane for 1 hour at room temperature. The secondary antibody solutuion was removed and the membrane washed as earlier. To detect HRP, Supersignal® West Pico Chemiluminescent Substrate working solution (ThermoScientific) was prepared by mixing equal parts the Stable Peroxide Solution and the Luminol/Enhancer Solution.

Membranes were then incubated in the working solution for 5 minutes. Emission was captured with autoradiograph film using and X-ray film processor.

2.10 ScanR microscopy

All fixed cell microscopy was performed on the ScanR unless otherwise stated. Cells were mounted either onto slides or plated in a 96 well optical plate (Corning), and fully automated image acquisition using a 20X or 40X air objective on the ScanR inverted microscope (Olympus) was conducted.

2.11 Live cell imaging - Timelapse microscopy

All Live cell imaging was performed on the IX81 inverted fluorescence motorised microscope (Olympus) equipped with a temperature controlled chamber stably adjusted to 37°C, an ORCA-Flash4.0 LT CMOS camera (Hamamatsu) and a CSU-X1 Spinning Disk confocal (Yokogawa). Imaging was performed using a 60X, 1.35NA oil objective and three-dimensional image stacks of 11 optical slices covering an 8 µm range, separated by 0.8 µm were collected every 6 minutes for 4 hours using Slidebook 6 software (Intelligent Imaging Innovations). Exposure times varied from 200-1000 ms for each channel and each frame.

2.12 StackReg registration software

To correct for movement of cell nuclei on the cell culture dish, the StackReg image registration plugin (Biomedical Imaging Group) was implemented. StackReg is available through FIJI, an image processing package distribution of ImageJ. After alignment, 2-D

maximum projection time-lapse sequences were analysed with a custom written particle tracking FIJI plugin.

2.13 Trackmate tracking software/plugin

The Trackmate plugin, available through FIJI, was used to perform single particle tracking (SPT) of 'spot-like' structures inside U2OS cells. Each spot is segmented in multiple frames and its trajectory is reconstructed by assigning it an identity over these frames, in the shape of a track. These tracks were then either visualized or used to yield further analysis results.

2.14 Recipes

10X TBE (1 L)

Tris base	108 g
Boric acid	55 g
EDTA	7.5g
ddH_2O	made up to 1 litre

Hyrbidisation buffer

Formamide	500 µl
Dexran Sulfate	200 µl
Triton X-100	100 µl

20X SSC	100 µl
ddH_2O	Made up to 1000 µl

Metaphase spread hypotonic solution

Sodium Citrate	8 g
ddH2O	Made up to 1 litre

2.15 $CaCl_2$ competent cell preparation

Stock commercial competent DH5α or Stbl2 E.coli cells were plated onto an LB agar plate without antibiotics and grown overnight at 37°C. A single colony of E.coli was picked from the plate and used to inoculate a 10 ml starter culture of LB. This culture was grown overnight at 37°C with shaking and used to inoculate 1 litre of LB media at 37°C with shaking until the OD_{600} reached 0.4. At this point the cells were immediately put on ice and left to chill for 20 minutes, swirling occasionally to ensure even cooling. From this point forward, cells, and any bottles or solutions that they came into contact with were pre-chilled and kept at 4°C. The culture was split into four parts by pouring into sterile, disposable, ice cold 50 ml Falcon™ conical centrifuge tubes and harvested by centrifugation at 4000 rpm for 15 minutes at 4°C. Supernatant was decanted and the pellet resuspended in 25 ml of ice cold $MgCl_2$. Suspensions were combined into 2x 50 ml centrifuge tubes and the centrifugation step repeated. The resulting supernatant was decanted and the pellet resuspended in 40 ml of ice cold $CaCl_2$. This suspension was then

kept on ice for 20 minutes. Following this, cells were harvested by centrifugation once again for 15 minutes at 4°C and the resulting pellet resuspended in 12.5 ml of ice cold 85 mM $CaCl_2$ in 15% glycerol. Aliquots of 50 µl of cells were made, snap frozen in liquid nitrogen and stored at -80°C.

2.16 Oligo annealing

Specific oligos were resuspended in annealing buffer (10 mM Tris [pH 7.5], 50 mM NaCl, 1 mM EDTA) and mixed in equimolar concentrations. Approximately 2 µg of each primer was mixed in a total volume of 50 µl. Annealing was achieved by pipetting mixed oligos into a PCR tube and placing them in a thermocycler programmed to start at 95°C for 2 minutes, and then gradually cooling to 25°C over 45 minutes.

Chapter 3

3 Investigating the Spatial Distribution of γH2AX Around a Nascent Double-Strand Break

3.1 Introduction

3.1.1 Formation of γH2AX at regions distal to the break site

Upon DSB induction, γH2AX molecules can form foci linearly covering chromatin up to and beyond 1 megabase (Mb) away from the break site. Previous biochemical studies conducted by the Bonner lab estimated that γH2AX formed around DSBs induced by various genotoxic agents involved chromatin regions containing around 2 Mb of DNA (Rogakou *et al.*, 1998). Their estimate was based on the assumption of maximal and uniform H2AX phosphorylation within nucleosomes around DSBs. In mammalian cells, γH2AX is bound by MDC1 which interacts constitutively with the MRN complex, thereby activating ATM. This interaction of MDC1 and γH2AX has been proposed to amplify the γH2AX signal (Stewart et al. 2003; Stucki et al. 2005). In addition, it has been hypothesised that MDC1 mediates a feed-forward mechanism that promotes the ATM-dependent spread of γH2AX into chromatin at distances further away from the break (Stucki and Jackson, 2006). This hypothesis was based on 2D IF studies analogous to those by the Bonner lab, demonstrating comparable reduction in the size of γH2AX foci in cells lacking ATM or MDC1 function. However, data obtained using Chromatin immunoprecipitation (ChIP) to measure γH2AX and H2AX densities in nucleosomes along chromosomal DNA strands broken during V(D)J recombination in G1 phase lymphocytes suggested a more nuanced picture.

Savic et al. 2009 revealed the principal way by which ATM and MDC1 cooperate to generate γH2AX along broken DNA strands, at least in G1 cells, is through the

phosphorylation of H2AX in chromatin proximal to DNA breakage sites. This results in the formation of γH2AX at high densities near DSBs rather than a continued spreading of γH2AX further and further away from the break site. Furthermore, Savic et al. 2009 observed that the ATM-dependent formation of γ-H2AX along DNA strands 200–600 kb from breakage sites did not require MDC1, but γH2AX was still formed up to 2500 kb away. This indicated that there was a soluble pool of activated ATM able to phosphorylate H2AX at distances further away from DSBs along disrupted DNA fibers (**Fig. 3.1**). The authors thus concluded that ATM promotes H2AX phosphorylation through MDC1-dependent mechanisms proximal to DSBs, and MDC1-independent mechanisms distal from DSBs.

3.1.2 ATM activation and diffusible pATM

Activation of ATM is considered to be site specific and occurs at DSBs. However, many targets of ATM do not actually localise at the break site, indicating that some fraction of activated ATM (pATM) diffuses from the break site and phosphorylates its targets throughout the nucleus. Indeed, one study observed the initial accumulation of pATM at break sites upon laser stripe-induced DNA damage followed by an overall increase in pATM signal throughout the nucleus (Kruhlak *et al.*, 2006). It is possible then that the resulting concentration gradient of pATM molecules could be a defining factor in the spread of γH2AX. Notably, when chromatin is induced to relax by treatment with chloroquine or trichostatin, ATM is activated globally and ATM substrates that would be phosphorylated at the site of breaks, such as H2AX, fail to become phosphorylated, whereas substrates present elsewhere in the nucleus, such as p53, can still be

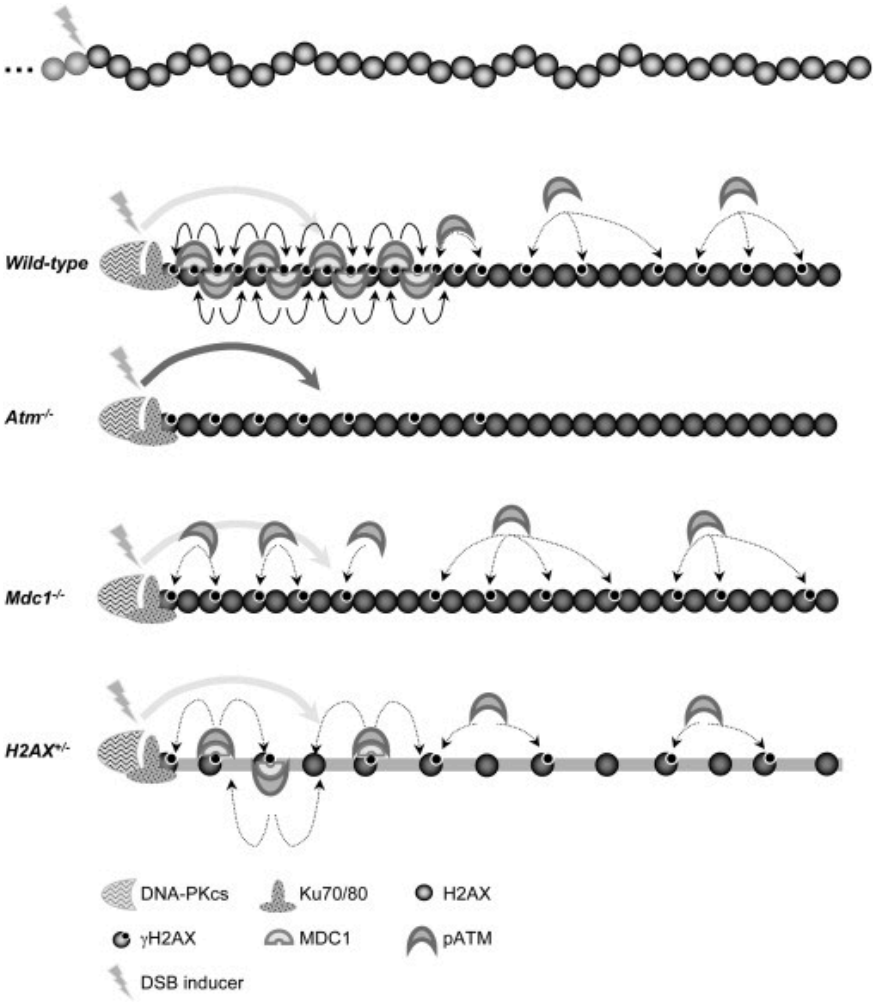

Figure 3.1. Models depicting how γ-H2AX forms along DNA strands broken in G1 phase cells

Adapted from Savic et al, 2009. In wild-type cells, the γ-H2AX self-reinforcing mechanism generates and maintains γ-H2AX at high densities near DNA ends and soluble ATM forms γ-H2AX at lower densities over sequences further away from DSBs. DNA-PKcs may contribute to γ-H2AX formation near DNA ends. In ATM deficient cells, DNA-PKcs generates γ-H2AX at low densities near DNA ends, but not over sequences further away from DSBs. In MDC1 deficient cells, soluble ATM generates γ-H2AX at low densities both near DNA ends and over sequences further away from DSBs. In H2AX haploinsufficient cells, the γ-H2AX self-reinforcing mechanism is not as effective as in wild-type cells and generates γ-H2AX at low densities near DNA ends, but soluble ATM forms γ-H2AX over sequences further away from DSBs as in wild-type cells.

phosphorylated (Bakkenist and Kastan, 2003). This indicates that ATM activation is not dependent on direct binding to DNA breaks, but may result from changes in the structure of chromatin.

The premise that diffusible pATM phosphorylates H2AX distally could indicate that such a chromatin mark could be deposited non-linearly and does not require 'tracking' along the DNA fibre. In fact γH2AX formation at unprotected telomeres can form discontinuously (Meier *et al.*, 2007). The 'intra-TAD model' for γH2AX domain establishment, posited by (Aymard and Legube, 2016), suggests that the flexibility and local movements of the chromatin fibre inside the topologically associated domain (TAD) brings distant nucleosomes within spatial proximity of ATM. Phosphorylation of any nucleosome containing H2AX within a TAD would occur if a break persisted long enough and the DNA damage signal was sustained. Such a model would be in line with the observation made by (Savic *et al.*, 2009), in which neither lower levels of H2AX nor a persistent DSB changed the spreading capability of γH2AX. Also, in *Saccharomyces cerevisiae*, the H2A phosphorylation equivalent to γH2AX, γH2A, can skip over heterochromatic regions (Kim *et al.*, 2007), further supporting the idea that γH2AX may not spread through chromatin tracking.

3.2 Establishment and Characterisation of a Cell Based System to Analyse the Spatial Distribution of γH2AX

Taking the challenge of stochastic interactions into consideration, the most ideal way to practically address this issue would be to use a cell based system in which the association of the break site and a distal chromatin region is non-random and can be inducible.

Although extensively used as a marker of DSBs, little is known about how γH2AX is spatially distributed around a nascent DSB in mammalian cells and how the DDR affects chromatin function and gene expression beyond the immediate region *in cis*. From the data presented in the current literature we hypothesise that γH2AX can spread in *trans* unto an unbroken chromosome in human cells. (**Fig. 3.2**).

To this end I have attempted to create a novel system whereby two independent artificially created DNA segments stably inserted into the genome of human bone osteosarcoma epithelial cells (U2OS) can be tethered together through the use of a novel TetR:2xFLAG:LacI fusion protein (**Fig. 3.3A**). Upon expression of the fusion protein the two distinct chromatin regions are tethered through binding of the tet repressor protein to the array of tet operator sequences and binding of the lac repressor to the array of lac operator sequences. This U2OS-derived cell line will be used for ChIP analysis in the presence of the TetR:2xFLAG:LacI fusion protein to monitor the extent to which γH2AX spreads from the break site in *cis* and *in trans*.

A tandem sequence of FLAG peptides was inserted between the two repressor proteins. The function of the 2xFLAG peptide would be twofold. First, the peptides could be used as a tag for detection of the recombinant fusion protein by immunofluorescent

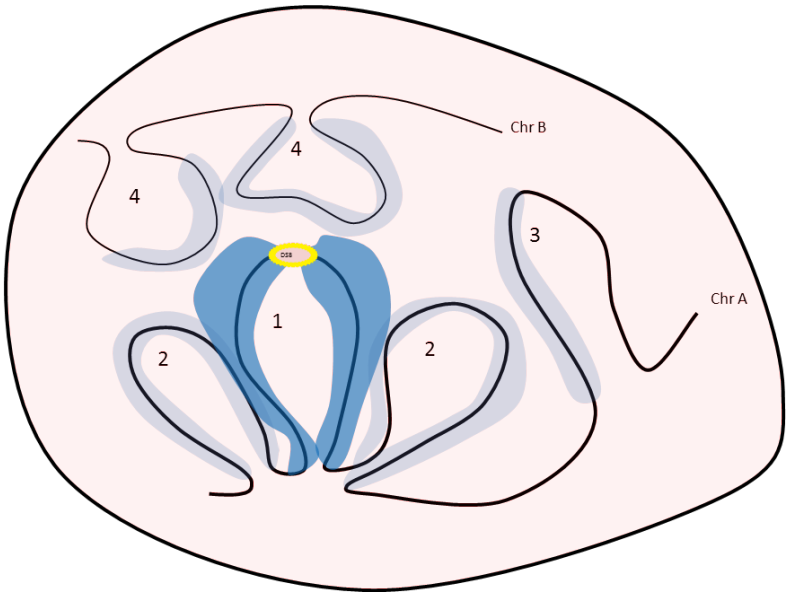

Figure 3.2. Hypothesised 3D interactions between a DSB and the local chromatin

IRIF, as seen by immunofluorescence are probably not a representation of γH2AX spreading linearly. Rather γH2AX spreads to chromatin segments (blue) found in the vicinity of a nascent DSB(yellow): (**1**) at high density proximal to the break site, (**2**) spreading linearly at lower densities to regions distal to the break site, (**3**) spreading intra-chromosomally to regions distal to the break site but that have been folded into proximity and (**4**) spreading to regions of other unbroken chromosomes that may happen to be in vicinity of the break.

staining or western blot. Second, to avoid mis-folding of the fusion proteins the peptides would act as a linker and thus ensure the two proteins fold independently (**Fig. 3.3B**).

An I-SceI mediated site specific DSB can be induced on one DNA segment but not the other, giving the opportunity to address the possibility of *in cis* and *in trans* spreading of DDR induced chromatin modifications. I-SceI mediated DSB induction was inducible through an import system (Soutoglou, Jonas F. Dorn, *et al.*, 2007) using plasmid I-SceI-GR-RFP. This plasmid contains a glucocorticoid-receptor chimera fused to the I-SceI restriction endonuclease that is translocated from the cell cytoplasm to the cell nucleus upon binding to the synthetic ligand triamcinolone acetonide (TA).

Two plasmid constructs: pLAU44-I-sceI-pCI Puro (tetO) and pLAU43 (lacO) and (**Fig. 3.4**) were stably transfected into U2OS cells and randomly integrated into the genome after antibiotic selection.

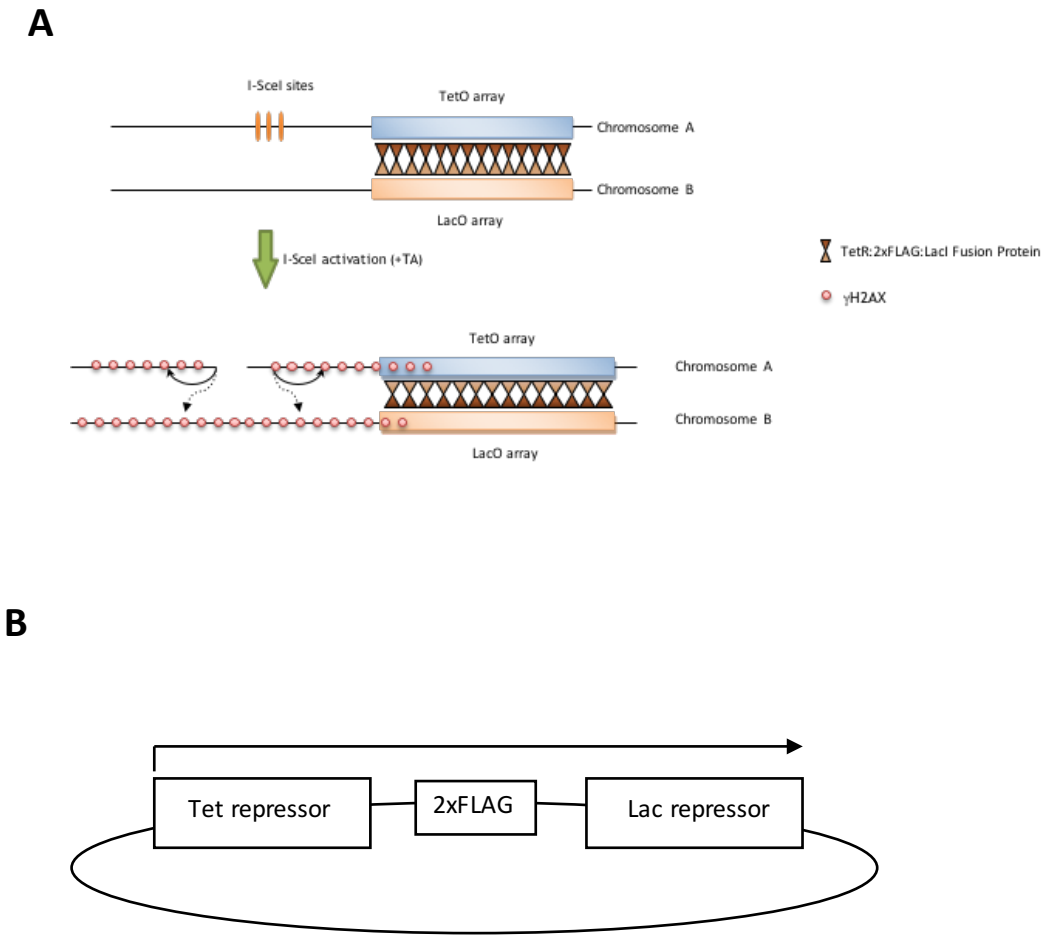

Figure 3.3. Model system to address the 3D DDR in U2OS cells

(**A**) Schematic representation of a unique cell based system in which a single site specific DSB can be induced in a cell and though the use of a novel TetR:FLAG:LacI fusion protein, two distinct chromatin regions containing tetO and lacO binding arrays can be tethered. The I-SceI cut site is located adjacent to the tetO array so that a site-specific break can be introduced in the vicinity of the region of association. (**B**) Schematic representation of the TetR:FLAG:LacI fusion protein. Transcription of Tet and Lac repressor occurs in the same reading frame and results in a fusion protein that simultaneously expresses both proteins The FLAG peptides as a linker between the two proteins enabling TetR and lacI to fold into higher order structure independently of each other.

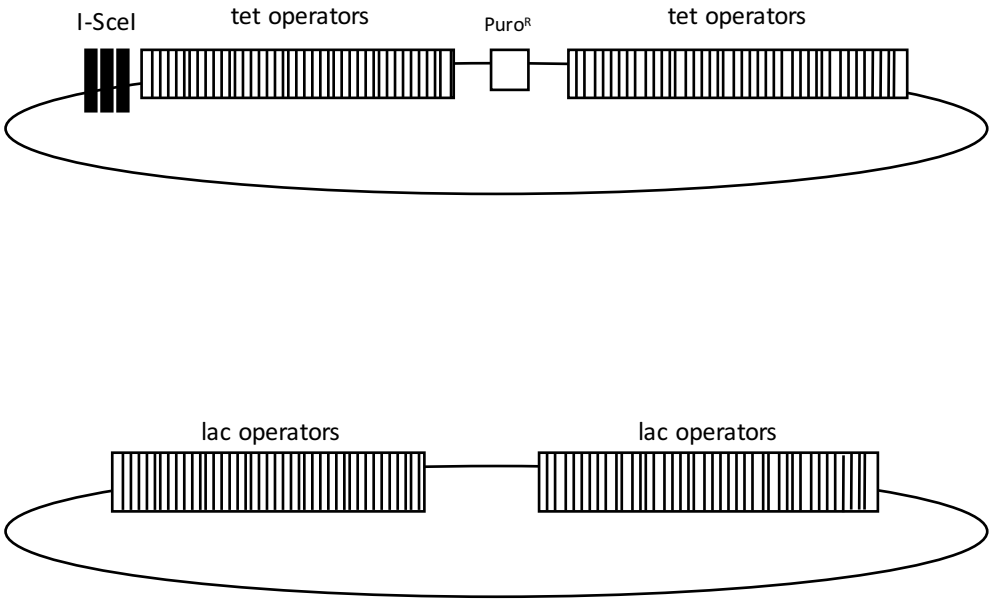

Figure 3.4. Key stable integrants of the U2OS-tetO-lacO cell line

Schematic representation of two plasmid constructs stably integrated into the genome of U2OS cells. Top: plasmid pLAU44-I-SceI-pCI Puro containing two arrays totalling approximately 180 tandem tet operator sequence repeats. A selectable marker conferring resistance to puromycin is located between the two arrays. An I-SceI triple cut site is adjacent to the arrays. Bottom: plasmid pLAU43 containing two arrays totalling approximately 170 tandem lac operator sequences.

3.2.1 Constructing pLAU44-IsceI-pCI Puro

Plasmid pLAU44-IsceI-pCI Puro was constructed to be stably integrated into the genome of U2OS cells. Stable cell line generation in mammalian cells involves the transfection of the 'gene of interest' (tetO repeats with adjacent I-SceI recognition sequence) together with a mammalian antibiotic selection marker; in this case puromycin **(see materials and methods)**. Resistance to puromycin is conferred by the puromycin N-acetyl-transferase gene (pac) from Streptomyces. pLAU44-IsceI-pCI Puro was generated in order to include the resistance gene on the same plasmid construct so that upon transfection and uptake of the plasmid, any cell showing resistance to puromycin antibiotic would be expected to also harbour the 'gene of interest'.

Plasmid pLAU44 (Lau *et al.*, 2004) was used as the parent plasmid and contained two independent arrays of approximately 120 tandem copies of the *E. coli* Tn10 Tet operator (tetO) sequence. Random base pairs of sequence are interspersed between each operator sequence. In order to be able to induce a DSB in the system, I sub-cloned a small insert (henceforth referred to as I-SceI triple array) composed of an array of 3 I-SceI restriction sites (**Fig. 3.5.**) into plasmid pLAU44. The expectation was that having an array of three cut sites spanning close to 200 bp (approx. 140 bp of DNA is wound around histones) would increase the probability of I-SceI accessing its recognition sequence and increase the cutting efficiency.

Upon repeated transformation of the ligation reaction between linearised pLAU44 and the I-SceI triple array into DH5α *E. coli*, little or no colonies grew on Kanamycin selective plates. Of the small population of colonies that did grow, after diagnostic restriction digest of plasmid recovered from *E. Coli*, only undigested or

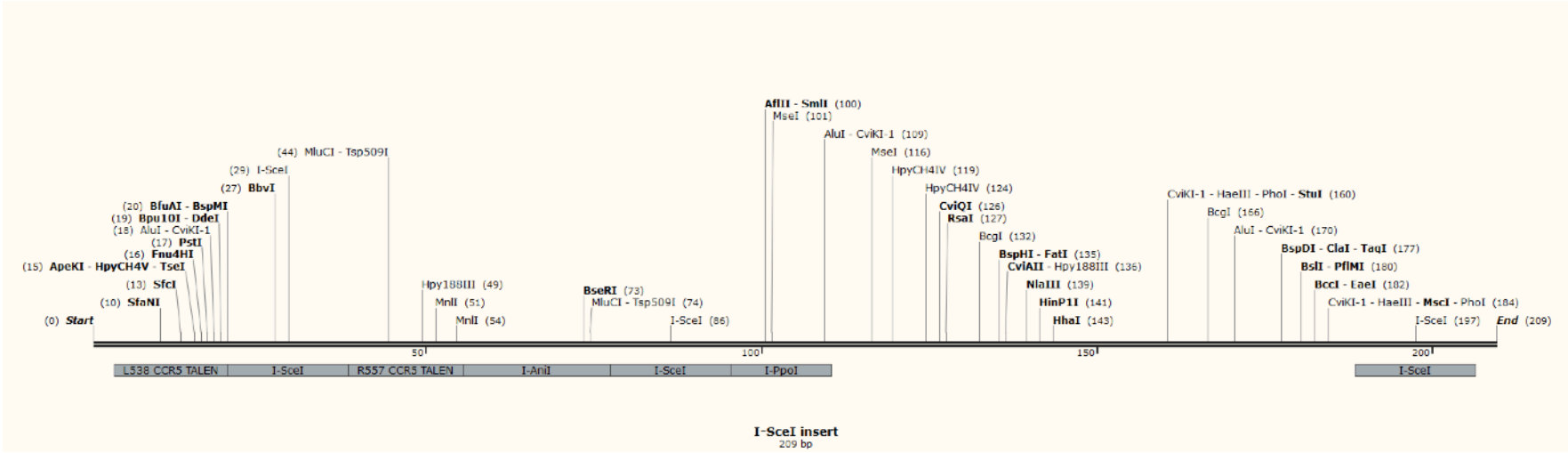

Figure 3.5. The I-SceI triple cut site array

Image showing the features of the I-SceI triple array site.

possibly recircularised plasmid was recovered. Zero ligated plasmid was present. These results suggested that two things could be occurring. First, the insert and vector may not have ligated successfully, thus leaving linearised plasmid which is unable to be propagated in *E. Coli*. Enough varied ligation conditions were tested to suggest that this may not have been the reason for a lack of recombinants. Second, ligation is occurring at some level of efficiency, however the plasmid is unstable in *E. Coli* and could be undergoing minor deletions and/or rearrangements. As certain sequences in *E. coli*, and direct repeat sequences such as those in pLAU44 and pLAU43 are unstable in many *E. coli* strains, I decided to use a strain of competent *E. coli* (MAX Efficiency™ Stbl2™ Competent Cells) that have been specifically designed for cloning unstable inserts. Stbl2 Competent Cells have the *Rec*A1 single point mutation in the ATPase domain of RecA, a protein that is essential for recombination and general DNA repair, and reduces plasmid recombination and increases plasmid stability. In addition, these cells have a unique genotype that allow for stable cloning of direct repeat sequences and tandem array genes. Transformation of the pLAU44-I-SceI ligation into Stbl2 competent cells yielded colonies from which recombinant DNA was isolated, showing successful ligation of vector and insert after diagnostic restriction digest. Plasmid pLAU44-IsceI-pCI Puro was finally generated by ligation of pLAU44-I-SceI and pCI Puro.

3.2.2 Characterisation of the U2OS-tetO-lacO Cell Line

The U2OS tetO-lacO stable cell line was generated by sequential transfection and stable selection of the pLAU44-I-SceI-pCI Puro and pLAU43 plasmids in. Stable cell lines were generated according to the protocol as described in (MATERIALS AND METHODS). After

transfection of pLAU44-I-SceI-pCI Puro and confirmation of stable insertion into the U2OS genome through antibiotic selection, the same process was conducted for the pLAU43 plasmid. Before transfection into U2OS cells, all plasmids were linearised with restriction enzymes that cut within non-essential regions. When generating a stable cell line the transfected plasmid undergoes recombination during chromosomal integration, and this recombination event could happen at any region within the plasmid. Controlled linearisation of plasmids before transfection would reduce the likelihood of this recombination event occurring within essential regions. Because the process of non-targeted stable integration of foreign DNA into cells is a random one, the constructs would be expected to be inserted into random loci on random chromosomes.

Stable insertion of pLAU44-IsceI-pCI Puro

Plasmid pLAU44-I-SceI-pCI Puro was transfected and selection of stable transfectants was performed according to the protocol (see materials and methods). A concentration of 2.5 µg/ml of Puromycin was used for selection, which was previously determined to be the optimal antibiotic concentration for this cell line (data not shown). Epi-fluorescence analysis of the selected clones was undertaken through transient transfection, in 96 well plates, of the tetracycline repressor protein fused to green fluorescent protein (TetR-GFP). Upon transfection of this plasmid, TetR-GFP is expressed and binds to the tet operator sequences that were stably inserted in U2OS cells. After identifying transfected clones in multi-well dishes that were positive for GFP foci but exhibited only one GFP focus per cell, cells were taken through a second round of clonal

selection by limiting dilution to ensure purity of the clones. Clones positive for only one GFP focus, henceforth referred to as U2OS-tetO, were selected for testing.

Inducible DSB in U2OS-tetO cells

Following the selection process described above, analyses were undertaken to see whether a site specific DSB could be induced in the cells. U2OS-tetO cells were transiently transfected with TetR-GFP and I-SceI-GR-RFP, treated with triamcinolone acetonide(TA) for 2 hours the following day and then fixed and stained by IF to visualise the DSB using an α-53BP1 antibody. Co-localisation of a 53BP1 focus with the TetR-GFP focus showed that a DSB could induced on the tetO array (**Fig. 3.6**).

Stable insertion of lacO

Stable transfection and selection of the pLAU43 plasmid was performed on the newly created U2OS-tetO cell line in the same way as the pLAU44-I-SceI-pCI Puro plasmid. However, after many unsuccessful attempts to sub-clone a eukaryotic selection marker into pLAU43, co-transfection of pLAU43 was instead performed with a separate plasmid containing the neomycin resistance gene that confers resisters to G418. As the selection marker was expressed from the co-transfected plasmid, the molar ratio of the plasmid carrying the 'gene of interest' to the plasmid carrying the selection marker was set at 10:1 to increase the likelihood that any cell containing the selection marker would also contain the 'gene of interest'. Epi-fluorescence analysis of the resultant monoclonal cells

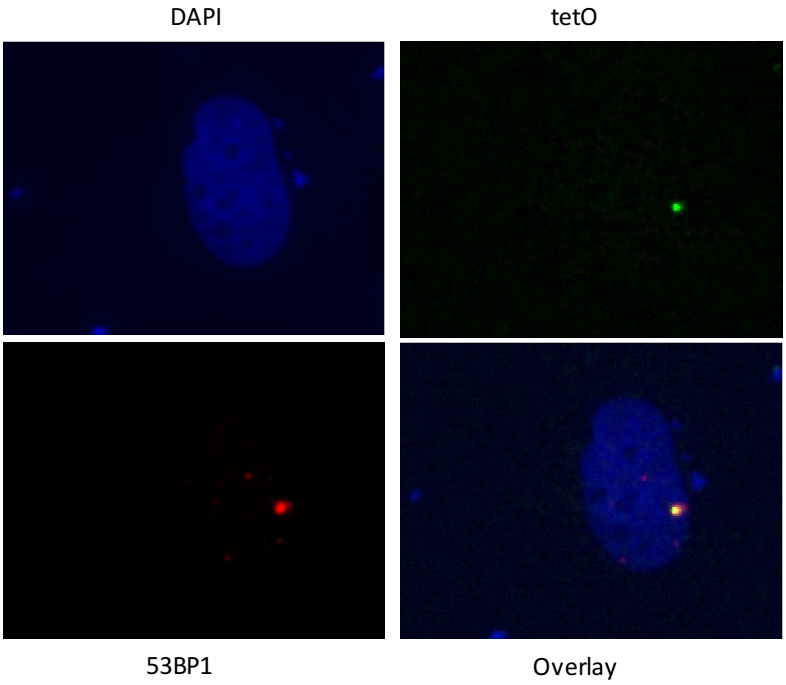

Figure. 3.6. I-SceI-GR-RFP can induce a DSB in U2OS-tetO cells

Immunofluorescence image showing co-localisation of immunostained 53BP1 (red) with the tetO array (green) in U2OS-tetO cells. TetR-GFP was transiently transfected to visualise the tetO array.

was undertaken through transient transfection, in 96 well plates, of the lac repressor protein fused to red fluorescent protein (LacI-RFP). Upon transfection of this plasmid, LacI-RFP is expressed as one protein and binds to the lac operator sequences now stably inserted in U2OS-tetO cells. This confirmed stable cell line is henceforth referred to as U2OS-tetO-lacO. (**Fig. 3.7**)**.**

pLAU44-IsceI-pCI Puro and pLAU43 are located on distinct chromosomes

Metaphase spread FISH was performed on the U2OS-tetO-lacO cell line to confirm that pLAU44-IsceI-pCI Puro and pLAU43 plasmids were integrated into separate parts of the genome (**Fig. 3.8**)

3.2.3 Attempts to Locate the Genomic Position of the Inserts

pLAU44-I-sceI-pCI Puro and pLAU43 plasmids were stably transfected and incorporated into the genome of U2OS cells through non-targeted, random integration after linearization of plasmids with NdeI. In an attempt to pinpoint the specific genomic loci that pLAU44-IsceI-pCI Puro and pLAU43 plasmids were integrated into the genome, two cloning based strategies were employed: inverse PCR and linker-mediated PCR. Because these methods work best with DNA templates whose sequence complexity is less than 1×10^9 bp, it is unlikely that PCR will work when total mammalian genomic DNA is used as a template. Therefore, both of these approaches involved the isolation of genomic DNA and digestion with a restriction enzyme that cuts many times in the plasmid and the genome. As the integrated plasmids were linearised with NdeI before stabl

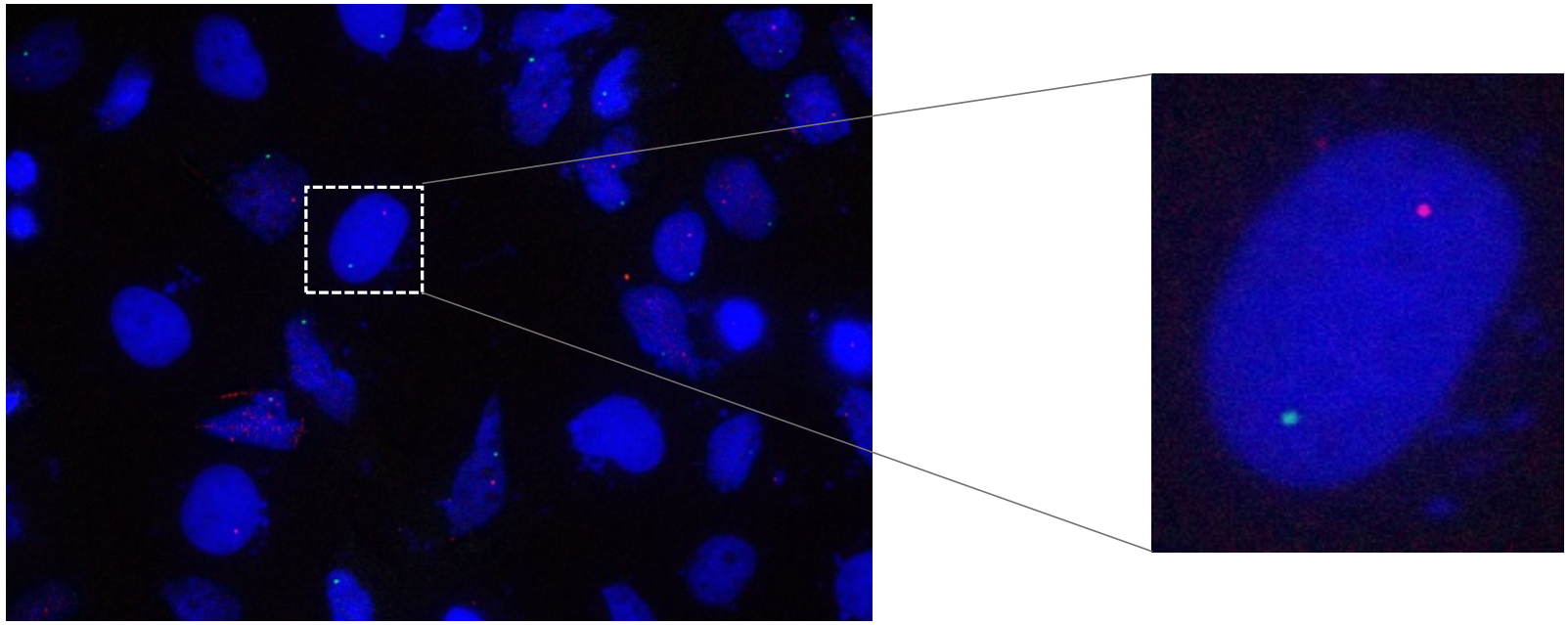

Figure. 3.7. Visualisation of U2OS-tetO-lacO cells

Left: Monoclonal population of U2OS tetO-lacO cells. tetO and lacO arrays are visualised by transient transfection, expression and binding of TetR-GFP (green) and LacI-RFP (red) to their respective binding arrays. Note, not every cell displays tetO and lacO arrays because not all cells were succesfully transfected. Right: Magnified image of an exemplary interphase nucleus showing the tetO (green) and lacO (red) arrays. Each array is integrated at a single genomic locus.

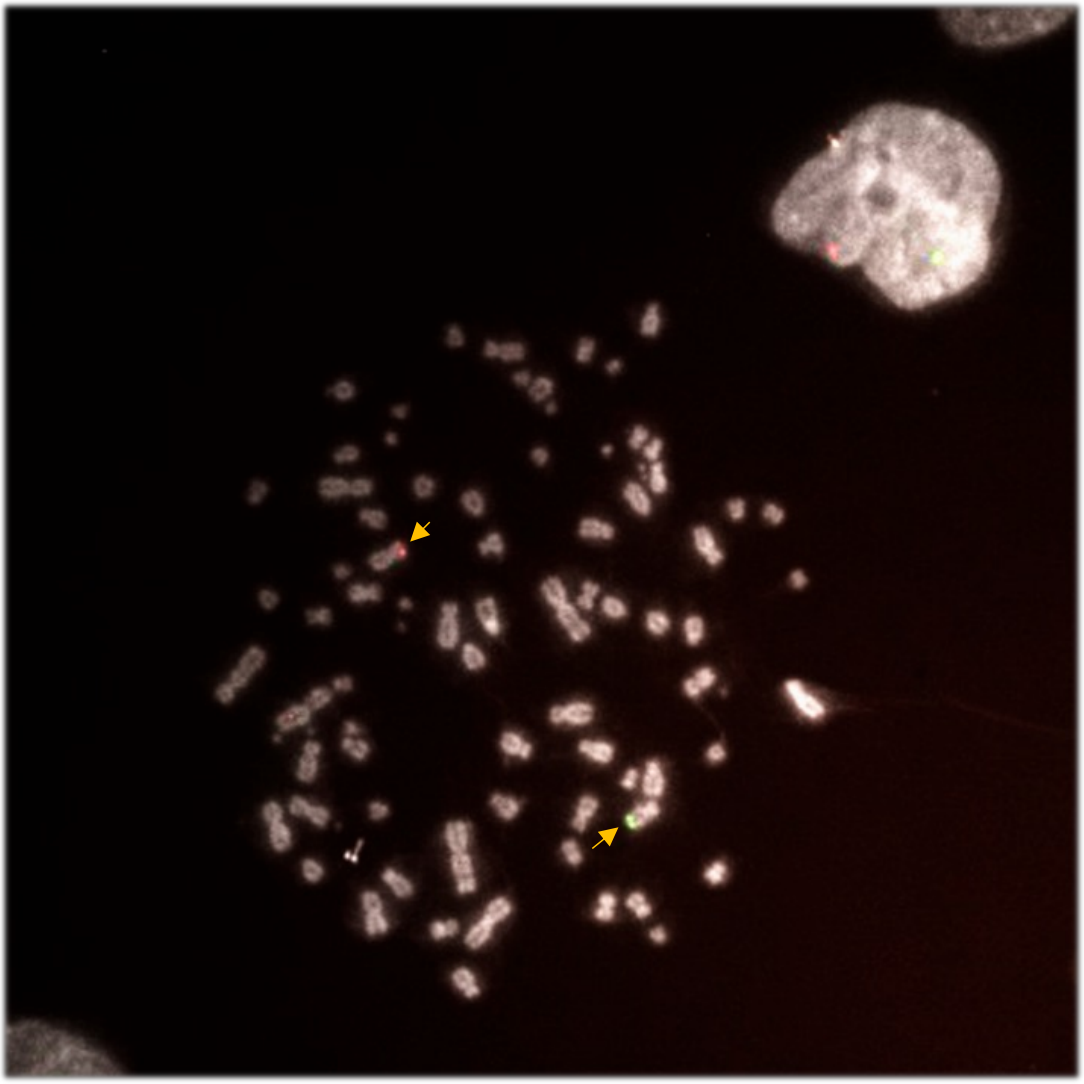

Figure. 3.8. tetO and lacO arrays are located on distinct arrays

2D metaphase spread FISH image of U2OS-tetO-lacO cells. tetO and lacO arrays are labelled with ATTO488 (green) and ATTO550 fluorescent (red) dNTPs respectively. Image is a 2D max projection of 7 optical slices in the Z-axis.

transfection, it was possible to approximate the junction where the known plasmid region would start (henceforth referred to as the plasmid start point) and 'unknown' genomic DNA would end. Making use of this knowledge, primers were designed to anneal between the plasmid start point and the first restriction cut site.

Linker-mediated PCR strategy

Using the linker-mediated PCR approach, isolated genomic DNA was digested using AluI, a restriction enzyme that has a 4 base recognition sequence and would, in theory, be expected to cut the genome every 256 bp. The fragmented genomic DNA was purified and ligated to a double stranded 'linker' (two single stranded oligos annealed together) consisting of 25 bp of random DNA sequence.

Because AluI generates blunt ends when it cuts DNA, the adaptor was designed to have 5'-phosphates attached to both termini to encourage ligation. Forward and reverse primers designed to anneal to the linker and to the 'known region' of the plasmid so amplification of the ligated genomic DNA would occur. (**Fig. 3.9A**)**.** With the aid of the NCBI BLAST function, linkers were designed with minimal homology to the human genome to avoid the possibility that primers designed to anneal to the linker could also anneal to other regions in the genome. However despite much optimisation, this approach was unsuccessful and failed to yield specific PCR product.

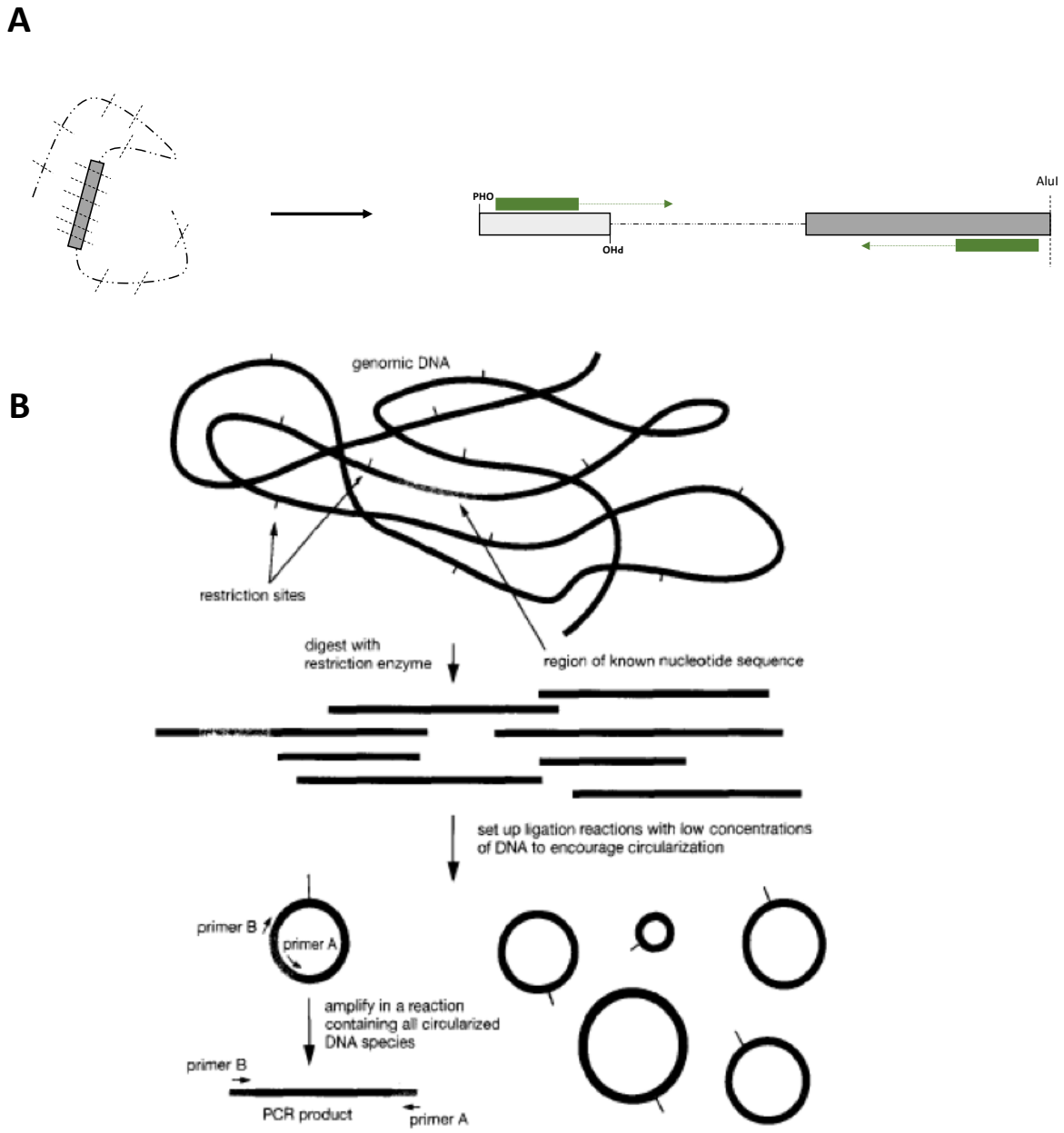

Figure. 3.9. Cloning based approaches to locating the genomic position of stably integrated inserts

(**A**) Schematic representation of linker-mediated PCR approach to determining the genomic location of tetO and lacO arrays. Genomic DNA is harvested and digested with AluI restriction enzyme (4 base cutter) that cuts many times in both the genome and 'known region' DNA. Double stranded linker is ligated to digested genomic DNA and PCR primers are designed to anneal to double stranded linker DNA and known region DNA. *Left:* dashed and dotted line represents genomic DNA. Grey box represents integrated known region DNA (tetO or lacO plasmid). Dashed lines represent digestion with AluI restriction enzyme. *Right:* light grey box represents double stranded linker DNA with 5' phoshate groups at the termini. Dashed and dotted line represents genomic DNA. Dark grey box represents integrated known region DNA. Green boxes represent specifically designed PCR primers. (**B**) Left: Schematic representation of inverse PCR approach. Adapted from Joseph Sambrook, David W. Russel -Molecular Cloning: A Laboratory Manual. Right*:* schematic of the known region DNA pLAU44i-pCI-Puro plasmid integrated into genomic DNA, digested with BamHI restiction enzyme.

Inverse PCR strategy

Standard PCR amplifies segments of DNA that lie between forward and revers inward-facing primers. In contrast, inverse PCR was used to amplify 'unknown' genomic DNA that flanks the ends of a known DNA sequence for which no primers are available. (**Fig. 3.9B**). Isolated genomic DNA was digested with BamHI, a restriction enzyme with a 6 base pair recognition sequence that cuts multiple times in pLAU44-I-sceI-pCI Puro. Individual restriction fragments of genomic DNA were converted into circles by intramolecular ligation and circularised DNA used as template in PCR. The 'unknown' genomic DNA was then amplified by two primers designed to anneal to the region of known DNA (integrated plasmid DNA) that pointed in opposite directions. Conditions that favour the formation of intramolecular circles over concatenates during ligation needed to be achieved by keeping the molar concentration of DNA ends low. These conditions needed optimising, as it would be difficult to calculate an appropriate concentration when the DNA molecules in the population differ in size and when the proportion of damaged termini is unknown. Therefore, a series of ligation reactions with a range of DNA concentrations was set up.

After much optimisation of the ligation step, conditions were achieved that generated PCR bands discernible on an agarose gel, indicating that circular DNA resulting from intramolecular ligation was achieved (**Fig. 3.10A**). In order to improve the specificity of the PCR, nested primers were employed in a second round of PCR, using the product of the first round as a template. This approach reduced the number of amplified product bands that were detectable by agarose gel electrophoresis, suggesting that the number of off-target amplified products was reduced. (**Fig. 3.10B**).

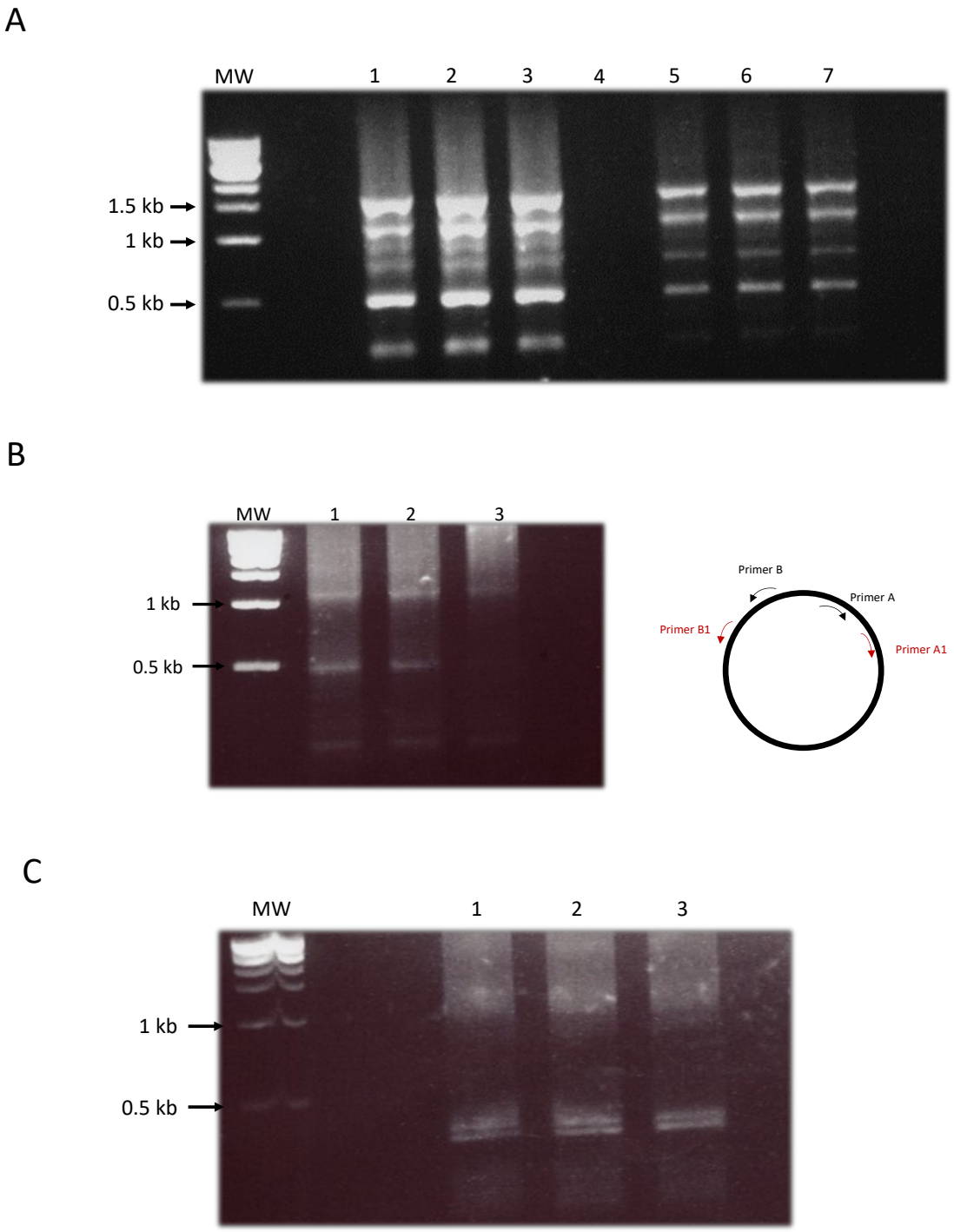

Figure 3.10. Attempts to obtain discrete gel electrophoresis bands for DNA sequencing

(**A**) Agarose gel electrophoresis image showing bands obtained from PCR of genomic DNA that had been digested and ligated. 5 µg of genomic DNA was digested and the resulting reaction products were ligated under conditions that favour formation of intramolecular circles. *Lanes 1-3:* bands from PCR conducted with annealing temperature of 58˚C. *Lanes 5-7:* bands from PCR conducted with annealing temperature of 63˚C. Genomic DNA was run on a 1 % gel (**B**) *Left:* Agarose gel electrophoresis image showing the results of a second round of PCR using nested primers. All three lanes are repeats and contain the same genomic DNA. *Right:* Schematic showing the position of nested primers on ligated circular DNA. Primer set A/B was used in the first round of PCR. Nested primer set A1/B1 were used in the second round of PCR. Genomic DNA was run on a 1 % gel (**C**) Agarose gel electrophoresis image showing bands obtained from the nested PCR in 'B', run instead on a 2 % gel.

The 500 bp product was selected for extraction and sequencing, because this band was the most discrete and had less surrounding background product. However sequencing failed to identify a specific amplification product, instead containing unreadable mixed sequences. In an attempt to improve the purity of this product I employed gel electrophoresis using a 2% agarose gel, and increased the running time to 90 minutes, resultin in fractionation of the 500 bp band into two separate products (**Fig. 3.10C**)**.** However, sequencing again failed to identify the insert, revealing the presence only of plasmid.

3.2.4 Testing the TetR:FLAG:LacI fusion protein

Western blot analysis

To confirm expression of the fusion protein I employed SDS-PAGE and western blot analysis. The TetR:FLAG:LacI plasmid construct was transfected into U2OS cells and whole cell lysate was analysed by western blotting as described in materials and methods. α-LacI antibody identified bands of the expected molecular weight for TetR:FLAG:LacI (**Fig. 3.11C**). Anti-TetR protein however failed to identify this band (**Fig. 3.11A**).

IF microscopy analysis

The TetR:FLAG:LacI fusion protein was constructed from the parent plasmid, pCDNA6-TetR by ligation of a FLAG linker peptide followed by ligation of the Lac repressor gene (LacI). Immunofluorescence experiments were conducted to test whether the components of the TetR:FLAG:LacI fusion protein were able to bind the tetO and lacO operator sequences respectively. Upon transient transfection of U2OS-tetO-lacO cells

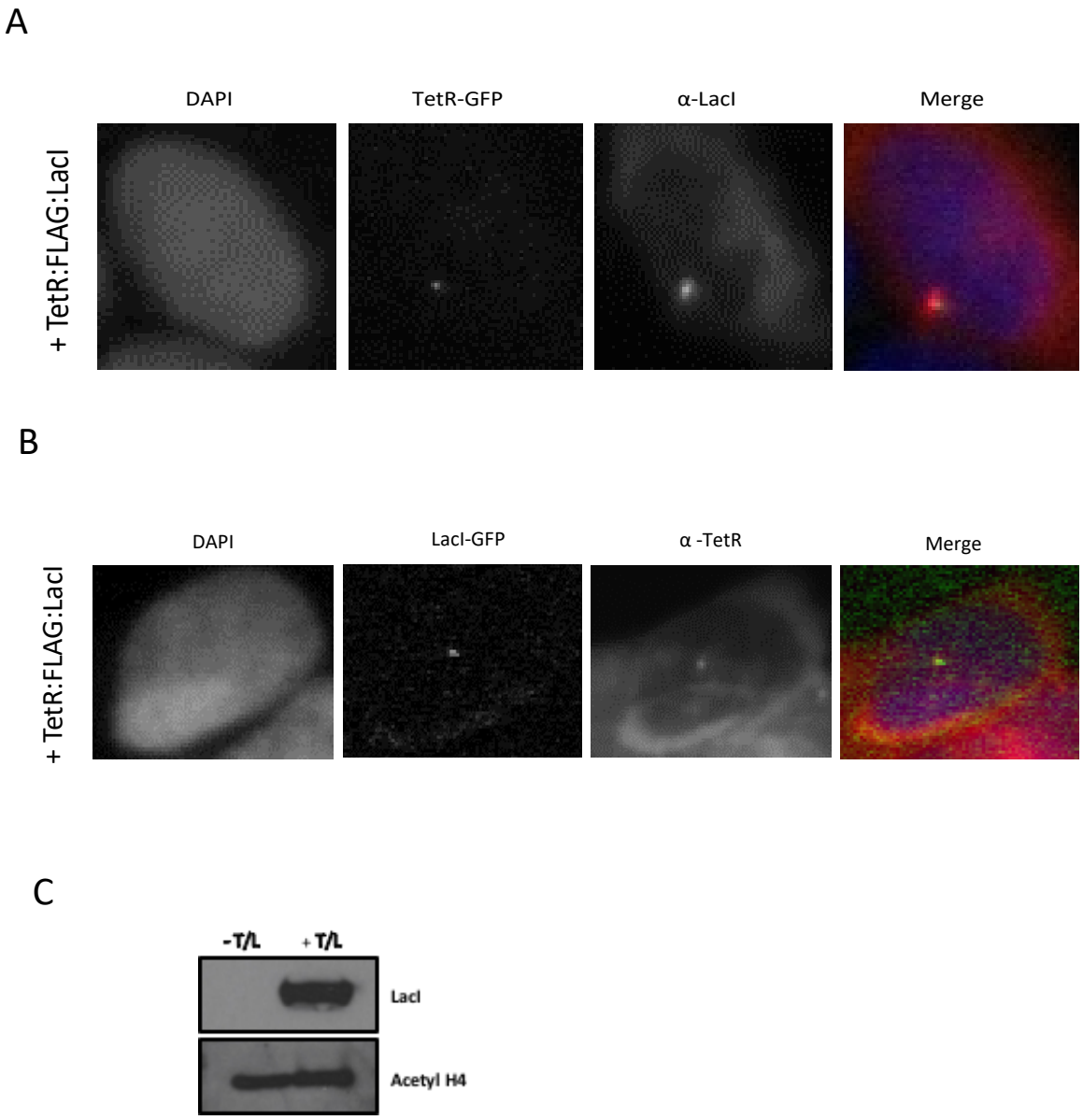

Figure. 3.11. TetR:FLAG:LacI fusion protein is expressed and binds correctly

(**A**) U2OS-tetO-lacO cells were transiently transefected with the TetR:FLAG:LacI fusion protein. The tetO array was visualised by transient transfection of TetR-GFP. Cells were immunostained with an antibody against LacI. (**B**) U2OS-tetO-lacO cells were transiently transfected with the TetR:FLAG:LacI fusion protein. The lacO array was visualised via transient transfection of LacI-GFP. Cells were immunostained with an antibody against TetR. (**C**) Whole cell lysates from naive U2OS cells after expression of the TetR:FLAG:LacI fusion protein were analysed by immunoblotting with an antibody to LacI.

with either TetR-GFP (to detect the tetO array) or lacI-GFP (to detect the lacO array), cells were immunostained with α-LacI antibody or with an α-TetR antibody respectively to detect the TetR:FLAG:LacI fusion protein. Both experiments confirmed co-localisation of the GFP-tagged teto and lacO operator sequences with the TetR:FLAG:LacI fusion protein, indicating that both the TetR and LacI components of the fusion protein were active (**Fig. 3.11A**). Anti-TetR antibody was able to bind TetR by immunofluorescence despite its previous inability to identify bands a TetR by western blot. It is possible that the denaturing conditions of SDS-PAGE destroyed the epitope the α-TetR antibody binds to. In any case these initial results suggested that the TetR:FLAG:LacI fusion protein was expressed in cells, TetR and LacI segments are able to fold independently and correctly, and are able to bind properly to their respective operator sequences.

Further testing of the fusion protein was conducted, this time on the U2OS-tetO-lacO cell line to confirm the two distinct arrays could be tethered upon transient transfection of TetR-GFP, LacI-RFP and the fusion protein together. Each time all three plasmids were transfected, U2OS-tetO-lacO cells would display numerous aggregates throughout the nucleus (henceforth referred to as 'clumping'). Where usually U2OS-tetO-lacO cells would display one green spot and one red spot upon transfection of TetR-GFP and LacI-RFP respectively, following transfection of TetR-GFP, LacI-RFP and TetR:FLAG:LacI together, multiple green and red aggregrates were observed (**Fig. 3.12**). Clumping occurred in the nucleus of cells strictly after simultaneous transfection of TetR-GFP, LacI-RFP and TetR:FLAG:LacI, but not after transfection of any combination of two out of the three plasmids. This phenomenon made it difficult to visualise and analyse

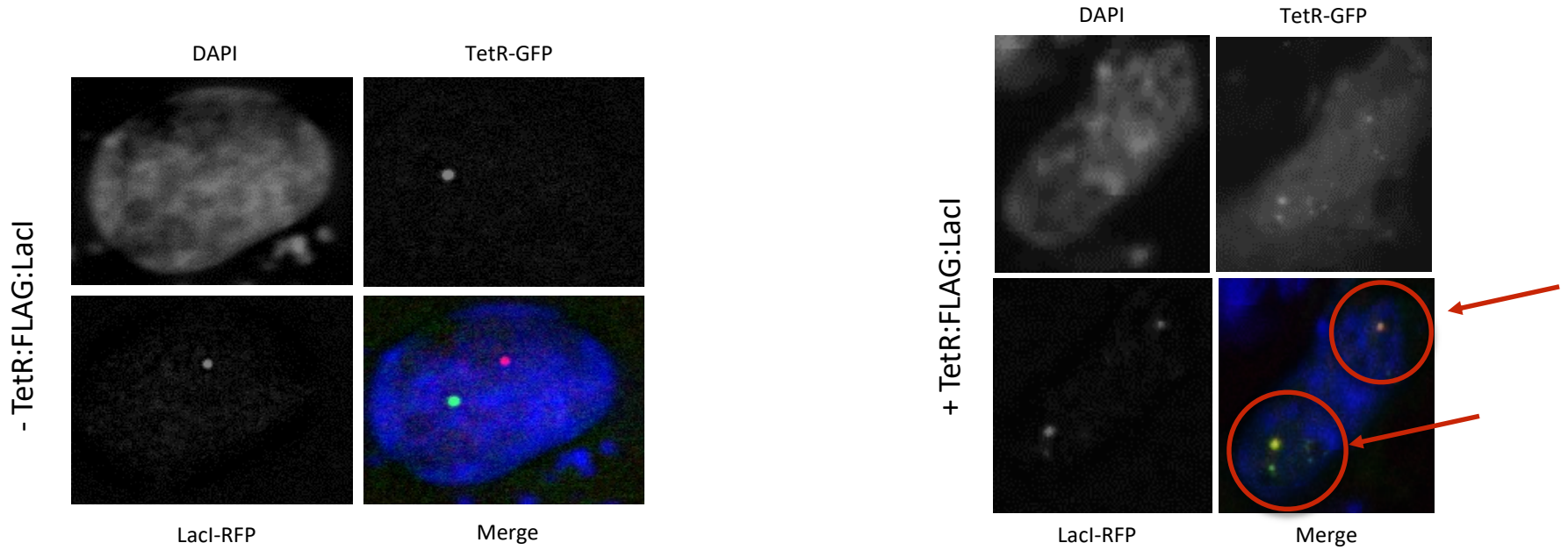

Figure. 3.12. Transfection of TetR-GFP, LacI-RFP and TetR:FLAG:LacI causes 'clumping'

Left: Fluoresence image showing tetO array (TetR-GFP)) and lacO array (LacI-RFP) in U2OS-tetO-lacO cells in the absence of the TetR:FLAG:LacI fusion protein. *Right:* Fluoresence image showing tetO array (green) and lacO array (red) in U2OS-tetO-lacO cells transfected with the TetR:FLAG:LacI fusion protein. Transfection of all three constructs causes aggregate-like structures in the nucleus

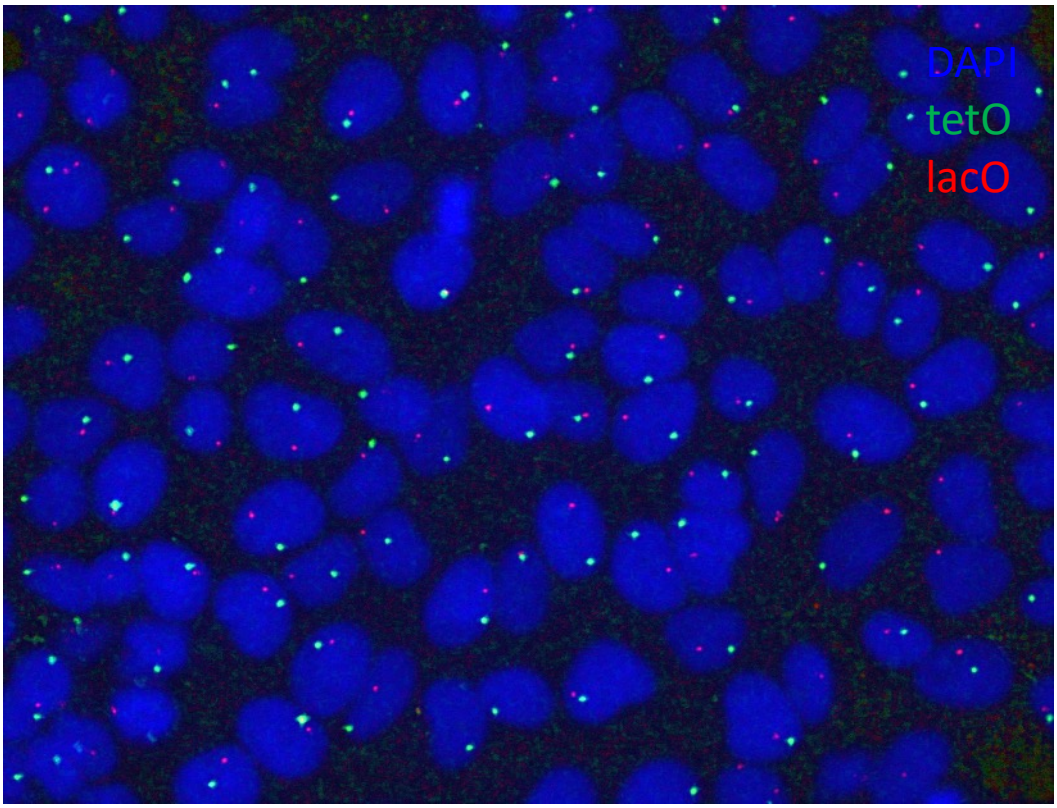

Figure 3.13. Two-dimensional FISH image of U2OS-tetO-lacO cells

U2OS-tetO-lacO cells showing tetO (green) and lacO (red) arrays visualised by 2D-FISH. tetO and lacO FISH probes incorporated with fluorescently labelled dNTPs were hybridised to their complementary sequences in the nucleus of U2OS-tetO-lacO cells. Note, every nucleus displays a tetO and lacO array at a single locus.

the effect of the fusion protein. In order to circumvent this issue, two-dimensional fluorescence in situ hybridisation (2d-FISH) was performed.

2D-FISH analysis

Two colour 2D-FISH was performed as described in materials and methods. Probes comprised of tetO (ATTO488) and lacO **(**ATTO 550) arrays containing fluorescent nucleosides were generated by direct labelling of pLAU44-I-SceI-pCI puro and pLAU43 plasmid DNA using a nick translation kit (**Fig. 3.13**) to reduce non- specific hybridisation by the probes, the labelled pLAU44-I-SceI-pCI puro and pLAU43 plasmids were digested with restriction enzymes to remove the ampicillin gene and other unwanted sequences.

No clumping was observed in nuclei transfected with the TetR:FLAG:LacI fusion protein after visualising probes by FISH (**Fig. 3.14**)**,** enabling clear observation of any interaction between the tetO and lacO arrays.

In addition, an additional advantage of using FISH was that it reduced the number of plasmid constructs needed to test the functionality of the TetR:FLAG:LacI fusion protein from three (TeRt-GFP, LacI-GFP, TetR:FLAG:LacI) to one (TetR:FLAG:LacI only). This increased the number of nuclei that could be scored by reducing cell death, and increasing the chance of the fusion protein of being taken up by cells.

Quantification of distances between the tetO and lacO arrays

Transfection of the TetR:FLAG:LacI fusion protein in nuclei in which the arrays were now visualised by FISH never showed a co-localisation of tetO foci with lacO foci. However, a subset of nuclei did consistently show a pairing of foci (**Fig 3.14**)**.** Transfected wells had a greater number of nuclei exhibiting paired foci than in untransfected wells (**Fig. 3.15A**). To determine the number of nuclei that exhibited paired foci upon transfection of the fusion protein, and then to quantify this, I attempted to compute the distances in microns between tetO and lacO foci in the absence and presence of the fusion protein.

ScanR acquisition software was used to acquire images on the Olympus ScanR microscope and ScanR analysis software was used for image processing, object detection, and gating (see methods). The data analysis software is based on an interactive cytometry-oriented approach for handling large numbers of multidimensional data sets. The image data generated are displayed in two-dimensional scatter plots or one-dimensional histograms.

After acquiring images of a cell population, nuclei were detected and segmented using the Object detection module. tetO and lacO foci were defined as distinct sub-objects and detected using the Spot Detector module. This allowed for several different parameters to be set and adapted to the objects and sub-objects of interest. Images and objects were linked reciprocally to any data point related to them and so, by clicking on a data point, the respective image was shown on the display window and the respective object highlighted. Conversely, by clicking on an object in the image display window, the related data points in the scatter plots and histograms were highlighted. Using these

options, clustered data populations of interest could be gated via graphical tools. For example, discrimination between nuclei that looked normal (suitable nuclei) and nuclei

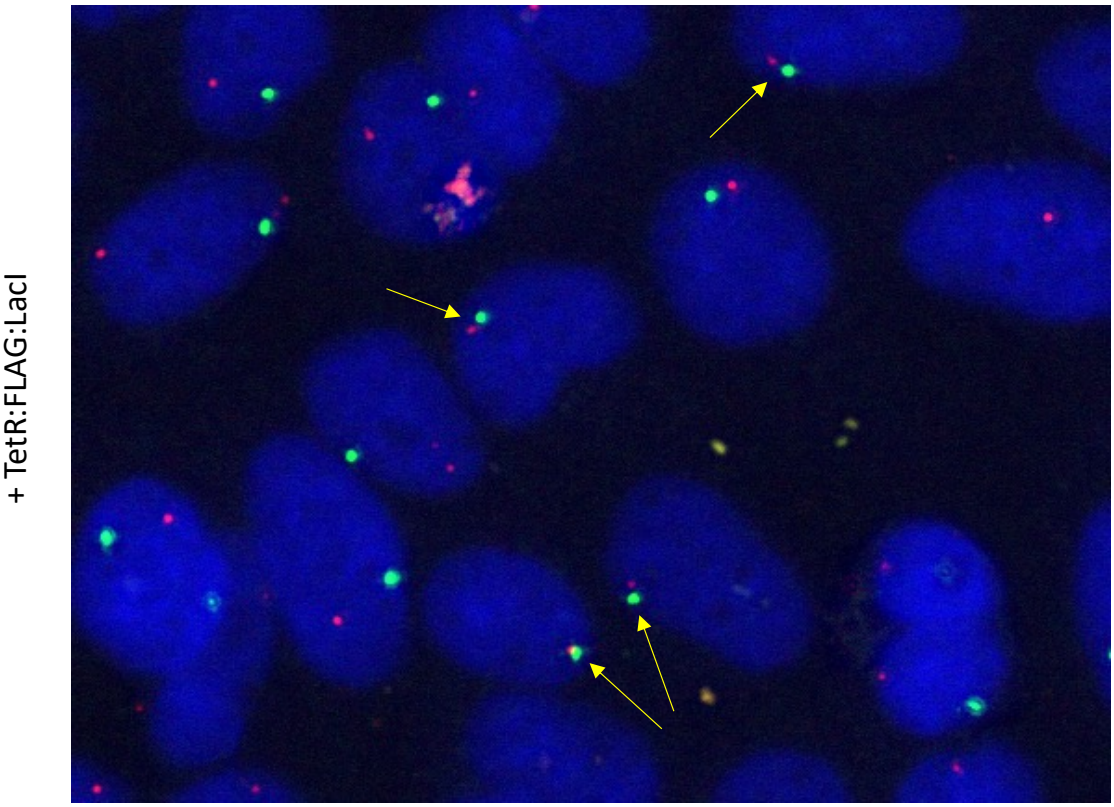

Figure 3.14. Transfection of the TetR:FLAG:LacI fusion protein gives rise to paired tetO and lacO arrays

2D-FISH image of U2OS-tetO-lacO cells displaying tetO (green) and lacO (red) arrays in close proximity upon transfection of the TetR:FLAG:LacI fusion protein

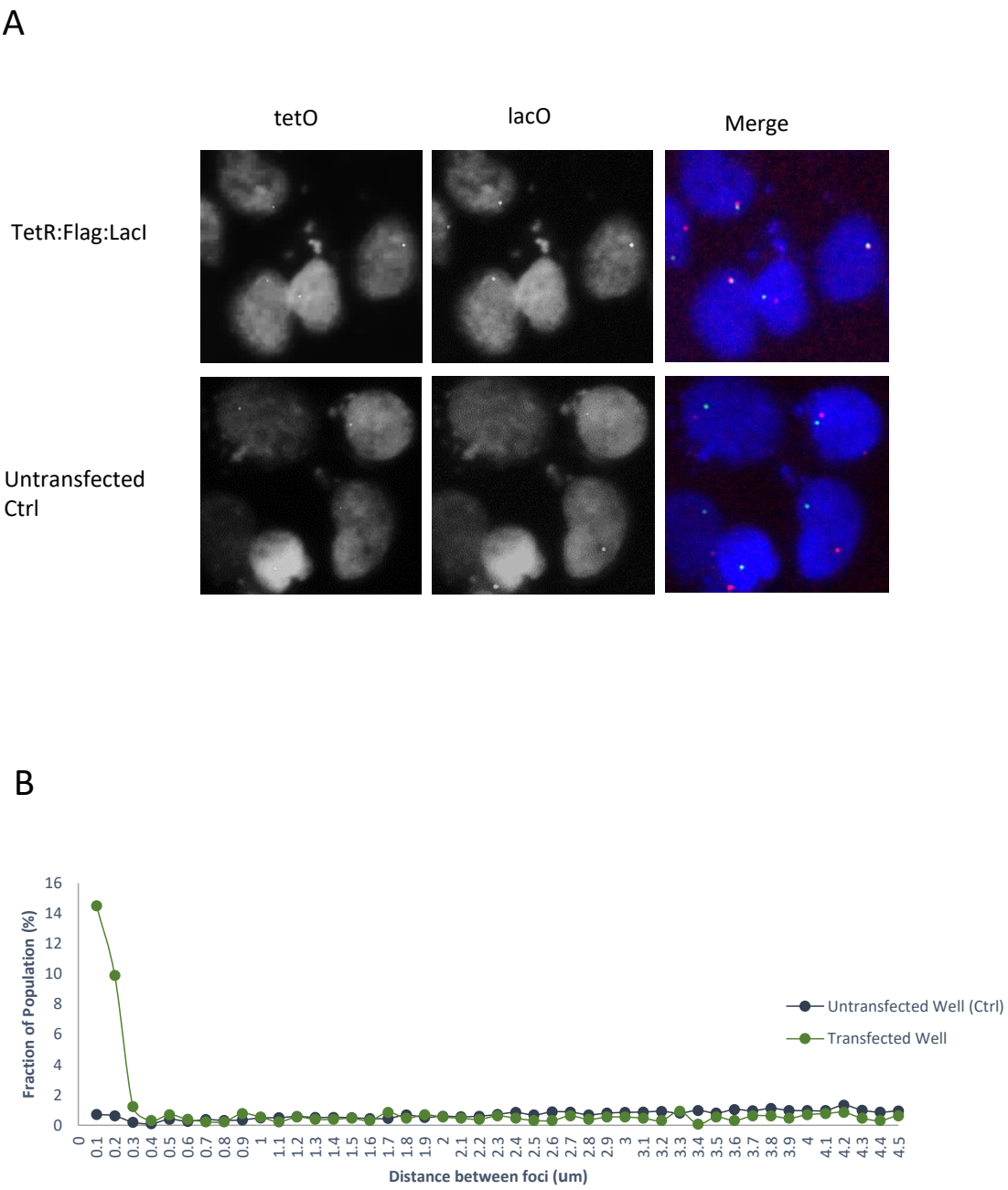

Figure 3.15. Inducible association of two independent DNA segments

(**A**) Expression of TetR:FLAG:LacI results in preferential association of the tetO and lacO arrays, U2OS-tetO-lacO cells were analyzed by two-colour FISH. (**B**) Quantification of the results obtained in (B). Minimum distances were calculated between tetO and lacO inserts in U2OS-tetO-lacO cells.

that overlapped to give the illusion of one large nucleus (unsuitable nuclei), was made based on their length and 'round-ness'. These parameters were selected from those available, as Elongation factor and Circularity factor. Those nuclei that were determined to be suitable were then selected and gated. Only nuclei that contained two foci per cell, one green (tetO) and one red (lacO), were gated. All of the parameters and gates applied to the imaged cells, including the X, Y coordinates of every single focus in a population, were exported and analysed in Microsoft Excel.

In Excel, the nuclei were sorted and filtered according to the gates they were initially selected for previously on scanR analysis. The aim was to use an intuitive method to see whether I could observe a greater reduction in distance between green and red foci in nuclei transfected with the fusion protein than between green and red foci in untransfected cells. The first step was to calculate the minimum distance observed between one green focus and all the red foci in the population. This was done for every green focus in the population. The minimum distances returned from the calculation were expected to represent the distance between a green and red focus in one nucleus. Pythagoras' Theorem was used to calculate distances between foci:

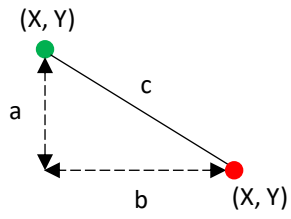

$c = (a^2 + b^2) \wedge 0.5$

Where **c** = distance in µ, **a** = X coordinate, **b** = Y coordinate. In Excel this was computed as $=MIN(((Xgreen - range\ Xred)^2+(Ygreen - range\ Yred)^2)^{0.5})$

Next, the minimum distances previously calculated were reviewed and a scale rising from 0.1 – 20 µm was put together to cover all of the distances returned. Following this, the number of minimum distances (representative of the distance between a green and red focus in one nucleus) that fell below each 0.1 µm 'bin' on the scale was calculated. The question asked was, for example, 'how many nuclei had a green and red focus that were less than 0.1 µm apart, or less than 5 µm apart?' The '=COUNTIF' function used to count spreadsheet cells based on single or multiple criteria was utilised and percentage of nuclei that fell below each 0.1 µm 'bin' was then calculated. The resulting data showed an approximately 20-fold increase in the number of nuclei that had green and red foci within a distance of 0 to 0.1 µm in cells transfected with the fusion protein compared to untransfected cells (**Fig. 3.15A**). Taken together these results indicated that the TetR:FLAG:LacI fusion protein was able to tether two stably integrated chromatin regions; tetO and lacO array, in a subset of cells.

3.2.5 Chromatin Immunoprecipitation Analysis of γH2AX Around a DSB

After testing the TetR:FLAG:LacI fusion protein and confirming it was able to successfully tether tetO and lacO arrays, ChIP was used to analyse the 3D spatial spread of γH2AX around a DSB. ChIP is a multistep process, and the pre-optimised protocol employed in this thesis involves the treatment of intact cells with formaldehyde to covalently link protein to DNA. (**Fig. 3.16A).** The cross-linked nucleoprotein complexes are then sheared mechanistically by sonication and the resulting cross-linked DNA-protein complexes are enriched by immunoprecipitation with a primary antibody, bound to a secondary antibody that is captured by protein G magnetic beads. Cross-links are reversed

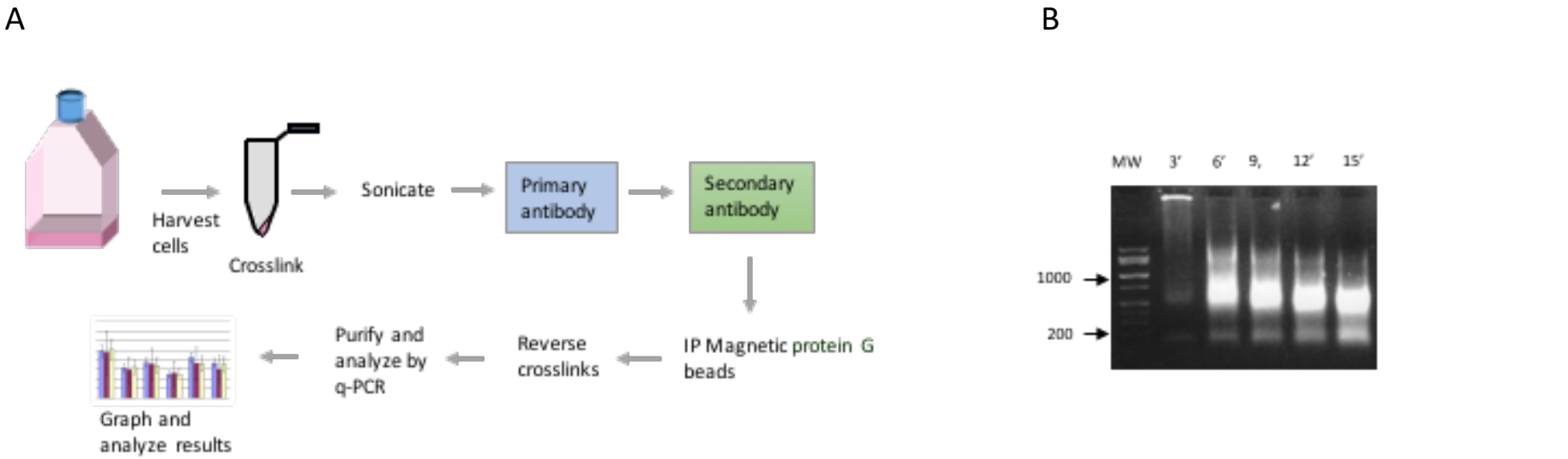

Figure. 3.16. ChIP procedure

(**A**) Cells are treated as necessary and harvested. DNA-binding proteins are cross-linked to DNA with formaldehyde in vivo. Cells are lysed to isolate the chromatin and sonicated to shear DNA along with bound proteins into small fragments. γH2AX histones are immunoprecipitated with a γH2AX-specific primary antibody which is bound by a secondary antibody that is in turn bound by protein G magnetic beads. Cross-linking is reversed to release the DNA and digest the proteins. Retrieved DNA is amplified and analysed by qPCR. (**B**) Cells were lysed and chromatin samples sheared for 3, 6, 9, 12 and 15 cycles of 30 sec ON/30 sec OFF with the Bioruptor Pico using using 1.5 ml Bioruptor microtubes (Cat. No. C30010016). Prior to de-crosslinking, samples were treated with RnaseA at 37°C for 1 hour. The fragmented chromatin is then de-crosslinked, purified and analyzed on a 2% agarose gel (MW corresponds to the 1Kb DNA molecular weight marker).

liberate the DNA, which is then analysed by real time PCR amplification with specific primers to detect and quantify specific genomic regions.

3.2.6 Chromatin fragment size optimisation

Efficient cell lysis and chromatin fragmentation is important for a successful ChIP experiment. Sonication was the preferred method of chromatin fragmentation as the ChIP assay was performed on cross-linked DNA and proteins. Sonication of chromatin is a key step in the protocol as it renders the chromatin soluble and dictates the resolution of the assay. The extent to which the location of a specific protein can be mapped in the genome ultimately depends on the degree to which DNA is fragmented, with the ideal DNA fragment size after sonication between 200 – 600 bp. Sonication conditions were optimised for U2OS cells (**Fig. 3.16B**). In brief, sonication was performed in a water bath sonicator at 4 °C to preserve chromatin from heat degradation. All samples were placed in the water bath and then removed at the allocated times. The majority of the DNA smear observed at 15 minutes was between the required DNA band size, and so moving forward, all chromatin was sonicated for 15 minutes.

3.2.7 Validation of qPCR primers

Specific qPCR primers were designed to anneal and amplify regions in the tetO (in *cis*) and lacO array (in *trans*). Because the sequence of the tetO and lacO insertions at their respective genomic sites is unknown, certain areas of the genome purify better than others, and sonication does not always create breaks at random, I generated sets of

primers to different regions within the tetO and lacO plasmids. All primer sets were run through BLAST to test for specificity. qPCR was performed on genomic DNA harvested from naïve U2OS using all primer sets, producing standard curves to test primer efficiencies. Two primer sets, one each to amplify regions in tetO and lacO insertions, displaying high specificity and efficiency were eventually picked.

3.3 ChIP Analysis

In order to first directly analyse γH2AX spread in *cis* to a DSB, exponentially growing asynchronous U2OS-tetO-lacO cells were transfected with I-SceI-GR-RFP and left for 24 hours. Cells were then treated with TA (10^{-7} M) for 2 hours to induce a single DSB at the tetO insertion site and ChIP was carried out followed by qPCR analysis of the recovered DNA. Repeated ChIP-qPCR experiments displayed minimal enrichment of γH2AX in the γH2AX IP sample compared to the beads only (no antibody) control sample and compared to a negative control genomic locus (**Fig. 3.17**). This indicated that after induction of a DSB in U2OS-tetO-lacO cells γH2AX levels at the tetO insertion site were barely above background levels, suggesting that I-SceI-GR-RFP was not efficiently cutting at its DNA recognition sequence. I concluded that this may have been a result of low transfection efficiency of I-SceI-GR-RFP. To circumnavigate this problem I generated U2OS-tetO-lacO cells stably expressing the I-SceI-GR-RFP endonuclease (**Fig. 3.18A**).

After induction of DSBs with TA in the newly created U2OS-tetO-lacO-I-SceI cell line, greater than 70% of cells showed translocation of I-SceI-GR-RFP from the cytoplasm

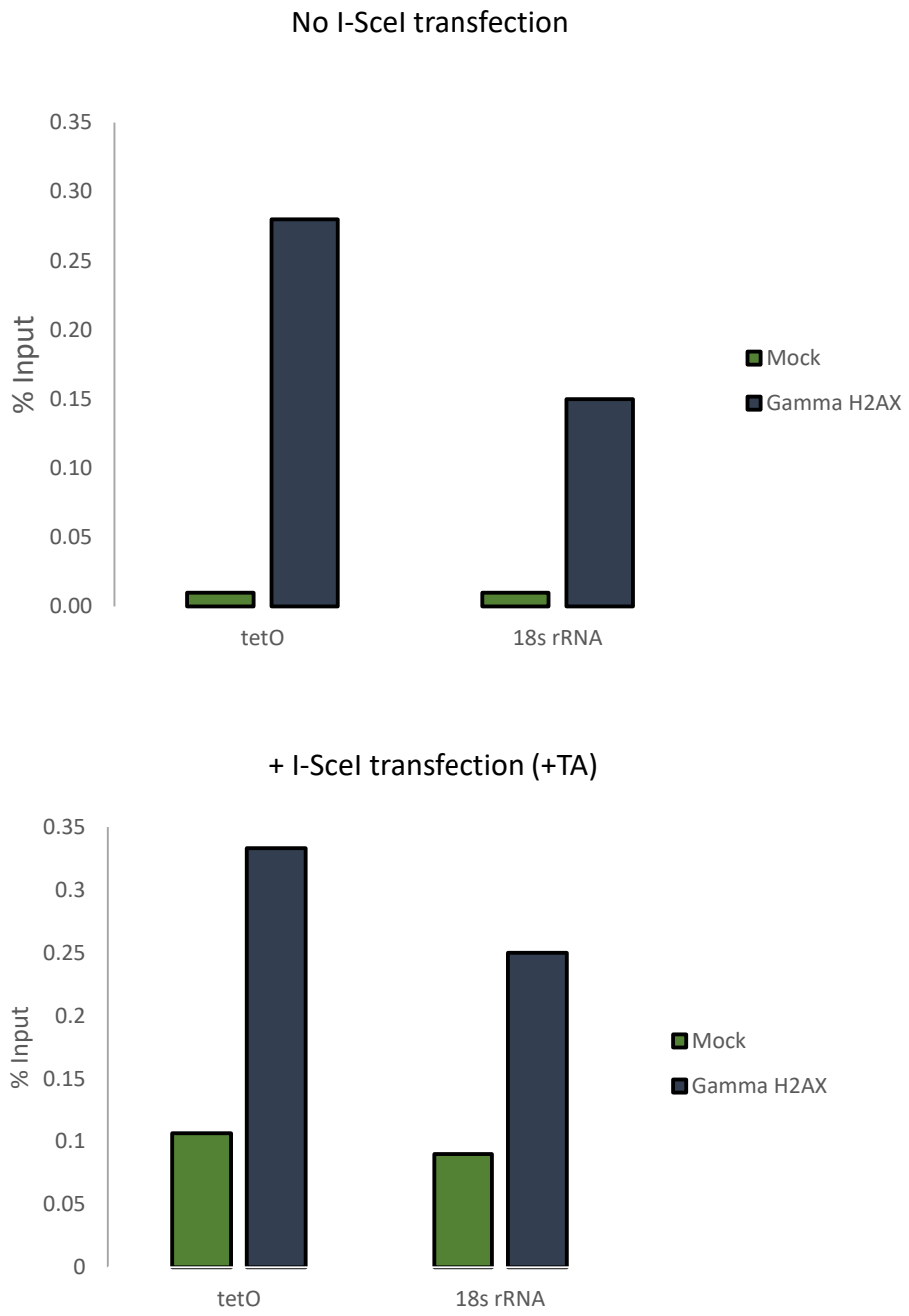

Figure 3.17. No significant increase in γH2AX signal at an I-SceI-induced DSB

U2OS-tetO-lacO cells were transfected with or without I-SceI-GR-RFP. No meaningful enrichment of γH2AX at tetO insertion sites was observed in the presence of a DSB. No meaningful difference in γH2AX signal was observed at tetO insertion sites compared to the control 18s rRNA locus.

A

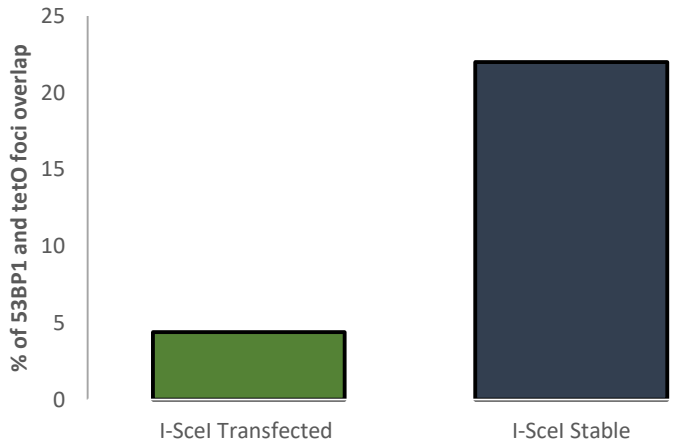

B

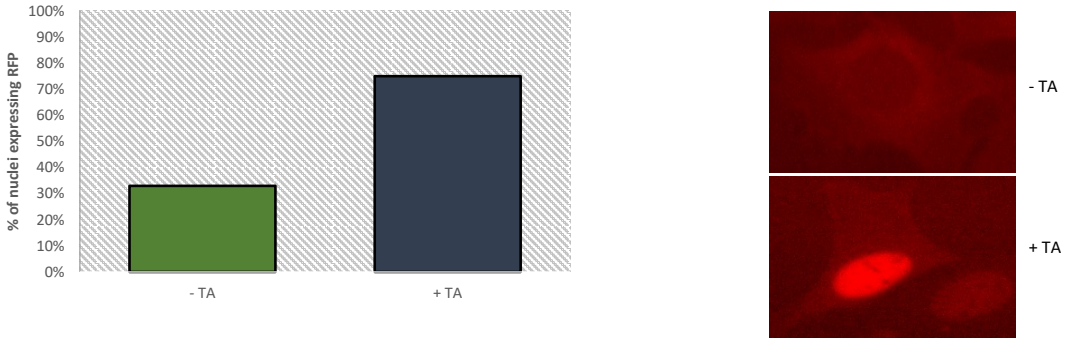

Figure 3.18. U2OS-tetO-lacO-I-SceI cells generate single DSBs upon the addition of TA

(**A**) U2OS-tetO-lacO-I-SceI cells are able to generated greater numbers of single DSBs in a population of cells than U2OS-tetO-lacO cells transfected with the I-SceI endonuclease. Inudction of a DSB is measured by appearance of immunostained 53BP1 at the tetO insertion site. (**B**) Incubation with the synthetic ligand triamcinolone acetonide causes nuclear translocation of I-SceI-GR-RFP from the cytoplasm to the nucleus in U2OS-tetO-lacO-I-SceI cells

to the nucleus compared to approximately 30% of cells in the absence of TA (**Fig. 3.18B**), as observed by numbers of cells expressing RFP in the nucleus. The presence of I-SceI-GR-RFP in the nucleus in 30% of cells even in the absence of TA was likely due to leaky expression of I-SceI, as observed by other groups (Grove *et al.*, 2008; Kwon *et al.*, 2012; Mund *et al.*, 2012). I optimised and used an immunoFISH protocol to determine the efficiency of cutting in U2OS-tetO-lacO-I-SceI cells before attempting to re-analyse γH2AX levels by ChIP. ImmunoFISH, a technique that combines immunofluorescence with a standard FISH technique, enabled simultaneous detection of endogenous 53BP1 at DSBs, and the tetO and lacO inserts. As the tetO and lacO inserts were visualised by fluorescent probes instead of by transfection of TetR-GFP and LacI-RFP (**Fig. 3.7**), any low transfection efficiency issues were negated. A maximum number of tetO sites could thus be scored for appearance of 53BP1 at the array. U2OS-tetO-lacO-I-SceI cells showed a greater cutting efficiency than U2OS-tetO-lacO cells transfected with I-SceI-GR-RFP (**Fig. 3.18A**).

Using ImmunoFISH also offered an extra level of control in the system as it presented the opportunity to select specifically only for cells that had been transfected with the TetR:FLAG:LacI fusion protein. Upon transfection of TetR:FLAG:LacI, the LacI antibody was used to stain for presence of the fusion protein, and the tetO and lacO inserts were visualised by fluorescent probes (**Fig. 3.19**). Surprisingly, in those cells that were transfected with the fusion protein, there was no visible association of tetO and lacO insertions. Moreover, analysis of distances between tetO and lacO insertions showed no difference in association of tetO and lacO between cells transfected with the fusion protein and cells without the fusion protein. ImmunoFISH revealed that the fusion

protein was seemingly now no longer able to make its way effectively into the nucleus (**Fig. 3.19**). Due to time constraints and the time already invested in attempting to set up the system, the decision was made to change the direction of my PhD project.

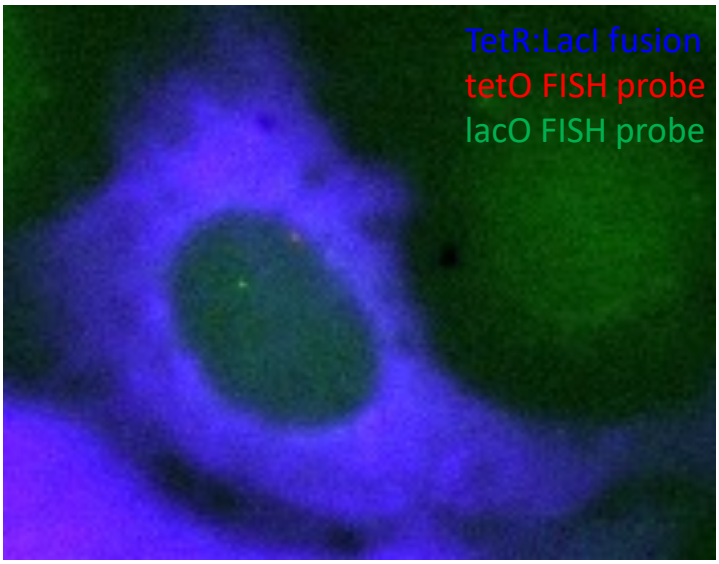

Figure. 3.19. TetR:FLAG:LacI is unable to induce tetO and lacO arrays to associate

ImmunoFISH image showing tetO array (red, lacO array (green) and antibody staining against LacI (blue) in a U2OS-tetO-lacO-I-SceI cell transfected with the TetR:FLAG:LacI fusion protein. tetO and lacO insertion sites are not induced to associate.

3.4 DISCUSSION

3.4.1 Key aspects of the construction system

Creating a cell based system to analyse γH2AX distribution and dynamics around a DSB was problematic in many ways. One of the more time consuming aspects of developing such a system was manipulation of the tet operator and lac operator-containing plasmids. pLAU44 (containing tetO arrays) and pLAU43 (containing lacO arrays) were both at least 11.5 kb in size and contained DNA de-stabilising repeat sequences. The arrays in each plasmid were organised in such a way that there were sections of random DNA sequences between each and every tetO or lacO operator sequence. The expectation is that this interspersed heterology would have a substantial effect in reducing recombination- and replication-based instability when cloning the plasmids into *E.* coli, as RecA pairing requires at least 25 nucleotides of homology (Hsieh, Camerini-Otero and Camerini-Otero, 1990). In spite of this consideration, both pLAU44 and PLAU43 proved difficult to propagate in *E. coli*.

Plasmid instability can be affected by a number of different factors, including the metabolic burden of plasmid maintenance, plasmid copy number, high positive selection pressure for a particular part of the plasmid (e.g. antibiotic resistance gene), genotype of the host strain and the recombinogenic potential of the plasmid sequences (Corchero and Villaverde, 1998). Plasmid instability can occur in the form of both structural and maintenance instability. Generally, the larger the plasmid and the more assorted the origin of its sequences are, the greater the likelihood that the plasmid will contain sequences that will be selected against by the host bacterial strain. To combat the issue of plasmid stability in the cloning involved in the generation of my system,

Stbl2™ competent cells containing the *Rec*A1 mutation, were used to great effect. Stbl2™ competent cells were cultivated at a reduced temperature of 30 °C. A low cultivation temperature has been reported to be beneficial for a higher stability, supposedly because of the reduced rate of bacterial growth (Liao, 1991). Additionally, the instability of plasmids was minimised by selecting smaller sized colonies from LB agar plates. Whilst pLAU44 was able to be cloned successfully using Stbl2™ competent cells, pLAU43 still proved refractory to transformation even into Stbl2™ competent cells.

Stable integration of the array plasmids was made into U2OS cells by transfection and selection of stable clones. This method of integration is random and therefore loci at which the plasmids have been integrated into was unknown. Determining the genomic insertion sites for tetO and lacO binding arrays would allow confirmation of the spread of γH2AX beyond the tetO insertion and into native chromatin surrounding the insertion site. Additionally, it would enable comparisons with the literature to be made concerning the distances γH2AX is able to spread at specific genomic locations.

To this end, a considerable amount of time was spent attempting to locate the genomic positions of the stably integrated tetO and lacO arrays through cloning based methods. The two strategies adopted in this thesis were linker-mediated PCR and inverse PCR. The inverse PCR method proved to be the more effective of the two; at least resulting in a successful PCR, although ultimately failing to incorporate any genomic sequence. While the inverse PCR approach has been well characterised in the literature, and has been shown to be an effective method for identifying flanking genomic DNA segments that lie outside primers that can be designed (Ochman, Gerber and Hartl, 1988), in practicality it required heavy amounts of optimisation. The

technique involved the digestion of genomic DNA, circularisation of restriction fragments, and amplification by oligonucleotides designed to prime DNA synthesis directed away from the core region of a known sequence, i.e., in the opposite direction of primers used in standard PCR.

The most problematic part of the protocol lay in obtaining the targeted digested DNA after ligation, because of the randomness of the ligation reaction. As oligonucleotides were designed to prime in opposite directions, ligation had to be performed in a way to encourage circularisation of DNA; a step that cannot be confirmed experimentally until the results of the PCR are run on an agarose gel. Low DNA concentrations were used to successfully favour intramolecular ligation. Ultimately, sequencing of the retrieved DNA revealed no genomic DNA was present and that only the known plasmid DNA was circularised. Bands of approximately 500 bp were excised from the inverse PCR reaction rather than those observed at approximately 1 kb (**Fig. 3.10B**). Although the larger of amounts of non-specific smearing at around the 1 kb band may have complicated the sequencing reaction, it is possible that DNA at this higher molecular weight may have contained genomic DNA.

The location of integration sites in the genome of human cells can be controlled by employing established gene-targeting methods using sequence-specific targeted cleavage events, such as transcription activator–like effector nucleases (TALENs). TALENs rely on the use of artificial proteins composed of a customisable sequence-specific DNA binding domain fused to a nuclease that cleaves DNA in a non-sequence-specific manner (Joung and Sander, 2013). The DNA binding domains are designed to provide the target specificity and the nucleases are able to introduce DSBs. The DSBs are

then repaired by mechanisms in cells that can be exploited to introduce insertions at the cleavage site.

Since the beginning of my PhD, alternative methods that were more efficient, easy to engineer and more affordable than TALENs have been developed for precise 'genome editing'. The gene targeting method using clustered regularly interspaced short palindromic repeats–associated nucleases (CRISPR/Cas9) (Cong *et al.*, 2013) is a technique that could have been applied in this thesis for stable integration of tetO and lacO arrays. The Cas9 nuclease is directed to cleave a target sequence by a guide RNA (gRNA). The Cas9 follows the guide RNA to the target sequence and cleaves DNA. Similarly, to the TALEN system, the CRISPR/Cas9 system can introduce mutations or insertions by 'co-injecting' a DNA construct with homology to target DNA on either side of the cleavage site. Both of the methods enable the targeted formation of DSBs at defined genomic sites of interest, substantially increasing the efficiency of recombination compared to the process of random integration through transfection and selection of clones.

3.4.2 Evaluating the experimental design

The work in this chapter described the steps taken to test the hypothesis that γH2AX spreads spherically into neighbouring chromatin both in *cis* and in *trans* in U2OS-tetO-lacO-I-SceI cells, and the attempts made to further characterise the cell based system I created in order to test this hypothesis. The new U2OS-tetO-lacO-I-SceI cell line was generated out of a necessity to improve the cutting efficiency of I-SceI-GR-RFP in the system. This cell line exhibited cutting of the tetO insert by I-SceI endonuclease even in

the absence of TA, as documented by other groups utilising the endonuclease. However, this would not have any bearing on the ChIP data as all experiments were conducted in the presence of TA anyway, and comparison of γH2AX enrichment was made between the broken tetO insert, the unbroken lacO insert and a genomic locus (which was not expected to be enriched for γH2AX) only. Moreover, as the efficiency of cutting was quantifiable (**Fig. 3.18A**), γH2AX levels in damaged cells could be normalised to γH2AX levels in undamaged cells at each genomic location assayed.

U2OS-tetO-lacO-I-SceI cells displayed a greater cutting efficiency than in U2OS-tetO-lacO cells transfected with I-SceI-GR-RFP, as measured by the co-localisation of 53BP1 foci with tetO foci using the immunoFISH technique. Despite greater than 70% of U2OS-tetO-lacO-I-SceI cells showing translocation of I-SceI-GR-RFP from the cytoplasm to the nucleus, only 22% of cells showed cutting at the tetO array indicating that although I-SceI was present in the nucleus after addition of TA, some molecules of I-SceI were not able to cut at its recognition sequence.

Upon induction, I-SceI is constitutively active and continues to cut intact sites as soon as they are repaired, resulting in a cycle of break and repair. In the case of immunoFISH, or any endpoint analysis technique for that matter, only a picture of the dynamic events occurring in the nucleus at the time of 'capture' is being observed. Thus, it is possible that when examining images of some nuclei in a population, cells have been fixed at a point when the site specific DSB has been repaired and 53BP1 molecules have dispersed from the break site. In this scenario, no 53BP1 signal would be observed and the tetO array would be scored as unbroken even though I-SceI is active at the site.

Enough molecules of 53BP1 would need to accumulate in order to be able to reach the detection limit of a microscope camera after immunostaining. In some cases, it is possible that I-SceI has generated a DSB and focal accumulation of 53BP1 has followed, but not enough molecules have been recruited to generate a signal that reaches the detection limit of the camera or a signal that is visible by eye. Similarly, to the previous scenario, the tetO array would be scored as unbroken even though I-SceI is active at the site. It is probable that the I-SceI cutting efficiency as measured by the co-localisation of 53BP1 foci with tetO foci is an underestimation of the endonuclease's activity.

The success of the inducible association system that I created was dependent on the ability of the TetR:FLAG:LacI fusion protein to tether two stably integrated arrays located on distinct chromosomes. Unfortunately, the fusion protein was ultimately not able to induce association of tetO and lacO arrays in cells. The integrity of the plasmids used for creation of the fusion protein was confirmed before use, and every step of the construction of the protein was validated by restriction digest. Restriction digests of the final plasmid construct of the fusion protein produced bands of the expected sizes. Although sequencing of the final plasmid construct was not performed, experimental tests suggested that the fusion protein was expressed in cells, that TetR and LacI proteins were able to fold independently and correctly, and that TetR and LacI were able to bind properly to their respective operator sequences. The function of the fusion protein was assessed by western blot analysis and FISH followed by quantitative analysis of distances between tetO and lacO arrays; these analyses all indicated that the protein functioned correctly. However, when the fusion protein was tested by staining against

the lacI portion of the protein by immunoFISH, it did not seem to show penetration of the nucleus. To check if this was simply an artefact of the immunoFISH technique, the fusion protein was tested again by the initial procedure of standard FISH and quantitative analysis of distances between tetO and lacO arrays (no selectivity of transfected cells). Still no association of tetO and lacO arrays was observed. Consequently, a shared decision was made to shift focus onto a different project in which results could be expected to be achieved in the time left of my PhD.

Chapter 4

4 Analysis of the Dynamics of a Single Double-Strand Break in Mammalian Cells

4.1 Introduction

4.1.1 The movement of DSBs can be either directed or stochastic

Many mathematical models based on cellular data have described active undamaged chromatin movement as a non-directional random walk over relatively short distances (Dion and Gasser, 2013). Movement of DSBs can be characterised as either directed or stochastic motion. The amplitude of stochastic motion, resembling the Brownian motion of particles, might be increased after DSBs due to massive chromatin modifications at the damaged locus leading to changes in its condensation state. These events could lead to an increase in the volume of nuclear space travelled by the damaged locus through random diffusion. By modelling chromatin fibres as looped polymers (Zhang and Heermann, 2014) revealed that faster movement, larger roaming and relocalisation at the periphery of a sub-compartment could be explained by the increased degree of freedom of DNA ends. Studies have shown that modifications of chromatin structure by chromatin remodelling enzymes could also increase local DNA diffusion through established links between ATP-dependent remodelling of local chromatin structure and large scale mobility. (Seeber, Dion and Gasser, 2013; Horigome *et al.*, 2014).

Alternatively, DSB mobility can be perceived to be directed; guided by a filament-driven mechanism. Evidence of this was provided by (Cho *et al.*, 2014)**,** who observed that DSBs triggered in ALT-telomeres by FokI nuclease resulted in long range and directional movement of the damaged telomere controlled by RAD51 filaments. This

finding was supported in the same year by (Lesterlin *et al.*, 2014), who observed RecA (Rad51 bacterial homolog) bundles that mediated homology pairing between distant sister chromatids following DSB induction in *Escherichia coli*. The linker of nucleoskeleton and cytoskeleton (LINC) complex has also been implicated in the directional movement of DSBs. By tracking 53BP1 foci with high resolution in live cells, Lottersberger et al. 2015 demonstrated a 53BP1-dependent mobility of DSBs via a LINC/microtubule-dependent mechanism that promotes the mobility of IR induced DSBs in PARP inhibitor treated BRCA1-deficient cells.

4.1.2 Roles of ATM AND DNA-PKcs in DSB repair

Upon detection of a DSB the DDR is rapidly initiated, largely relying on the recruitment and activity of the PI3K-related kinases ATM, ATR and DNA-PKcs through direct interactions with the MRN complex, ATRIP and the Ku heterodimer respectively. DNA-PKcs and ATM are primarily involved in DSB repair, whilst ATR responds to a wide range of DNA lesions, particularly those associated with DNA replication (Cimprich and Cortez, 2008)**.** ATM and DNA-PKcs have been proposed to participate in repair on three different levels: promoting efficient DNA repair by directly regulating the repair machinery, changing the local chromatin environment near a DSB and altering the cellular environment through checkpoint activation or cell apoptosis (Sirbu and Cortez, 2013).

The direct roles of ATM and DNA-PKcs in repair at the break site depends, for the most part, on their kinase activity. DNA-PKcs is a core component of the NHEJ machinery

whose function is two-fold: being required for tethering of broken DNA ends and the stable recruitment of the XRCC4/DNA ligase complex required for end joining (Calsou *et al.*, 2003). Accordingly, impairment of DNA-PKcs leads to end joining defects as measured by pulse field gel electrophoresis (PGFE) (Beamish *et al.*, 2000)**.** On the contrary ATM is actually dispensable for repair of most DSBs induced by IR (Aaron A. Goodarzi *et al.*, 2008), but is required for efficient repair of DSBs induced in heterochromatin (Beucher *et al.*, 2009) and is required to mediate the repair of DSBs with blocked DNA ends (Álvarez-Quilón *et al.*, 2014). Notably, ATM and DNA-PKcs preferentially phosphorylate their respective targets on Serine or Threonine residues followed by Glutamine (S/T-Q motif).

The prominent part that ATM plays in mediating all cell cycle checkpoints in response to DSBs through the action of p53 and checkpoint kinases 1 and 2 (CHK1/2) has been well characterised (Kastan *et al.*, 1992). DNA-PKcs has been demonstrated to selectively regulate the p53-dependent apoptosis pathway. Mice defective in DNA-PKcs displayed a decreased apoptotic response and lowered BAX expression following exposure to IR, suggesting DNA-PKcs serves as an upstream regulator of the p53-mediated apoptosis pathway. (Wang *et al.*, 2000). Furthermore, DNA damage-induced apoptosis was abolished in both DNA-PKcs $^{-/-}$ and p53$^{-/-}$ cells. Additionally, substituting Alanine for Serine18 led to a decreased apoptotic response, indicating that phosphorylation of p53 is important for DNA-PKcs-mediated apoptosis (Woo *et al.*, 2002).

DSBs can occur in various chromatin contexts including chromatin found in an open state and a more compacted state. Both of these chromatin contexts influence the

activation of the DDR and DNA repair efficiency. Repair in heterochromatin for example, is known to be more challenging for repair machinery presumably because repair proteins are physically occluded from accessing the break. ATM-dependent local chromatin changes promote a local environment conducive for repair. Histone H2B is monoubiquitylated near DSBs and this modification, typically associated with actively transcribed genes, when prevented, impairs NHEJ and HR in cells (Moyal *et al.*, 2011). Another mechanism by which ATM relaxes chromatin to promote repair is through phosphorylation of KRAB-associated protein (KAP-1), a transcriptional corepressor that works with histone methyltransferase and histone deacetylase complexes to promote heterochromatin function. ATM-dependent KAP-1 phosphorylation disperses the nucleosome remodeller CHD3 from DSBs and triggers concomitant chromatin relaxation (Goodarzi, Kurka and Jeggo, 2011). ATM is thus particularly important for repair of DSBS occurring in heterochromatin. (Aaron A. Goodarzi *et al.*, 2008).

Also, following a DSB, ATM can promote a local environment favourable for repair through the formation of γH2AX and consequently a γH2AX-MDC1 platform for recruitment of many DNA repair, DDR signalling and chromatin modifying factors including: RNF8 and RNF168, BRCA1 and 53BP1, and the ATP-dependent chromatin remodelling complexes SWI/SNF, SWRI and INO80.

Reports have described a DNA-PKcs dependent component to the G2/M checkpoint (Arlander *et al.*, 2008; Liu, Matsuda and Plunkett, 2008), raising the possibility of cross-talk between ATM and DNA-PKcs in DNA damage signalling. However it is important to note that several lines of evidence point to a distinct role between ATM and DNA-PKcs in the response to DSBs *in vivo*. When compared with the broad spectrum

of ATM substrates, the targets of DNA-PKcs remain largely undefined. Although a novel component of the DNA damage response, NR4A nuclear orphan receptors, have been shown to interact with DNA-PKcs as a substrate in DNA repair (Malewicz *et al.*, 2011). Moreover, those phenotypes associated with ATM and DNA-PKcs deficiencies are distinct. Where ATM knockout mice are sterile and predisposed to lymphomas, DNA-PKcs knockout mice are fertile but exhibit severe combined immunodeficiency (SCID) without increased incidence of tumourigenesis. The majority of evidence suggests that although ATM and DNA-PKcs are both activated by IR-induced DSBs, they cannot wholly substitute for each other in the DNA damage response *in vivo*, possibly because of distinct physiological targets.

The formation of cytologically discernible γH2AX foci plays a critical role in the retention of repair proteins at the sites of DSBs. While the ATM-dependent formation of γH2AX foci has been well established, the function of DNA-PKcs towards this modification is still relatively unclear. Some reports have shown an exclusively ATM-dependent formation of γH2AX foci (Burma *et al.*, 2001), and a requirement of ATM but not DNA-PKcs for γH2AX domain establishment at AsiSI-induced DSBs. (Caron *et al.*, 2015). On the other hand, one study has reported defective γH2AX formation in the DNA-PKcs-defective tumour line M059J (Paull et al. 2000), and more weight of evidence supports an at least partially redundant role for ATM and DNA-PKcs (Stiff *et al.*, 2004). In addition, although markedly attenuated compared with wild-type cells, cells from patients with ataxia-telangiectasia showed many DNA damage responses that are considered ATM dependent (Tomimatsu, Mukherjee and Burma, 2009).

The mechanism by which the DNA damage response promotes increased chromosome mobility is not yet fully clear. Insights into how the DDR kinases ATM and DNA-PKcs regulate chromosome dynamics will provide important information into how chromatin domains are maintained around a DSB and will have significant implications for the mechanisms potentially driving chromosomal translocations.

4.2 Development of a Cell-Based System to Investigate DSB Mobility

With the aim of directly studying the dynamics of a single DSB *in vivo* in living human cells, I have created a cell based system in which a DSB can be induced at a specific locus in the human genome and analysis of the movement of the DSB compared to an undamaged locus within the same cell can be followed in real time. U2OS-tetO-lacO-I-SceI cells stably expressing the meganuclease I-SceI and containing stable insertion of two artificially created DNA segments; tetO and lacO array, were utilised. Approximately 180 tandem copies of tetO sequences and 170 tandem copies of lacO sequences were located on two distinct chromosomes (as described in chapter 3) and were independent of one another (**Fig. 4.1**). A single I-SceI mediated DSB could be induced on the tetO

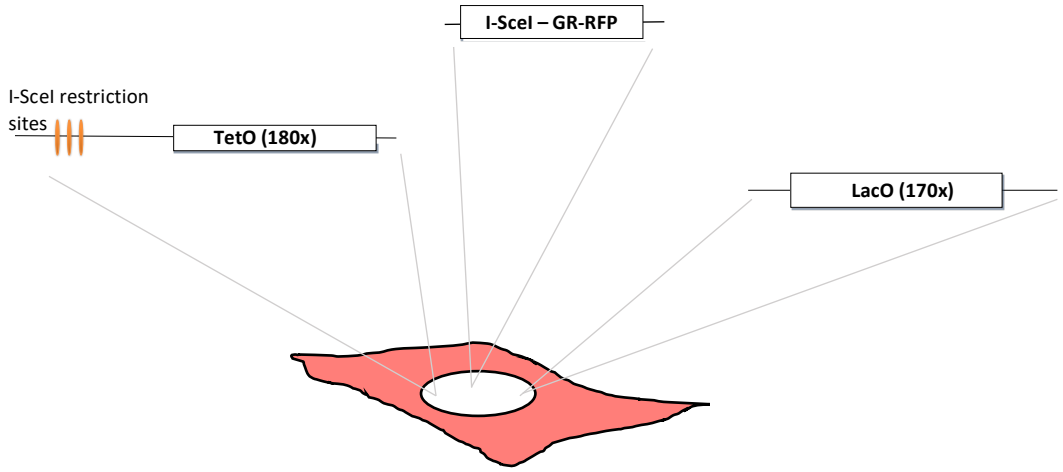

Figure 4.1. Schematic of U2OS- tetO-lacO-I-SceI cells showing key stable integrants

U2OS-tetO-lacO-I-SceI cells stably expressing I-SceI-GR-RFP and containing stable insertion of 180 tandem tet operator sequence repeats and 170 tandem lac operator sequence repeats. Three tandem I-SceI recognition sequences are positioned adjacent to the tet operator sequences

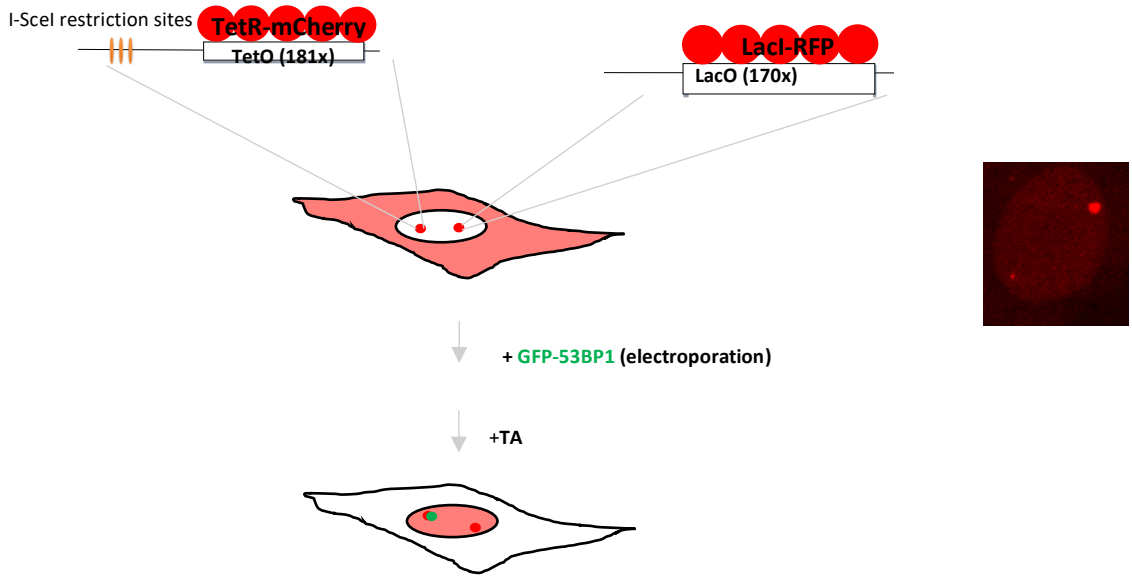

Figure 4.2. An experimental system to visualise and monitor the dynamics of a single DSB

Schematic representation of the I-SceI-inducible system. DSBs are triggered by treatment of cells with the steroid ligand triamcinolone acetonide (TA), resulting in relocation of the I-SceI-GR-RFP fusion protein (pink) from the cytoplasm to the nucleus. tet and lac arrays are visualised after transient transfection of TetR-mCherry and LacI-RFP respectively. Physical transfection by electroporation of GFP-53BP1 results in its accumulation at the I-SceI-induced DSB

array but not the lacO array upon the transient transfection of I-SceI-GR-RFP plasmid and the addition of the synthetic ligand triamcinolone acetonide (TA). To visualise the stable inserts, cells were transiently transfected by electroporation with TetR-mCherry and LacI-RFP which, on expression, bound to the tetO and lacO arrays respectively to give signals as red dots (**Fig. 4.2**). Exploiting the ability of 53BP1 to localise to DSB sites in nuclei, 53BP1 was used as a marker of DSBs. To be able to distinguish between the two red dots and identify which dot represented the array that could be broken, full length 53BP1 tagged with GFP at its N-terminus was transiently transfected into cells by electroporation.

4.2.1 Characterisation of the GFP-53BP1 protein

The GFP-53BP1 protein acted with the same dynamics as endogenous 53BP1, relocating to DSBs generated by X-ray irradiation, as marked by the appearance of γH2AX foci. (**Fig. 4.3A/B**)**.** GFP-53BP1 recapitulated hallmarks of the physiological functions of 53BP1 showing: largely homogenous pan-nuclear distribution in cells that were not induced with a DSB except for in nucleoli devoid of the protein and appearance of 53BP1 nuclear bodies (**Fig. 4.3C**). Finally, GFP-53BP1 was able to re-localise to a single DSB induced by I-SceI (**Fig. 4.4**).

4.2.2 Real-time dynamics of tagged loci

Live cell microscopy was used to create time-lapse movies to monitor the movement of tagged genomic loci. Exponentially growing U2OS-tetO-lacO-I-SceI cells were electroporated with TetR-mCherry, LacI-RFP and GFP-53BP1 DNA to a total of 2 µg and

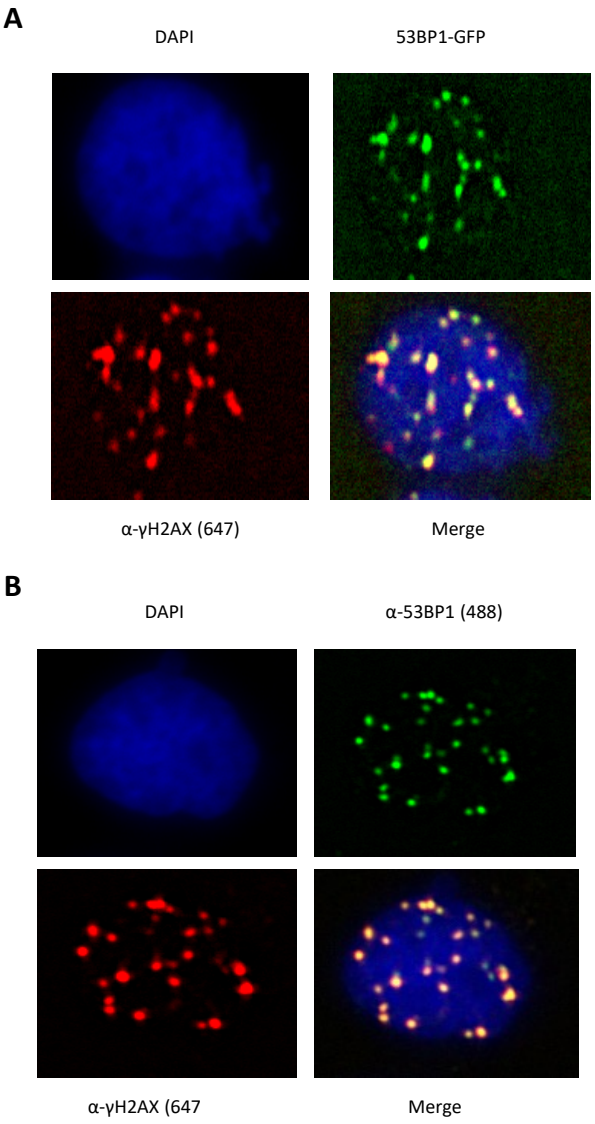

Figure 4.3. Characterisation of GFP-53BP1 dynamics in vivo

(**A**) Asynchronously growing U2OS cells transiently transfected with GFP-53BP1 were fixed and immunostained with an antibody to γH2AX. (**B**) Asynchronously growing U2OS cells were fixed and immunostained with antibodies to γH2AX and endogenous 53BP1. (**C**) A snapshot of live, exponentially growing U2OS cells showing nuclear localisation of GFP-53BP1

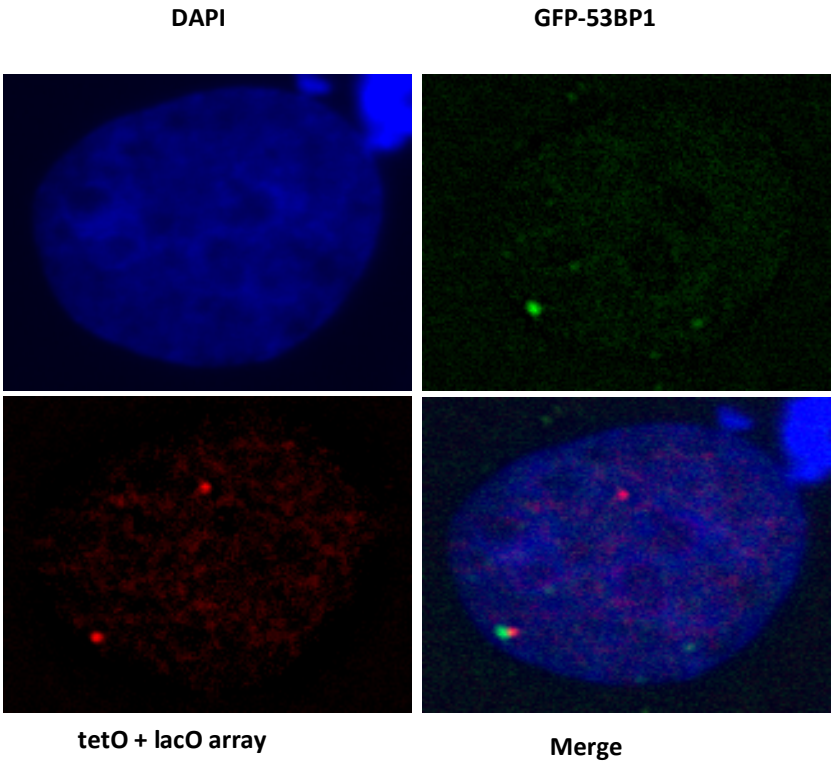

Figure 4.4. Re-localisation of GFP-53BP1 to a DSB in the U2OS- tetO-lacO-I-SceI cell line

Snapshot of a live exponentially growing U2OS-tetO-lacO-I-SceI cell line showing appearance of GFP-53BP1 (green) adjacent to the tetO locus (red) after induction of a DSB after addition of TA.

cells were plated in a glass bottom dish for imaging. Because the chamber belonging to the spinning disk confocal microscope in which cells would be imaged was not equipped with a CO2 input, the following day DMEM media covering the cells was replaced with CO2 independent media to deterioration of cells. Next, cells were incubated for 1 hour with SiR-DNA (SiR-Hoechst), a chemical that allows the labelling of nuclear DNA in live cells with high specificity and low background. SiR-DNA was used instead of the more conventional Hoechst 33342 as its emission and excitation in the far-red wavelength of light minimised phototoxicity and sample auto-fluorescence. In contrast Hoechst 33342 requires excitation by blue light which is damaging to cells. After incubation with SiR-DNA, cells were subjected to time-lapse recording (see materials and methods), and TA added after 1 hour to induce DSBs in nuclei (**Fig. 4.5**)**.** Cells were imaged in three channels: 405 nm, 488 nm and 561 nm.

Before time-lapse images were captured, varying parts of the imaging dish were surveyed in order to find nuclei that were suitable for imaging. To be deemed suitable for imaging, individual nuclei needed to display successful expression of TetR-mCherry, LacI-RFP and GFP-53BP1 as observed by two spots in the 561 nm channel and a pan nuclear distribution of GFP-53BP1 signal in the 488 nm channel. In addition, nuclei should not have exhibited over expression of GFP-53BP1. Once suitable nuclei were identified, their X, Y, Z location in the dish was saved using the local Slidebook 6 program. This process was repeated to assemble a multipoint list of locations whose size was limited only by restrictions pertaining to imaging time between each capture. As captures were set to be taken at 4-minute intervals, this was the maximum time available for the microscope to move the motorised stage to the set points and acquire

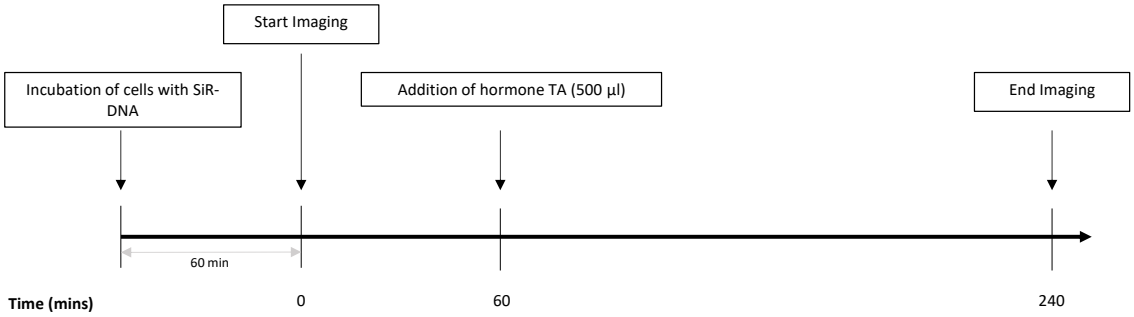

Figure 4.5. Schematic of live cell experimental procedure

Schematic representation of the experimental strategy used to capture time-lapse images of the dynamics of tetO and lacO loci in live cells. 1 hour before imaging commenced, pre-electroporated cells (TetR-mCherry, LacI-RFP, GFP-53B1) were incubated with silicon-rhodamine (Sir)-DNA stain. 500 µl of TA diluted in DMEM was added at 60 minutes into imaging.

images. Three-dimensional image stacks of 11 optical slices covering an 8 µm range, separated by 0.8 µm were collected every 6 minutes for 4 hours and then.

4.3. Analysing the Mobility of Undamaged and DSB-Containing Chromosomal Loci

Time-lapse imaging confirmed that after transient transfection of TetR-mCherry, LacI-RFP and GFP-53BP1 and following the treatment of U2OS-tetO-lacO-I-SceI cells with TA, the tetO locus was cut in live cells by I-SceI. This was demonstrated by GFP-53BP1 localisation to the tetO locus (**Fig. 4.6**). Appropriate cells were identified and picked for analysis of the movement of the tagged tetO and lacO loci.

4.3.1 Image Alignment

Direct analysis of dynamics of tetO and lacO loci by four-dimensional (3D + time) confocal microscopy in vivo was hindered by the global motion of the cell itself. The time intervals between the automated acquisitions of the 3D projected images was in the order of minutes, so it was not expected that the cell would remain in a fixed position on the imaging dish. The tagged loci under analysis moved relative to the co-ordinate system of the cell nucleus, but at the same time, this coordinate system rotates and translates as the cell moves. This whole cell movement superimposed a motion on the dynamics of the tagged loci in the nucleus of U2OS-tetO-lacO-I-SceI cells, not attributed to the tagged loci themselves, which needed to be removed. This operation, henceforth called alignment, can be achieved by various methods. In this study I used an Image J plugin called StackReg to achieve alignment (Thevenaz, Ruttimann and Unser, 1998). In brief, a cell was identified and followed across the entire time series of 40 frames. Each frame was used

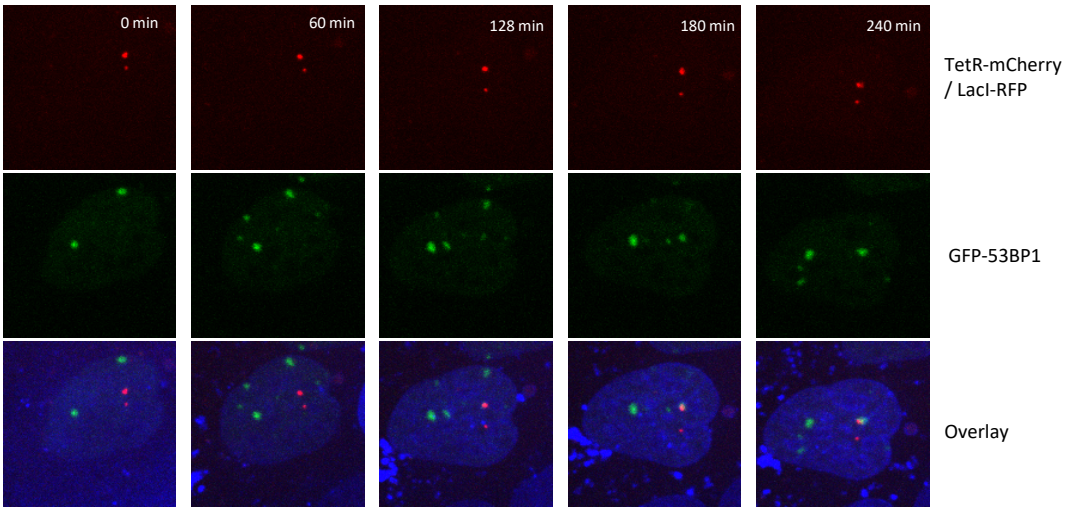

Figure 4.6. Visualisation of GFP-53BP1 at the tetO locus

Representative time points of a time-lapse series showing the appearance of GFP-53BP1 at the broken tetO locus after the addition of triamcinolone acetonide in U2OS-tetO-lacO-I-SceI cells. Triamcinolone acetonide was added at 60 minutes. Each time point is a maximum projection of three-dimensional stacks of 11 optical slices.

as a template to which the following frame was aligned so that alignment proceeded by propagation.

The movement of the cell nucleus was treated as rigid body transformation, consisting of translational and rotational components in the X, Y plane. Following alignment (**Fig. 4.7**), the spatio-temporal properties of the tagged loci were analysed.

4.3.2 Single particle tracking

A single particle tracking (SPT) approach was used to track and follow the movement of tetO and lacO loci. This was aided through the use of (Tinevez *et al.*, 2017), an open source FIJI plugin that allows automated, semi-automated and manual tracking of single particles. The goal of SPT was to segment and follow tagged loci (spot-like structures) over time. Each spot was segmented in multiple frames and its trajectory reconstructed by assigning it an identity over these frames, in the shape of a motional track. Tracks were checked for inconsistencies, such as loss of a spot in multiple frames, by visual inspection. Only appropriate tracks were used for analysis (**Fig. 4.8**). X, Y, Z coordinates were extracted from the track data, but since the time-lapse movies generated were 2d projections of 3D images, the function of Z was zero, so only X, Y co-ordinates were utilised.

4.3.3 Mean squared displacement

DSB mobility was estimated using mean squared displacement (MSD) (**Fig. 4.9**). The squared displacement from the track origin was averaged for all tetO and lacO loci under

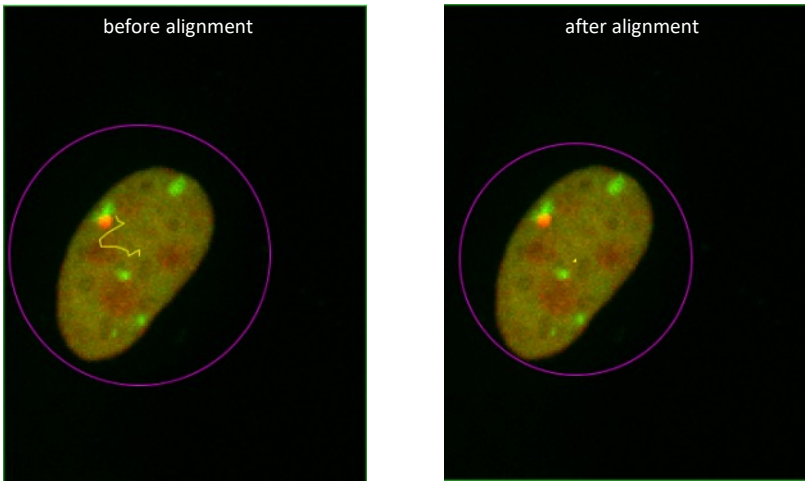

Figure 4.7. Recursive rigid body transformation alignment of images over a time series

Motional tracks (yellow) of the centre of mass of a cell nucleus before and after image alignment over a time-lapse series. Translational and rotational motion of the whole nucleus was corrected by rigid body transformation.

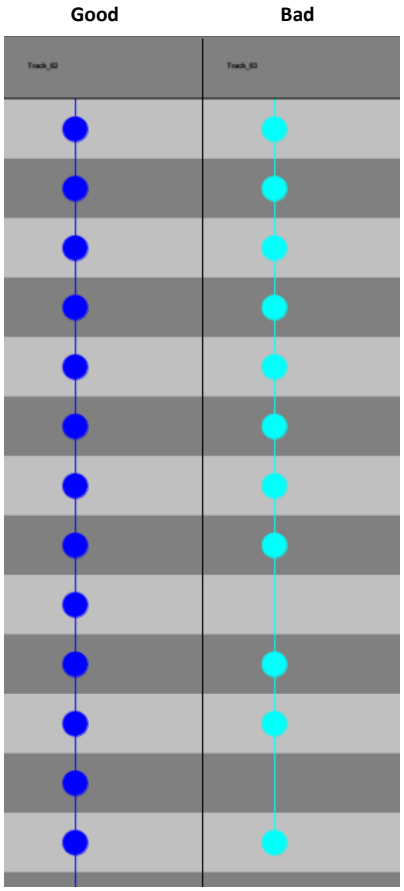

Figure 4.8. Visual inspection of motional tracks

Example of a track map showing disappearance of tracked spots in certain time frames (cyan). A track is laid on pane, arranged vertically over time. Each spot is displayed as a solid circle in the map. Tracks were inspected for missing spots in any time frame. Tracks with missing spots were not taken for analysis

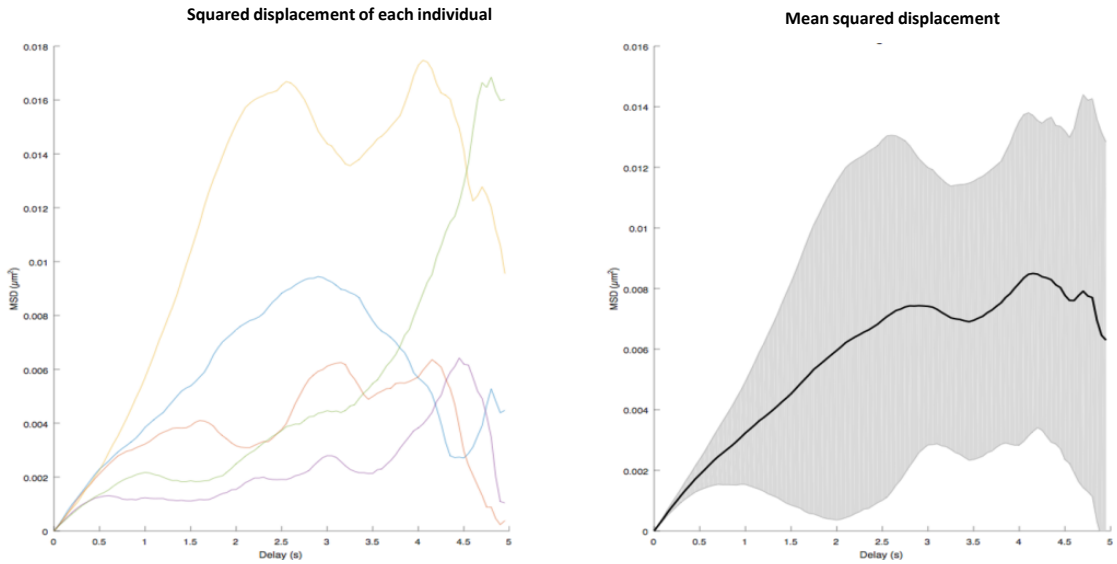

Figure 4.9. Plotting mean squared displacement curves

Left: Squared displacements of a single particle is calculated. Right: The average displacement of each individual is calculated to give the mean square displacement.

given conditions and was plotted against time for each experiment. MSD was calculated according to the formula:

$$\mathrm{MSD} \equiv \langle (x - x_0)^2 \rangle = \frac{1}{N} \sum_{n=1}^{N} (x_n(t) - x_n(0))^2$$

Where $\mathbf{x_n(0)}$ represents the reference position of a particle, $\mathbf{x_n(t)}$ represents the position of a particle determined in time, and ***N*** is the number of particles to be averaged.

4.3.4 Data collection considerations and criteria

Adopting a time-lapse imaging approach gave rise to a number of difficulties when attempting to analyse the dynamics of tetO and lacO loci in the complex nuclear environment. The majority of these issues stemmed from endeavouring to image enough nuclei to be able to make confident statistical inferences about the data obtained. Rigorous and meticulous steps were taken to ensure precise measurements of mobility. Many of the nuclei imaged were not suitable for analysis and were rejected (**Fig**. **4.10**)**.** In the following section, I will explain the reasons for rejecting specific nuclei and the measures taken to ensure accurate analysis. Kept away

Three plasmid DNA constructs were physically transfected at the same time by electroporation to enable visualisation of tetO loci, lacO loci and GFP-53BP1 in the system. The success of the experimental system relied on the ability to transiently co-express every element of the transfection DNA complex in the same cell. Although electroporation is a highly efficient strategy for the introduction of foreign DNA, and

Reason for Discarding	Number of Nuclei discarded	% of Total
Over-rotation of the nucleus	400	12.8%
No TetR-mCherry and LacI-RFP together	1568	50.0%
No GFP-53BP1	184	5.9%
Leaky cutting of I-SceI	208	6.6%
Gaps in motional tracks	588	18.8%
Merging of tetO and lacO in Z-axis	15	0.5%
Over-rotation of neighbouring nuclei	150	4.8%
Abnormal morphing of nucleus	23	0.7%

Total no.of suitable nuclei	173
Total no. of nuclei discarded	2963
Total no. of nuclei imaged	3136

Figure 4.10. Nuclei excluded from motional analysis.

A number of imaged nuclei were unsuitable for analysis of the dynamics of tetO and lacO loci and were consequently excluded. The table lists the number of nuclei scored.

even after optimisation of the ratio of each plasmid, the simultaneous transfection of three separate plasmids did not always result in expression of all three proteins in the same cell. As a result, a number of nuclei that were imaged could not be scored for tetO and lacO movement because there was a lack of expression of TetR-mCherry, LacI-RFP or GFP-53BP1. These nuclei were 'discarded' and not used for analysis

As previously shown, even in the absence of TA there was a subset of cells that expressed I-SceI-GR-RFP in the nucleus. In these cells, I-SceI-GR-RFP could then act and generate a DSB before the addition of TA. So, when examining time-lapse movies, there were nuclei in which GFP-53BP1 accumulated at the broken tetO locus, giving rise to 'leaky cutting' before the addition of TA at the 60-minute timepoint. In order to analyse the mobility of the tetO locus under native conditions (without a DSB) in the first hour, nuclei displaying GFP-53BP1 at the tetO locus were discarded.

The StackReg plugin available through FIJI was used to align images and correct the individual frames for shift and rotation of cell nuclei during imaging. However, there were some nuclei that exhibited too much movement for the alignment process to be effective. In addition, there were some instances in which the nucleus of interest showed limited motion, but alignment was unable to be applied to that nucleus because a neighbouring nucleus exhibited motion that affected the alignment process.

To limit the movement of cells and to reduce the number of nuclei discarded, cells were plated in such a way that they were approximately 80% confluent at the time of the experiment. Nuclei that underwent extensive morphological changes were also excluded from analysis. In some cases, tetO or lacO loci were seemingly close to the nuclear membrane, and changes in the nuclear morphology resulted in apparent motion

of loci. This motion can lead to overestimation of loci mobility, and so these nuclei were not included in analysis.

Although time-lapse images were taken in 3D; X, Y, Z dimensions, analysis was performed in 2D on 3D projected images. In some instances tetO and lacO foci were positioned close to one another or seemed to merge. Whilst the optical merging was most likely just due to an overlapping in the Z dimension only, and not an actual co-localisation of the two loci, their tracking during the course of the experiment is hindered. The tracking software cannot distinguish between the two loci spots, and so loci in nuclei exhibiting this phenomenon cannot be tracked and are consequently excluded from analysis.

As alluded to earlier (**Fig. 4.8**), only those nuclei in which appropriate motional tracks were extracted were included in analysis. Upon expression of TetR-mCherry and LacI-RFP the tetO locus was consistently observed to have a larger spot and give a stronger signal than the lacO locus. On occasion, tracked lacO loci would vanish from the image most likely due to lack of detection of its weak signal. Increasing the exposure time in the 555 nm channel worked to capture the lacO signal for the entire imaging time in some cases; however there were still some instances in which this was not effective.

Live cells were initially incubated with the fluorescent dye Hoechst 33258 to stain nuclear DNA. Hoechst 33258 is excited by UV light at around 350 nm and emits blue fluorescent light at around 461 nm. Repetitive excitation by UV light and emission of blue light over the 4-hour imaging time caused phototoxicity in cells and resulted in a mass accumulation of GFP-53BP1 to nuclear foci, making analysis difficult. To combat

this, silicon-rhodamine-Hoechst (SiR-Hoechst or SiR-DNA) was used to great effect. SiR-DNA is a far-red DNA stain excited and emitted in the far-red spectrum of light through the attachment of carboxylated SiR derivatives, that displays minimal cell toxicity. Throughout the length of imaging, captures were taken every 6 minutes. To increase the number of positions in the imaging dish and so increase the number of cells that could be captured in the 6-minute interval, the use of a DNA stain was negated. Without the need to image in a third fluorescent channel, the time it took to image at each position in the dish was reduced. In addition, the SiR-DNA stain was rendered redundant as GFP-53BP1 presented as pan-nuclear staining and could be used to identify and demarcate cell nuclei.

4.3.5 Reduced mobility of the DSB-containing tetO locus compared to the undamaged lacO locus

To directly investigate the mobility of a genomic locus containing a DSB and an undamaged genomic locus in the nuclear space, MSD plots were created. The movement of the tagged undamaged lacO locus was compared with the movement of the tagged damaged tetO locus at which an I-SceI-induced DSB was generated. At the end of the 4-hour imaging period the roaming range of the tetO locus was observed to be lower than that of the lacO locus, showing a reduction in MSD from approximately 2.7 μm^2 to 2.1 μm^2 (**Fig. 4.11A**). There was a statistically significant difference between the MSD of tetO and lacO from the point of induction of a DSB at 1 hour as determined by one-way ANOVA ($p<0.001$). The average displacement made by tetO and lacO loci per 6-minute time step was calculated, with lacO loci exhibiting a greater displacement

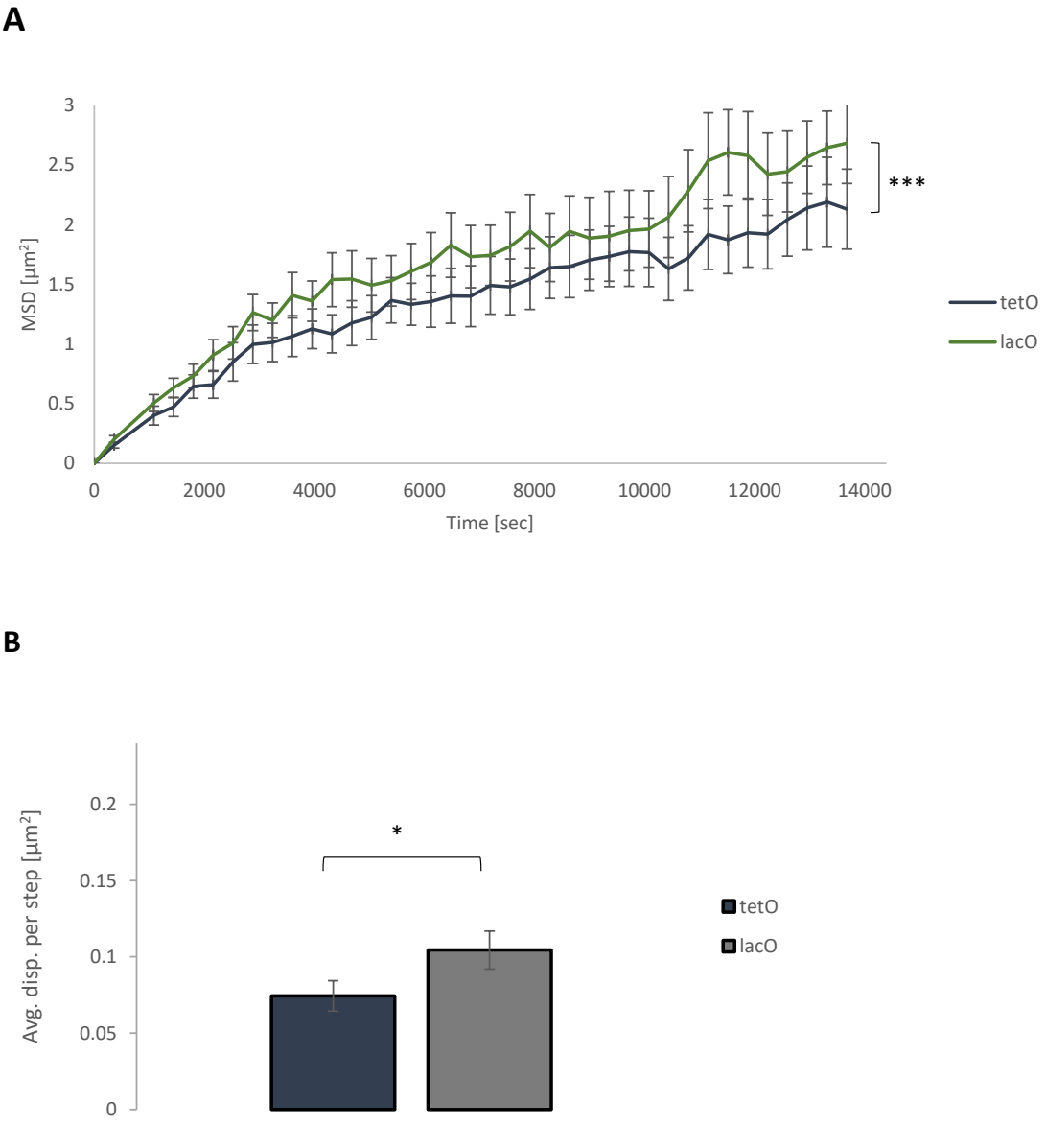

Figure 4.11. Mobility of a single DSB-containing locus is decreased compared to an intact undamaged locus

(**A**) MSD plots of the intact lacO locus and the single DSB-containing tetO locus. Triamcinolone acetonide was added at 3600 secs to generate an I-SceI-induced DSB. *** $P<0.001$ for the entire time series, assessed by one-way ANOVA. Error bars represent the SEM. (n = 63). (**B**) Bar graphs of the average displacement of the lacO and tetO locus per 360-second (6-minute) interval. *$P<0.05$, assessed using two-tail paired *t*-Test. Errors bars represent the SEM.

per step than tetO loci (**Fig. 4.11B**), and the nuclear area roamed by lacO was 1.5 times higher than tetO (nuclear area roamed is proportional to $[MSD]^{3/2}$). The basic quantity characterising motion in various diffusion simulations is the MSD as a function of time. Through analysis of the curvature of an MSD plot, normal Brownian diffusion can be distinguished from deviations such as directed, anomalous and confined diffusion.(Saxton, 2007) (**Fig. 4.12**)**.**

Comparing my MSD plots with those in (**Fig. 4.12**)**,** tetO and lacO loci appear to move with similar diffusion characteristics and can be adjudged to undergo a mixture of random Brownian motion and anomalous sub-diffusion. Sub-diffusion occurs in various biological systems and is caused by viscoelasticity of the surrounding medium, obstruction by immobile obstacles and binding events (Lukacs *et al.*, 2000; Guigas, Kalla and Weiss, 2007).

In normal diffusion, the MSD is proportional to time and the diffusion coefficient is constant:

$$\mathbf{MSD = 4D}t$$

The diffusion coefficient, D, was estimated from the slopes of the MSD plots using a linear fit. (**Fig. 4.13**)**.** The fit is only made on the first 25% of the curve, following the recommendations of (Saxton, 2007). The gradient of an MSD plot for a particle undergoing a 2D walk is equal to 4D. Squared displacements were calculated from 3D-projected 2D images rather than 3D images; a process expected to give a slight underestimate in values as Z-axis displacements were not taken into account. As such, D was multiplied by a correction factor of 1.22 to factor in this conversion (Chubb *et al.*, 2002). Two linear regressions were fitted for each MSD plot; before the induction of a

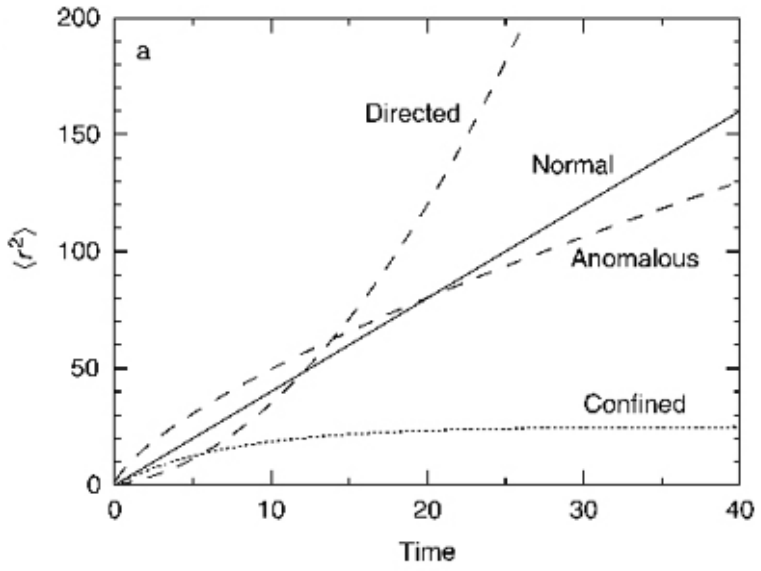

Figure 4.12. Types of diffusive motion experienced by single particles

Adapted from MJ Saxton, 2007. Mean-squared displacement $\langle r^2 \rangle$, as a function of time for normal diffusion, where the slope equals the diffusion coefficient (D) times twice the number of dimensions in which movement is measured (d), anomalous sub-diffusion, directed motion and confined motion. The mobility of a particle moving according to Brownian motion within confined space will generate a curve that levels off at larger time intervals.

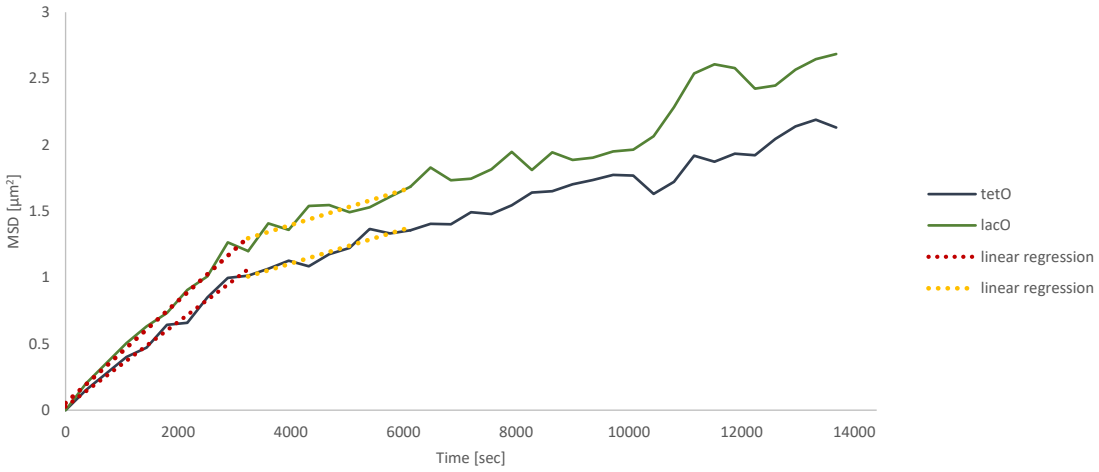

Figure 4.13. Estimating the diffusion coefficient of lacO and tetO loci

Linear regressions of the first 25% of MSD curves was made. The gradient of an MSD curve was used to estimate the diffusion coefficient, D.

DSB via addition of TA at 3600 seconds, and after (**Fig. 4.13**). The diffusion coefficients for the undamaged lacO locus were calculated to be $1.22x10^{-4}$ $\mu m^2/s$ before addition of TA and $3.05x10^{-5}$ $\mu m^2/s$ after addition of TA. The diffusion coefficients for the tetO locus were $9.15x10^{-5}$ $\mu m^2/s$ before addition of TA and $3.05x10^{-5}$ $\mu m^2/s$ after addition of TA. The diffusion coefficients calculated before the addition of TA for lacO and tetO were similar and after the addition of TA were identical, confirming that both loci moved with similar diffusion characteristics, and suggested that induction of a DSB did not affect the diffusional motion of a genomic locus.

In order to be sure the observed difference in mobility of the tetO locus compared to the lacO locus was a result of the induction of a DSB alone, and not simply due to an inherent lower mobility of the tetO locus, the mobility of the tetO locus was examined in the absence of TA. In the absence of TA, no translocation of I-SceI endonuclease to the nucleus takes place and therefore cutting at the inserted I-SceI triple cut site does not occur, consequently resulting in no DSB. Under this condition, the MSD of the tetO locus increased, and a statistically significant difference between the unbroken tetO locus and the tetO locus containing a DSB was determined ($p< 0.001$) (**Fig. 4.14A**).

The cutting efficiency of the I-SceI endonuclease, as determined earlier in this thesis by calculating the frequency of appearance of GFP-53BP1 at the tetO locus, was approximately 25%. As a result, there were a number of nuclei that upon transfection of GFP-53BP1, did not display GFP-53BP1 at the tetO locus even in the presence of TA; indicating that I-SceI endonuclease did not cut at its recognition sequence. These nuclei were deemed to not contain an I-SceI induced DSB at the tetO locus. The MSD of these

A

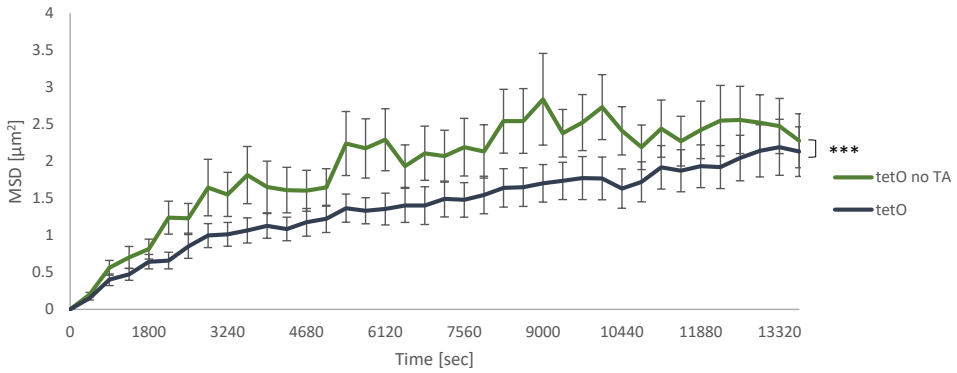

B

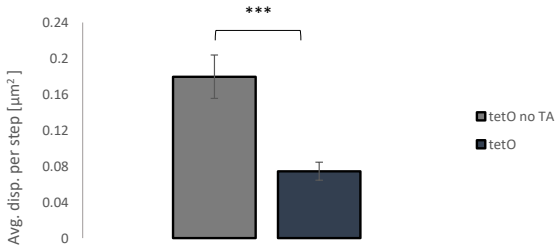

C

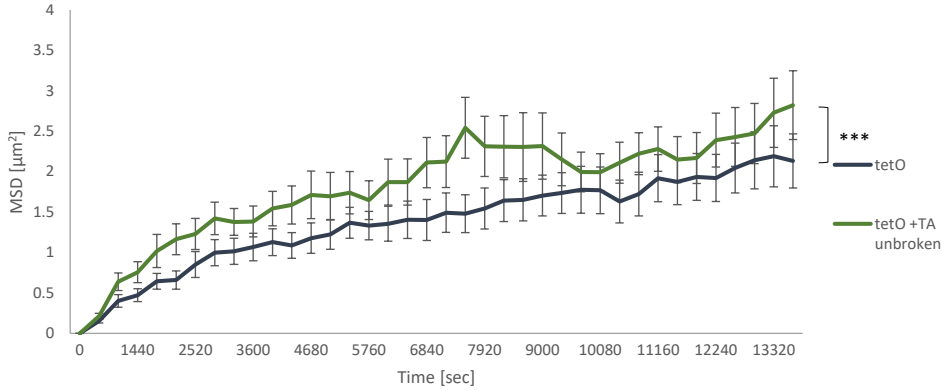

D

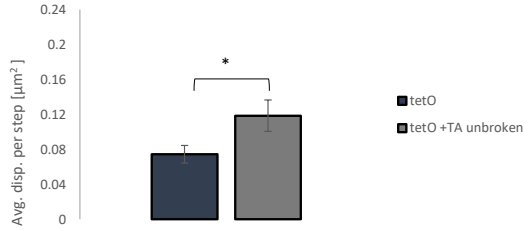

Figure 4.14. Mobility of a single DSB-containing locus is decreased compared to the same locus without a DSB

(**A**) MSD plots of the single-DSB containing tetO locus, and the intact tetO locus in the absence of a DSB (n = 57). *** *P*<0.001 for the entire time series, assessed by one-way ANOVA. Error bars represent the SEM. (**B**) Bar graphs of the average displacement, per 360-second (6-minute) interval, of the DSB-containing tetO locus and the intact tetO locus in the absence of a DSB. **P*<0.05, assessed using two-tail paired *t*-Test. Errors bars represent the SEM. (**C**) MSD plots of the single-DSB containing tetO locus, and the tetO locus in the presence of TA, but containing no DSB (n = 53). *** *P*<0.001 for the entire time series, assessed by one-way ANOVA. Error bars represent the SEM. (**D**) Bar graphs of the average displacement, per 360-second (6-minute) interval, of the DSB-containing tetO locus and the tetO locus in the presence of TA but containing no DSB. ***P<0.001, assessed using two-tail paired *t*-Test. Errors bars represent the SEM.

unbroken tetO loci in the presence of TA was calculated and also increased compared to broken tetO loci yielding a statistically significant difference (**Fig. 4.14C**). The MSD of unbroken tetO loci both in the presence and absence of TA was observed to be at similar levels to those of the lacO locus, showing no statistically significant differences. (**Fig. 4.15**).

4.4 The extent of mobility of a single DSB is influenced by ATM but not DNA-PKcs inhibition

To investigate the roles that ATM and DNAPKcs might play in the dynamics and mobility of a DSB, I analysed the effect of ATM and DNA-PKcs activity on DSB mobility using the specific ATM and DNAPKcs small molecule inhibitors Ku55933 and Nu7441 (Zhao *et al.*, 2006), respectively. U2OS-tetO-lacO-I-SceI cells were incubated with 10 µM of either Ku55933 or Nu7441 inhibitors for 1 hour prior to commencement of live cell imaging. The rest of the experimental procedure (**Fig. 4.5**) was unchanged. One of the cellular hallmarks of ATM deficiency is reduced phosphorylation of the heterochromatin building factor KAP-1. (Guo *et al.*, 2015). Radiation induced recruitment of ATM and subsequent phosphorylation of KAP-1 is hampered after specific inhibition of ATM kinase as observed by immunofluorescence staining. (**Fig. 4.16A**). A characteristic of inhibition of the catalytic activity of DNA-PKcs is demonstrated by the presence of persistent γH2AX foci at long periods post break induction (Cowell, Durkacz and Tilby, 2005; Yamauchi *et al.*, 2017). Inhibition of DNA-PKcs recapitulated this occurrence. (**Fig. 4.16B**). This was confirmation that small molecule inhibitors Ku55933 and Nu7441 were able to inhibit the activities of ATM and DNA-PKcs in *vivo* respectively.

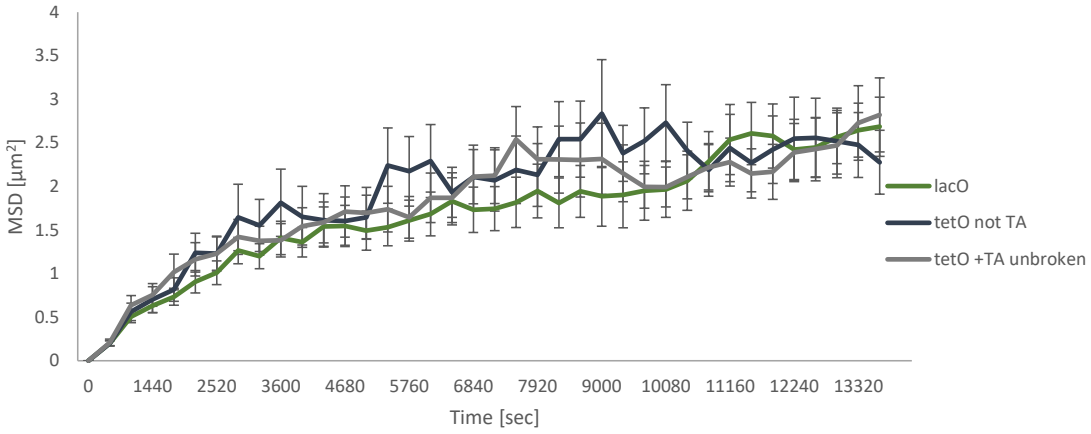

Figure 4.15. Intact loci show no significant difference in mobility

MSD plots of lacO and intact tetO loci. Error bars represent the SEM.

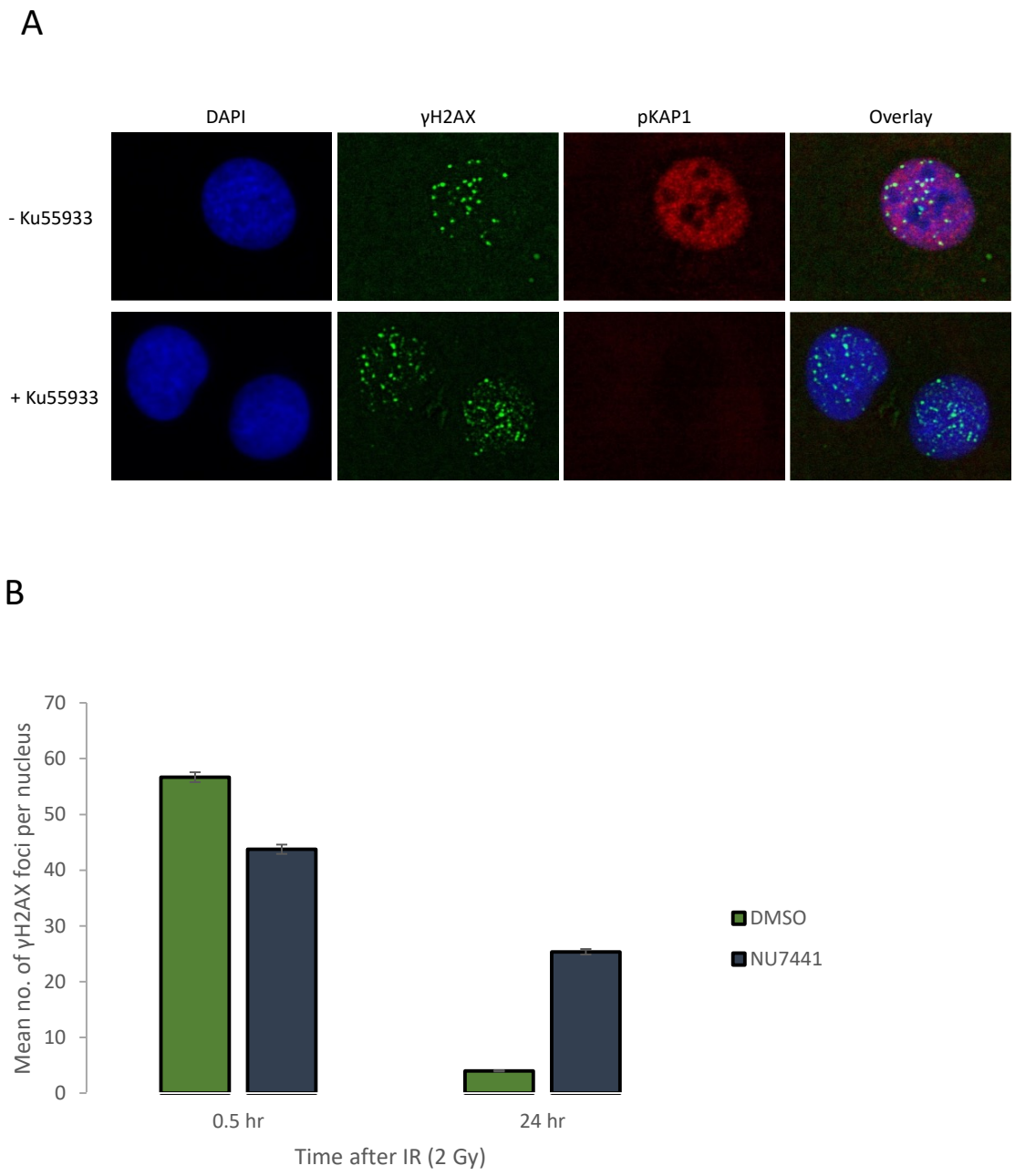

Figure 4.16. Effects of KU-55933 and NU7441 on IR-induced phospho-KAP1 and γH2AX focus formation and decay

(A) Immunofluorescence detection of γH2AX and pKAP1 in U2OS-tetO-lacO-I-SceI cells either treated with solvent alone (control, DMSO) for 1 hour prior to X-ray irradiation (2 Gy) or treated with 10 µM KU55933 for 1 hour prior to X-ray irradiation (2 Gy). (**B**) Effect of DNA-PKcs inhibitor (NU7441) on the number of γH2AX foci in U2OS-tetO-lacO-I-SceI cells treated with either solvent alone (control, DMSO) or 10 µM NU7441 for 1 hour prior to X-ray irradiation until the time of fixation (0.5 hour or 24 hours after X-ray irradiation). Error bars represent SEM.

Inhibition of ATM in U2OS-tetO-lacO-I-SceI cells showed a clear reduction in the mobility of the broken tetO locus. The total roaming range after the imaging observation period of the broken tetO locus after treatment with ATM inhibitor was reduced compared to the wild-type DSB-containing tetO locus: wild type DSB-containing locus gave a final MSD of 2.13 μm^2, and ATM inhibited DSB-containing locus gave a final MSD of 1.8 μm^2. (**Fig. 4.17A)**. This reduction in mobility was statistically significant as determined by one-way ANOVA for the entire time series ($p = 0.017$). The diffusion coefficients for both the wild-type DSB-containing tetO locus and the ATM inhibited DSB-containing tetO locus before DSB induction were identical ($9.15x10^{-5}$ $\mu m^2/s$). However, upon induction of a DSB there was a strong decrease in the diffusion coefficient from $3.05x10^{-5}\mu m^2/s$ for the wild-type DSB containing locus to $9.15x10^{-7}$ $\mu m^2/s$ for the ATM inhibited DSB-containing locus.

Observation of the curvature of the MSD plots indicated a change in diffusion from anomalous sub-diffusion for the wild-type DSB containing locus to confined diffusion for the ATM inhibited DSB-containing locus. The confined mobility of the ATM inhibited DSB containing locus led to a reduction of the sampled volume within the cell nucleus from 3.18 μm^3 to 2.4 μm^3. Inhibition of DNAPKcs in U2OS-tetO-lacO-I-SceI cells showed no effect on the mobility of a DSB (**Fig. 4.17B**). Analysis of the MSD curves indicated no statistical or significant difference between the wild-type DSB containing locus and the DNA-PKcs inhibited DSB containing locus.

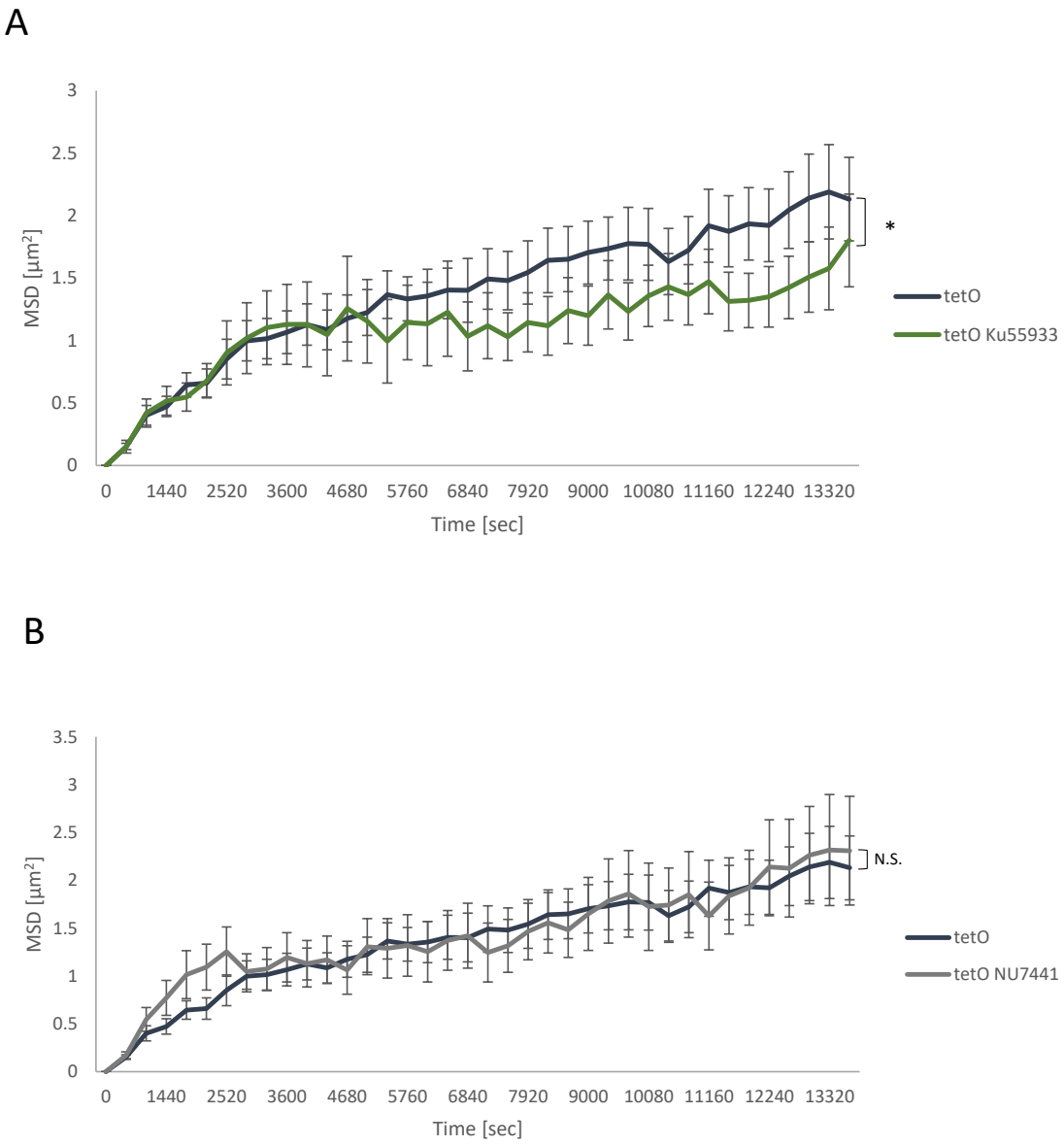

Figure 4.17. Inhibition of ATM not DNAPKcs constricts the mobility of an I-SceI-induce DSB

(A) MSD plots of single DSB-containing tetO loci in the presence or absence of ATM inhibitor (KU55933). * P<0.05 for the entire time series, assessed by one-way ANOVA. Error bars represent the SEM. (n = 26). (B) MSD plots of single DSB-containing tetO loci in the presence or absence of DNAPKcs inhibitor (NU7441). Error bars represent the SEM. (n = 23).

4.6 Discussion

To examine the mobility of a single DSB, DNA damage was introduced by I-SceI endonuclease at the tetO locus and the spatial dynamics of the tetO locus was compared to the unbroken control lacO locus. The broken tetO locus exhibited a motion with an MSD of 2.1 μm^2 compared to the MSD of 2.7 μm^2 of the unbroken lacO locus over the 4-hour time period monitored. The statistically significant reduction in mobility of the DSB-containing tetO locus compared to the intact lacO locus was analogous to findings by (Falk *et al.*, 2007). In that study, in which they generated DNA damage by γ-irradiation and marked DSBs through accumulation of GFP-NBS1, they reported a decrease in the mobility of IRIF after irradiation when compared to the mobility of IRIF before irradiation in cells. (Kruhlak *et al.*, 2006) showed that after their initial appearance, GFP-53BP1 IRIF exhibited limited diffusional motion with an MSD of 0.9 μm^2 over the 50 min time period monitored. In another study it was reported that IRIF generated by X-ray and marked by 53BP1-GFP displayed an MSD of 0.78 μm^2 after 100 minutes. (Becker *et al.*, 2014a). While the MSD values calculated for IRIFs by the groups mentioned are much lower than that calculated for a single DSB at the tetO locus in this thesis, it must be noted that the observation period in this study was much longer, covering 240 minutes. Therefore, a higher MSD would be expected. Fittingly, the tetO MSD of 2.1 μm^2 was strikingly akin to that reported by (Jakob *et al.*, 2009) who, through analysis of the motional activity of GFP-53BP1 foci in live U2OS cells after generating DSBs by low-angle nickel and X-ray irradiation, observed an MSD of approximately 2.2 μm^2 4 hours after irradiation.

The decreased mobility of a DSB compared to an undamaged locus observed in this thesis was in contrast to another study in which it was reported that IRIF generated by

γ-irradiation were substantially more mobile than labelled undamaged chromatin domains approximately 1 Mb in size (Krawczyk *et al.*, 2012).

On comparison of the MSD plots of the tetO locus with that of the lacO and control loci, it is apparent that even before the induction of DSB the tetO locus exhibits a lower MSD than undamaged control loci. This can be explained by the 'leaky cutting' phenomenon previously alluded to in which some cases, the I-SceI endonuclease was able to reach the nucleus and cut at its recognition sequence, resulting in the appearance of GFP-53BP1 foci at the tetO locus before the addition of TA. As a result, a less mobile DSB would lower the MSD values observed.

The $1.22x10^{-4}$ $\mu m^2/s$ diffusion coefficient for the lacO locus was almost identical to the diffusion coefficient of lacO arrays stably inserted at the 5p14 locus reported by (Chubb *et al.*, 2002) in human HT-1080 cells. This value is approximately 4-fold lower than the coefficient estimated for budding yeast (Marshall *et al.*, 1997), suggesting that human chromatin experiences greater resistance to motion than yeast chromatin. The undamaged nucleoplasmic 5p14 locus monitored in the study by (Chubb *et al.*, 2002), exhibited greater displacement (0.23 μm^2) after 10 minutes, and was significantly more mobile than an undamaged 13q22 locus (0.1 μm^2) that was located at the nuclear periphery. These MSD values were lower than those observed in my data of the lacO (0.5 μm^2) and unbroken tetO locus (0.4 μm^2) after 12 minutes. Consequently, it is possible to infer that the lacO and tetO arrays were stably integrated at loci in the U2OS genome that were not located at the nuclear periphery.

Here I have presented data demonstrating that the mobility of a single DSB at a defined locus is reduced when the activity of ATM is inhibited. The diffusion coefficient

of the ATM inhibited DSB is decreased in comparison to the wild-type DSB, indicating a greater resistance to motion in the absence of ATM. However, this decrease in mobility of a single DSB is not echoed when cells are treated with DNA-PKcs inhibitor. No difference in mobility of a DSB was observed in wild-type cells compared to DNA-PKcs inhibited cells. This data suggests that the kinase activity of ATM and not DNA-PKcs plays a significant role in the dynamics of single I-SceI DSBs.

Chapter 5

5 Discussion

5.1 Attempts to Investigate the Spatial Distribution of γH2AX Around a DSB

A hallmark of the cellular response to DNA double strand breaks is histone H2AX phosphorylation by ATM. H2AX is unevenly distributed throughout chromatin and is rapidly phosphorylated to form γH2AX to distances estimated to extend up 2 megabases around DSBs. (Rogakou *et al.*, 1998; Rogakou, 1999). Yeast H2A is phosphorylated locally in chromatin upon DSB formation (forming γH2A) with a comparable distribution pattern to mammalian systems, although spreading occurs over a reduced distance (Shroff *et al.*, 2004). Studies in yeast systems have shown that while γH2A can spread in *cis* surrounding the break site, it can also spread *in trans* onto unbroken chromosomes located in close spatial proximity (Renkawitz *et al.*, 2013). Although the majority of data in the current literature presents the well characterised *in cis* spread of γH2AX, there are strong indications that it can also occur *in trans* in mammalian systems; analogous to the findings shown in budding yeast. The determinants that control γH2AX distribution are still yet to be elucidated mainly because of the intrinsic limitations of available DSB induction methods. Methods used to generate DSBs in various experimental systems include, alpha particles, UV damage, laser-induced damage, radiomimetic drugs and gamma-irradiation. These methods produce damage indiscriminately throughout the genome, which is inappropriate for subsequent ChIP analyses.

In order to investigate this, I worked to develop a novel inducible system whereby two independent artificially created DNA segments stably inserted into the U2OS genome, could be tethered together through the use of a novel TetR:FLAG:LacI fusion protein and the possibility of *in trans* spreading of γH2AX could be addressed by ChIP analysis. Upon expression of the fusion protein the two distinct chromatin regions would be tethered through binding of the Tet repressor protein to the array of tet operator sequences and binding of the lac repressor to the array of lac operator sequences. U2OS-tetO-lacO cells containing stably integrated tetO and lacO binding arrays were successfully generated. The binding arrays were visualised either through transient transfection of Tet and Lac repressor proteins fused to GFP and RFP respectively, or through hybridisation of specific fluorescent FISH probes. The key element of the inducible association system was the TetR:FLAG:LacI fusion protein. In initial testing, the fusion protein appeared to be able to successfully induce tetO and lacO arrays to associate. However, further testing confirmed that the fusion protein was unable to recapitulate this action and pointed to a lack of nuclear entry as a possible explanation for this. After retrospective examination of the construction steps of the TetR:FLAG:LacI fusion plasmid, I recognised that the fusion protein was not constructed with an attached nuclear localisation signal (NLS). I did not proceed to re-clone the fusion protein attached with an NLS due to time constraints and no guarantee that the protein would function even with the attached NLS. Any future work relating to this system would therefore begin with testing the function of the TetR:FLAG:LacI fusion protein with a cloned NLS.

5.1.1 Implications of three-dimensional spatial dynamics of chromatin changes around a DSB

Although I was ultimately unable to successfully develop the inducible association system, there are nevertheless meaningful implications to a possible spread of chromatin changes in 3D around a DSB in mammalian cells.

It has been observed that an initial accumulation of ATM activated at DSBs upon laser stripe-induced DNA damage preceded an overall increase in ATM throughout the nucleus (Kruhlak *et al.*, 2006). This ability of ATM to diffuse away from the break site has been suggested to be a defining factor in the spread of γH2AX (γH2AX spatial distribution hypothesis) (Savic, 2013). RNF 168, the ubiquitin ligase functioning downstream of ATM in the DDR, displays properties similar to ATM in that hypothesis. The RNF168-dependent generation of lysine 63-linked polyubiquitin chains focally around DSBs on histone H2A, among others (Panier *et al.*, 2012), is dependent on the preceding H2A monoubiquitylation via RNF8. This is in turn dependent on MDC1 and serves as an anchor and primer for polyubiquitylation assembly (Doil *et al.*, 2009b). Although a requirement for initial recruitment and activity, subsequent ubiquitylation of chromatin seems independent of RNF8. It therefore appears that RNF168 has an autoregulatory effect on its own chromatin recruitment and signal amplification capacity. The indication here, is that the major way that RNF168 is regulated at break sites is through overall availability, as shown by (Gudjonsson *et al.*, 2012). In that study, the size of 53BP1 foci formed around site-specific breaks was increased in cells lacking TRIP12 and UBR5, two HECT domain ubiquitin E3 ligases that control accumulation of RNF168.

The proposed mechanism by which RNF168 could lead to spatial ubiquitylation and 53BP1 recruitment is similar to the spatial formation of γH2AX as generated by ATM.

(**Fig. 5.1**)**.** The association of RNF168 with chromatin requires the action of RNF8-mediated ubiquitylation of histone H2A, subsequently creating binding sites for RNF168. This is comparable to the formation of γH2AX/MDC1 binding sites for ATM. Although in contrast to ATM, which can phosphorylate γH2AX itself, RNF8 is essential for RNF168 function at break sites. (Doil *et al.*, 2009b). RNF168 may be able to polyubiquitylate neighbouring nucleosomes and create new binding sites irrespective of RNF8 (Panier *et al.*, 2012). Importantly, the RNF168-mediated ubiquitylation has not been shown to have any DNA tracking ability and so the ubiquitylation may depend on the proximity of potential substrate nucleosomes. It is thus possible that RNF168-mediated ubiquitylation could 'jump' between chromatin regions in a non-linear manner. The ability of 53BP1 foci to grow significantly larger than a γH2AX-containing region, in proportion to the amount of available RNF168 in the cell (Gudjonsson *et al.*, 2012), strongly supports the idea that RNF168-mediated ubiquitylation spreads beyond the confines of γH2AX-coated chromatin regions.

Interestingly, (Chapman *et al.*, 2012), demonstrated a minimal overlap between 53BP1 and γH2AX IRIF staining by 3D-SIM and showed that the most prominent γH2AX signals corresponded to regions peripheral to 53BP1 signal. The evidence presented by the authors provides 3D structural evidence that the predominant way in which RNF168 induces 53BP1 binding is not through ubiquitylation within the region that RNF8 generates the seeding monoubiquitylation, but within the region of RNF168's

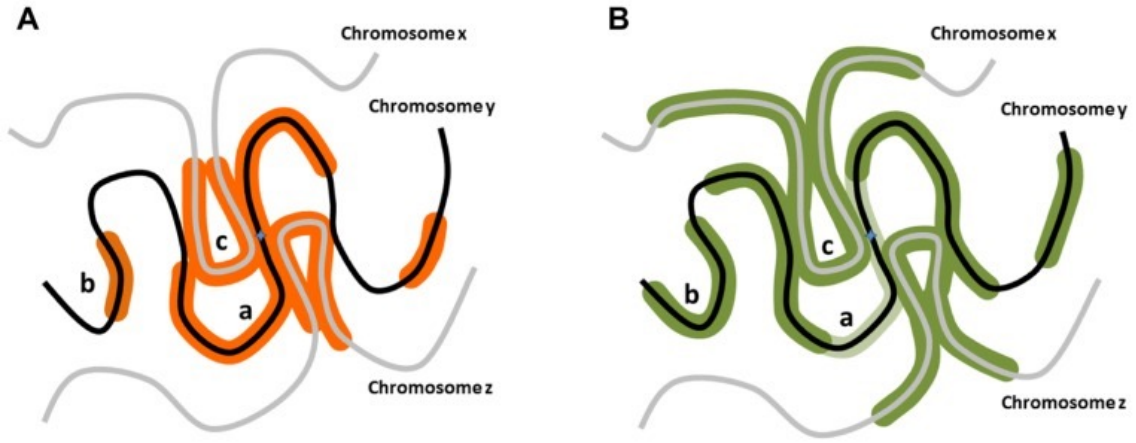

Figure 5.1. Potential distribution of DNA damage associated modifications around nascent DSBs

Taken from (Savic 2013). **(A)** When a DSB occurs on a chromosome y, aside from the confirmed linear phosphorylation in the vicinity of the break site along chromosome y (a), H2AX could be phosphorylated on distal chromosomal regions of the same chromosome (b), or on regions of different chromosomes (chromosomes x, z) in the vicinity of the break site (c). **(B)** RNF168 polyubiquitylation-dependent 53BP1 distribution could exhibit distribution analogous to γH2AX, but potentially more expanded distally from the break site. Notably, in G2 stage of the cell cycle in particular, 53BP1 distribution pattern may be only partially overlapping with the γH2AX region as it is excluded from the vicinity of the break site bound by BRCA1 (light green; (Chapman et al. 2012)

autoregulatory signal amplification. This suggests that 53BP1 may be able to spread away from DSBs in a three-dimensional manner, as hypothesised with γH2AX.

Previous studies have implicated both and ATM (Kruhlak *et al.*, 2007; Shanbhag *et al.*, 2010), and DNA-PK (Pankotai *et al.*, 2012), in inducing break-associated gene repression, together with the components in the polyubiquitylation pathway and the PBAF chromatin remodelling complex (Ui, Nagaura and Yasui, 2015). Most of these proteins are regionally recruited to the vicinity of nascent DSBs, not directly at the break site itself. Such recruitment is guided by DDR mediated chromatin changes; thus, it is reasonable to speculate that if they spread spherically into undamaged chromatin, that the factors involved in gene repression would follow suit. (**Fig. 5.2**)**.** If true, this would be a paradigm shift in our understanding of the effect of the DDR signalling on the function of neighbouring chromatin.

5.1.2 Conclusion

Since the seminal discovery of γH2AX, the changes to chromatin induced by DNA damage have been the subject of intense investigation. Significant advances have been made in elucidating the interaction networks governing the DDR and the spatial organisation of this network. However, the spatial organisation of γH2AX around a DSB in mammals is still yet to be fully uncovered. The formation of γH2AX is a key component in DDR signalling at DSBs and plays an important role in DNA repair. Initial reports have indicated some sort of spatial regulation of the DDR, but the question of whether γH2AX accumulates *in trans* in a non-linear fashion has been unanswered. Presently, many investigations into the mechanisms that regulate γH2AX are conducted using two-

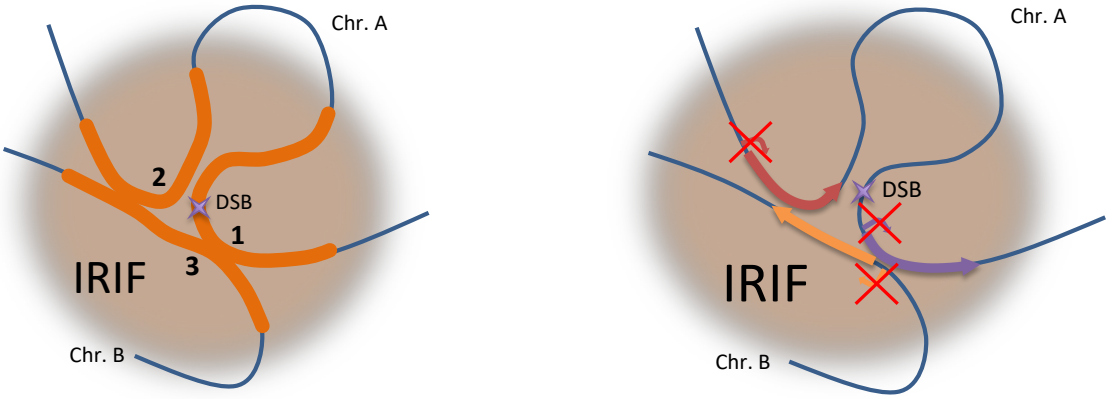

Spatial organisation model

Transcriptional consequence hypothesis

Figure 5.2. Spatial IRIF model

IRIF, as seen by immunofluorescence, are probably not a representation of γH2AX or 53BP1 spreading linearly. Rather, they are present at any chromatin segment (orange) found in the vicinity of the nascent break (star): *in cis* proximal to the break site (**1**), at regions distal to the break site, but folded into proximity (**2**) or regions of other chromosomes, if they happen to be in the break vicinity as well (**3**). Spreading of chromatin changes in trans are indicative of the broader function of DDR signalling in the proximity of the break. One of the more striking consequences of DDR signalling is localised transcriptional silencing. Although verified only *in cis*, the potential ability of the DDR machinery to affect the chromatin structure of non-linearly adjacent DNA segments allows speculation to be made that other DDR functions, namely transcriptional repression, can occur *in trans* as well.

dimensional IF techniques. Although IF based studies are informative, they cannot provide information regarding the density of γH2AX at specific chromosomal sequences; ChIP based analyses offer this possibility. In this thesis the steps I took to develop an experimental system in which two distinct chromatin regions would be induced to associate through the use of a novel fusion protein have been laid out. I constructed two DNA binding arrays and stably inserted them into the genome of U2OS human osteosarcoma cells, with one array also containing an I-SceI endonuclease target site. ChIP would then be performed to look for the extent of the spread of γH2AX *in cis* and *in trans*. Unfortunately, the fusion protein was ultimately unable to induce association of the distinct chromatin regions. However, a functional cell based inducible association system would offer a specific and targeted approach to addressing the spatial effect of a DSB on chromatin.

5.2 Dynamics of Distinct Chromosomal Loci and Factors that Affect DSB Mobility

5.2.1 Chromatin motion and DSB mobility

In this thesis I used a cell-based system in which the dynamics of a single DSB at a specific genomic locus could be compared to the dynamics of another intact genomic locus in living cells, using time-lapse microscopy. Both genomic loci were visualised using the LacI-lacO and TetR-tetO binding systems.

Early investigations often depicted the nucleus as a static structure, containing immobile chromatin held in precise positions. However, constant changes in the composition of nucleosomes, posttranscriptional modifications of histones and shifts in

nucleosome positioning give a clearer picture of the dynamic nature of chromatin (Campos and Reinberg, 2009). Various reports have highlighted the role of higher-order chromatin structure, chromatin dynamics and the non-random organisation of the genome in the maintenance of genomic integrity (Misteli and Soutoglou, 2009). These studies explored the biological implications of chromatin dynamics by following both intact and damaged chromatin in fixed and living cells. Some of these studies utilised methodologies that are indirect, such as tracking of DNA damage repair foci formed by fluorescently tagging repair proteins after DNA damage (Jakob *et al.*, 2009). The spatio-temporal characteristics of commonly established markers of DSBs such as γH2AX and 53BP1 suggest that they should be considered as indirect markers of DSBs. Other studies used indirect methods such as incorporating labelled deoxy-NTP (dNTP) analogues during replication (Zink *et al.*, 1999), or expressing core histones tagged with photoactivatable fluorescent proteins after laser induced DNA damage (Kruhlak *et al.*, 2006). While these studies have provided considerable insights into repair dynamics and the dynamics of chromatin, undamaged and broken alike, they are limited in their ability to score the dynamics of specific chromosomal loci.

The development GFP-Lac repressor (LacI) fusion proteins that were able to bind lacO arrays integrated in the genome of yeast cells enabled the microscopic analysis of the position of chromosomal loci in living cells (Robinett *et al.*, 1996). The LacI-lacO system was followed by development of the TetR-GFP-tetO system (Michaelis, Ciosk and Nasmyth, 1997), making it possible to track the movement of tagged chromosomal loci in yeast accurately and independently of nuclear movement. In these systems the GFP-fused repressors concentrate at their respective operator sites, generating a visible fluorescent spot.

I have demonstrated that a chromosomal locus containing a single DSB exhibited less motion, a lower average displacement per time step and roamed a smaller area of the nucleus than a distinct undamaged chromosomal locus. This observation was in agreement with studies by Soutoglou et al. (2007) who demonstrated a positional stability of a single I-SceI-induced DSB and by Becker et al. (2014a) who confirmed a general positional stability of damaged chromatin domains with limited mobility in a sub-micron range. Additional studies have also reported relatively immobile DSBs (Falk *et al.*, 2007; Jakob *et al.*, 2009)**.** However, other studies have revealed contrasting data pointing to an increased mobility and large-scale movements of DSBs (J. A. Aten *et al.*, 2004; Gandhi *et al.*, 2012; Krawczyk *et al.*, 2012; Cho *et al.*, 2014). It is clear that there are mixed conclusions in the current literature regarding mobility of DSBs and DSB-containing chromatin regions in mammalian cells. Contradictory reports could be due to a number of different factors: significant differences between the model systems used and the epigenetic patterns of the models, the number of induced DSBs, the way breaks are visualised and the way their mobility is measured. Other important factors to consider are the phase of the cell cycle in which DSBs are induced, the chromatin context of the DSB and the mechanism of DNA repair employed. Another plausible explanation for the discrepancies of reports of DSB mobility could lie in the nature of the broken locus. Krawczyk et al. 2012 showed that DSBs induced by the topoisomerase II inhibitor etoposide, were substantially more mobile than DSBs generated by irradiation; two methods that are likely to generate breaks at different positions throughout the genome. Another example of the position of DSBs in the genome dictating mobility was presented by (Cho *et al.*, 2014), who observed a difference in mobility between sub-telomeric DSBs and more internal DSBs. The method of introduction of DSBs could also

be a factor in the contradictory reports of DSB mobility. High-LET particles and microlasers, frequently used in studies to generate DSBs, produce a high density of DNA breaks at the site of induction (Sachs, Chen and Brenner, 1997). Such a high density of breaks may lead to chromatin fragmentation, releasing short DNA fragments that could be more mobile than DSBs generated by other methods. Accordingly, high clustering and mobility was observed after exposure to high energy α-particles (J. A. Aten *et al.*, 2004), while irradiation with ultra-soft-X-rays resulted in immobile lesions (Nelms *et al.*, 1998).

Despite a higher-order spatial organisation, chromosomes in the interphase nucleus move constantly. Consistent with the higher-order structure of the genome, whole chromosomes undergo Brownian motion within a small nuclear area and this confinement is evolutionarily conserved from budding yeast to mammalian cells (Masuzawa *et al.*, 2000; Heun *et al.*, 2001; Chubb *et al.*, 2002). The properties of chromatin mobility differ quantitatively between organisms however. Movement of undamaged loci can be followed in living cells by taking measurements of the position of a locus over time and calculating its MSD. From the MSD, quantitative movement parameters such as the diffusion coefficient can be calculated. Work from several studies has established that human loci have smaller diffusion coefficients than budding yeast; 4.8×10^{-5} to 1.25×10^{-4} $\mu m^2/s$ for human cells (Görisch, Lichter and Rippe, 2005; Jegou *et al.*, 2009) and 5×10^{-4} to 1×10^{-3} $\mu m^2/s$ for budding yeast (Marshall *et al.*, 1997; Dion *et al.*, 2012; Miné-Hattab and Rothstein, 2012). This indicates that human chromatin experiences greater resistance to motion than yeast chromatin. The diffusion coefficient I calculated for the undamaged lacO locus in the human U2OS-tetO-lacO-I-sceI cell line in this thesis was 1.22×10^{-4} $\mu m^2/s$, which is in agreement with the values for

human cells. Because human nuclei are approximately 80 times larger than yeast nuclei, it is expected that the total nuclear volume that chromosomal loci can explore in human cells is much smaller than in yeast. In addition, the mammalian genome is considerably larger than the yeast genome. Subsequently, DNA organisation is more constrained in mammalian nuclei than in yeast.

Seminal work undertaken by (Marshall *et al.*, 1997), showed that chromatin movement undergoes a diffusive random walk motion within the nucleus. However, this diffusive motion is constrained such that although chromatin can diffuse freely over sufficiently small spatial scales, a given chromosome region is confined to a small sub-region of the nucleus. Similarly, observation of all MSD graphs in this thesis suggested that both damaged and intact chromosomal loci underwent a mixture of random Brownian motion and anomalous sub-diffusion. Directional motion, such as that mediated by motor proteins would lead to an upwardly curving parabolic curve. This was not evident in my data therefore I can conclude the motion of chromosomal loci I observed is not a type of directed motility.

The observation in this thesis that a broken chromosomal locus exhibits reduced mobility compared to an intact undamaged locus has implications for the mechanism by which chromosomal translocations might form. As DSBs exhibit a limited range of motion they are unable to diffuse through the nucleus in the search for a translocation partner. The requirement for a chromosomal translocation to take place is the illegitimate joining of two DSBs. Therefore, it could be posited that translocations occur predominantly among neighbouring chromosomes whose positioning results in the interaction of two DSBs on distinct chromosomes. The interaction of these DSBs would

arise as part of their locally constrained motion. Soutoglou et al. 2007 demonstrated that in the absence of Ku80, chromosome ends separate and the majority of them do not undergo translocation and remain unrepaired. As such, there is no requirement for a long-range motion of DSBs to form translocations. A key functional implication of the reduced mobility of DSBs could be the protective role against genomic instability. An increased mobility of DSBs might increase the chance of an interaction between distant DSBs, however, limited DSB movement would prevent the spontaneous joining of two distant DSBs, as they would not be brought into spatial proximity. This might facilitate local repair of at least one of the breaks before they have chance to interact and join to form a translocation. Intriguingly, in yeast, in which long-range movements of DSBs have been evidenced, recombination sites on distinct chromosomes are significantly more frequent than in mammalian cells (Haber and Leung, 1996).

5.2.2 Influence of DDR kinases on DSB mobility

Induction of a DSB activates a complex signalling cascade to promote DNA repair. Initiated by binding of the MRN complex, ATM is recruited as an inactive dimer and activated as a monomer through autophosphorylation of serine 1981. DNA-PKcs, another member of the PIKK family is also recruited to sites of DSBs and participates in DNA damage signalling (Shiloh, 2003). Since phosphorylation by ATM and DNA-PKcs plays a significant role in DSB repair, I analysed the effect of ATM and DNA-PKcs activity on DSB mobility. The specific small molecule inhibitors Ku55933 and Nu7441 were used to inhibit ATM and DNA-PKcs respectively (Veuger *et al.*, 2003; Hickson *et al.*, 2004; Griffin *et al.*, 2005). The inhibitory qualities of Ku55933 and Nu7441 have been well characterised; exhibiting IC50 values for ATM and DNA-PKcs of 13 nM and 14nM

respectively in vitro. Through examination and analysis of MSD curves, a reduction in the MSD from 2.13 μm^2 for the wild-type DSB-containing tetO locus to 1.8 μm^2 for the ATM inhibited DSB-containing tetO locus was found at the end of the 4-hour observation period **(Fig. 4.17).** The reduction in mobility was statistically significant and led to a reduction of the sampled volume within the cell nucleus. This result is in agreement with a study by (Becker *et al.*, 2014a) , who showed that mobility of 53BP1-GFP foci was confined due to ATM inhibition. Another study demonstrated that persistent IRIF in cells treated with ATM inhibitor were significantly less mobile compared with IRIF imaged early after irradiation (Krawczyk *et al.*, 2012). I observed a strong decrease in the diffusion coefficient for the ATM inhibited DSB-containing locus and the bend observed in the MSD curve suggested a confinement of DSB mobility. However, inhibition of DNA-PKcs did not affect mobility of the DSB-containing tetO locus, suggesting a role for ATM kinase activity but not DNA-PKcs activity in the dynamics of DSBs. This observation was similar to that reported by (Caron *et al.*, 2015) who demonstrated that AsiSI-induce DSBs are able to cluster within repair centres in an ATM-dependent, but DNA-PKcs-independent manner.

As alluded to earlier in this chapter, a reduced mobility of DSBs could have important physiological consequences. If broken chromosome ends were highly mobile within the nucleus, the probability of illegitimate joining would be high every time two DSBs occurred within the same cell nucleus. A reduced mobility prevents illegitimate joining of spontaneously occurring distant DSBs since they cannot be brought into spatial proximity. The data presented in chapter 4 indicates that the kinase activity of ATM and not DNA-PKcs plays a significant role in the dynamics of DSBs, (V. Roukos *et al.*, 2013) contrastingly reported that inhibition of ATM or DNA-PK did not have any effect

on the number of DSBs that were able to pair. However, inhibition of DNA-PK increased chromosomal translocation frequency by almost an order of magnitude. Moreover, when the catalytic subunit of DNAPK was eliminated by siRNA, an increase similar to that observed after Ku70 knockdown was seen (Weinstock, Brunet and Jasin, 2007). This result distinguishes the mechanisms of DSB pairing and translocation formation and indicates that the kinase activity of DNAPK is essential to suppress translocations with no involvement in the physical pairing of DSBs.

ATM-dependent chromatin changes promote a local environment conducive for repair and the resulting chromatin context at the damaged locus may affect DSB mobility. Histone variant incorporation, histone PTMs and ATP-dependent chromatin remodelling are three processes that are key and play a direct role in the cellular response to DSBs (Shi and Oberdoerffer, 2012). Changes of the chromatin status at the damaged locus lead to a de-compaction and remodelling of the chromatin fibre to increase accessibility of the DSB for repair machinery. It is tempting to speculate that chromatin remodelling of chromatin could lead to an increased mobility of DSBs. In yeast, deletion of the actin-like protein 8 (Arp8) chromatin remodelling complex led to a decreased mobility of a DSB (Neumann *et al.*, 2012). In addition, in a recent study (Amitai *et al.*, 2017) used a quantitative 3D structured illumination microscopy (3D-SIM) technique that monitored the volume of a genomic locus to demonstrate that expansion of chromatin following a DSB requires the INO80 chromatin remodelling complex. However in mammalian cells, inhibition of TIP60, the major chromatin remodelling factor at DSBs did not affect DSB mobility (Jackson, Downs and Lowndes, 2000b; Ziv *et al.*, 2006; Sun, Jiang and Price, 2010).

Upon DSB induction, multiple lines of evidence point to a subsequent change in chromatin condensation. Several studies have reported that nuclease accessibility is enhanced at damaged chromatin in yeast and mammals, in an ATM and γH2AX-dependent manner (Aaron A Goodarzi *et al.*, 2008). The ATM-dependent phosphorylation of KAP1 following a DSB alters KAP-1 association with nuclease-resistant chromatin (Aaron A Goodarzi *et al.*, 2008) and causes 'global' nucleosome relaxation (Ziv *et al.*, 2006). Phosphorylation of histone H2AX by ATM following a DSB changes the folding of a chromatin fibre by de-stabilising the interaction between DNA and the H2AX-H2B dimer (Jackson, Downs and Lowndes, 2000a). In addition it has been shown that epigenetic modifications at the original sites of DSBs showed local chromatin decondensation manifested by increased H4K5 acetylation and decreased H3K9 dimethylation (Falk *et al.*, 2007; Robinson *et al.*, 2008). Based on the current literature, it is possible then to posit that the reduction in mobility of a single DSB that I observed in this thesis, is caused by a change in chromatin condensation state. The observation that the MSD curve shows a distinct confinement following ATM kinase inhibition suggests a mechanism of chromatin relaxation via its enzymatic activity.

It is important to consider that alternative or concerted actions could cause the observed reduction of a DSB after inhibition of ATM. Following DSB induction, ATM undergoes spatial re-localisation and catalytic activation. Although the total amount of nuclear ATM does not change (Brown *et al.*, 1997), a fraction is rapidly recruited to DNA break sites where the majority of it has been shown to stay for several hours (Andegeko *et al.*, 2001). ATM thus becomes an active component of the protein architecture that associates with the DSB site, and is responsible, either directly or indirectly, for numerous phosphorylation events and other PTMs within this structure. Initial reports

suggested that the physiological consequences of loss of ATM may not be the same as harbouring the inactive protein (Choi *et al.*, 2010). Further evidence to support this finding was obtained using mice with ATM mutations. ATM-knockout mice have long been known to recapitulate most symptoms characteristic of ataxia telangiectasia, with the exception of neurodegeneration, and so these mice presented a relatively mild phenotype (Barlow *et al.*, 1996; Elson *et al.*, 1996; Xu *et al.*, 1996). Strikingly, mice that produced physiological levels of kinase-dead ATM died early in embryogenesis, and expression of kinase-dead ATM in the immune system caused genomic instability in lymphoid cells (Daniel *et al.*, 2012; Yamamoto *et al.*, 2012). The mechanism for this observation is not yet understood. But as kinase-dead ATM was still recruited to sites of DSBs, it is possible that the presence of catalytically inactive ATM within the protein architecture severely disturbs the damage response network. It may also be possible to speculate that following treatment with ATM inhibitor, the presence of kinase dead ATM at DSB sites might hinder their mobility.

5.2.3 Conclusion

Since the first published live imaging experiments of the dynamics of chromatin by in vivo single particle tracking (Marshall *et al.*, 1997), there has been extensive investigation into the regulation and biological function of DNA movement. Unlike the directional separation of sister chromatids in mitosis, the motion of interphase chromatin is stochastic. Chromatin movement in eukaryotic nuclei is confined to sub-nuclear volumes and can be described as sub-diffusive, indicating that internal forces constrain chromatin movement (Chubb *et al.*, 2002; Bystricky, 2015). Movement of damaged chromatin in yeast has been established and is thought to facilitate the long-

range search for sequence homology during DNA DSB repair (Miné-Hattab and Rothstein, 2012). In mammals, a number of factors including the chromatin context of a DSB and the method of damage induction, influence whether DSB containing chromatin will show enhanced or reduced movement following damage induction. Various methods have been used to induce DNA damage and to visualise the spatial dynamics of DSBs. Use of the LacI-lacO and TetR-tetO binding approach, together with insertion of a single site-specific DSB generated by I-SceI endonuclease to visualise the dynamics of chromosomal loci, has been well established in yeast systems. This approach has also been used utilised in mammalian systems to monitor the mobility of DSBs (Soutoglou, Jonas F Dorn, *et al.*, 2007; V. Roukos *et al.*, 2013). However, a direct comparison of the mobility of a single DSB-containing chromosomal locus and an undamaged intact locus, under identical conditions in the same nucleus has been lacking. The system I have developed offers a precise method of directly monitoring mobility of a single DSB in mammalian cells.

In this thesis I have demonstrated that the mobility of a single I-SceI-induced DSB-containing chromosomal locus is reduced compared to an undamaged chromosomal locus. Furthermore, the data presented in thesis shows that the reduction in the mobility of an I-SceI-induced DSB is compounded by treatment with an ATM inhibitor but not a DNA-PKcs inhibitor. This suggests that the kinase activity of ATM and not the kinase activity of DNA-PKcs plays a significant role in the dynamics of DSBs. The picture painted by these results is one consisting of a reduction in movement of a chromosomal locus upon induction of a DSB, followed by an increase in movement caused by the activity of ATM at the break site. A reduced mobility of a DSB could have

implications in facilitating repair locally and might afford the cell an opportunity to repair a single break before any potential interaction with another DSB.

Finally, further insights into how DSB mobility impacts on genome stability could be achieved through the use of advanced time-lapse microscopy and super-resolution techniques, high resolution genome-wide approaches such as ChIP-seq and Hi-C, combined with the ability to induce targeted DSBs at different genomic locations.

Bibliography

Ahel, I. *et al.* (2006) 'The neurodegenerative disease protein aprataxin resolves abortive DNA ligation intermediates', *Nature*. Nature Publishing Group, 443(7112), pp. 713–716. doi: 10.1038/nature05164.

Ahnesorg, P., Smith, P. and Jackson, S. P. (2006) 'XLF interacts with the XRCC4-DNA ligase IV complex to promote DNA nonhomologous end-joining.', *Cell*, 124(2), pp. 301–13. doi: 10.1016/j.cell.2005.12.031.

Al-Hakim, A. *et al.* (2010) 'The ubiquitous role of ubiquitin in the DNA damage response', *DNA Repair*, 9(12), pp. 1229–1240. doi: 10.1016/j.dnarep.2010.09.011.

Allers, T. and Lichten, M. (2001) 'Differential timing and control of noncrossover and crossover recombination during meiosis.', *Cell*, 106(1), pp. 47–57.

Alpi, A. F. and Patel, K. J. (2009) 'Monoubiquitylation in the Fanconi anemia DNA damage response pathway', *DNA Repair*, 8(4), pp. 430–435. doi: 10.1016/j.dnarep.2009.01.019.

Álvarez-Quilón, A. *et al.* (2014) 'ATM specifically mediates repair of double-strand breaks with blocked DNA ends.', *Nature communications*. Nature Publishing Group, 5, p. 3347. doi: 10.1038/ncomms4347.

Amitai, A. *et al.* (2017) 'Visualization of Chromatin Decompaction and Break Site Extrusion as Predicted by Statistical Polymer Modeling of Single-Locus Trajectories.', *Cell reports*, 18(5), pp. 1200–1214. doi: 10.1016/j.celrep.2017.01.018.

Andegeko, Y. *et al.* (2001) 'Nuclear retention of ATM at sites of DNA double strand breaks.', *The Journal of biological chemistry*, 276(41), pp. 38224–30. doi: 10.1074/jbc.M102986200.

Arlander, S. J. H. *et al.* (2008) 'DNA protein kinase-dependent G2 checkpoint revealed following knockdown of ataxia-telangiectasia mutated in human mammary epithelial cells.', *Cancer research*, 68(1), pp. 89–97. doi: 10.1158/0008-5472.CAN-07-0675.

Aten, J. A. *et al.* (2004) 'Dynamics of DNA double-strand breaks revealed by clustering of damaged chromosome domains.', *Science (New York, N.Y.)*, 303(5654), pp. 92–5. doi:

10.1126/science.1088845.

Aten, J. A. *et al.* (2004) 'Dynamics of DNA Double-Strand Breaks Revealed by Clustering of Damaged Chromosome Domains', *Science*, 303(5654), pp. 92–95. doi: 10.1126/science.1088845.

Aymard, F. *et al.* (2017) 'Genome-wide mapping of long-range contacts unveils clustering of DNA double-strand breaks at damaged active genes', *Nature Structural & Molecular Biology*, 24(4), pp. 353–361. doi: 10.1038/nsmb.3387.

Aymard, F. and Legube, G. (2016) 'A TAD closer to ATM', *Molecular & Cellular Oncology*, 3(3), p. e1134411. doi: 10.1080/23723556.2015.1134411.

Bakkenist, C. J. and Kastan, M. B. (2003) 'DNA damage activates ATM through intermolecular autophosphorylation and dimer dissociation', *Nature*, 421(6922), pp. 499–506. doi: 10.1038/nature01368.

Baldeyron, C. *et al.* (2011) 'HP1α recruitment to DNA damage by p150CAF-1 promotes homologous recombination repair', *The Journal of Cell Biology*, 193(1), pp. 81–95. doi: 10.1083/jcb.201101030.

Baldock, R. A. *et al.* (2015) 'ATM Localization and Heterochromatin Repair Depend on Direct Interaction of the 53BP1-BRCT2 Domain with γH2AX.', *Cell reports*. Elsevier, 13(10), pp. 2081–9. doi: 10.1016/j.celrep.2015.10.074.

Barlow, C. *et al.* (1996) 'Atm-deficient mice: a paradigm of ataxia telangiectasia.', *Cell*, 86(1), pp. 159–71.

Bassing, C. H. *et al.* (2002) 'Increased ionizing radiation sensitivity and genomic instability in the absence of histone H2AX', *Proceedings of the National Academy of Sciences*, 99(12), pp. 8173–8178. doi: 10.1073/pnas.122228699.

Bassing, C. H. *et al.* (2003) 'Histone H2AX: a dosage-dependent suppressor of oncogenic translocations and tumors.', *Cell*, 114(3), pp. 359–70.

Beamish, H. J. *et al.* (2000) 'The C-terminal conserved domain of DNA-PKcs, missing in the SCID mouse, is required for kinase activity.', *Nucleic acids research*, 28(7), pp. 1506–13.

Becker, A. *et al.* (2014a) 'ATM alters the otherwise robust chromatin mobility at sites of DNA double-strand breaks (DSBs) in human cells.', *PloS one*. Edited by R. Hancock, 9(3), p. e92640. doi: 10.1371/journal.pone.0092640.

Becker, A. *et al.* (2014b) 'ATM Alters the Otherwise Robust Chromatin Mobility at Sites of DNA Double-Strand Breaks (DSBs) in Human Cells', *PLoS ONE*. Edited by R. Hancock. Public Library of Science, 9(3), p. e92640. doi: 10.1371/journal.pone.0092640.

Bekker-Jensen, S. *et al.* (2010) 'HERC2 coordinates ubiquitin-dependent assembly of DNA repair factors on damaged chromosomes', *Nature Cell Biology*, 12(1), pp. 80–86. doi: 10.1038/ncb2008.

Berger, J. M. *et al.* (1996) 'Structure and mechanism of DNA topoisomerase II', *Nature*, 379(6562), pp. 225–232. doi: 10.1038/379225a0.

Bernstein, N. K. *et al.* (2005) 'The molecular architecture of the mammalian DNA repair enzyme, polynucleotide kinase.', *Molecular cell*. Elsevier, 17(5), pp. 657–70. doi: 10.1016/j.molcel.2005.02.012.

Beucher, A. *et al.* (2009) 'ATM and Artemis promote homologous recombination of radiation-induced DNA double-strand breaks in G2', *The EMBO Journal*, 28(21), pp. 3413–3427. doi: 10.1038/emboj.2009.276.

Bewersdorf, J., Bennett, B. T. and Knight, K. L. (2006) 'H2AX chromatin structures and their response to DNA damage revealed by 4Pi microscopy', *Proceedings of the National Academy of Sciences*, 103(48), pp. 18137–18142. doi: 10.1073/pnas.0608709103.

Bianco, P. R., Tracy, R. B. and Kowalczykowski, S. C. (1998) 'DNA strand exchange proteins: a biochemical and physical comparison.', *Frontiers in bioscience : a journal and virtual library*, 3, pp. D570-603.

Botuyan, M. V. *et al.* (2006) 'Structural Basis for the Methylation State-Specific Recognition of Histone H4-K20 by 53BP1 and Crb2 in DNA Repair', *Cell*, 127(7), pp. 1361–1373. doi: 10.1016/j.cell.2006.10.043.

Boveri, T. (1914) *Zur Frage der Entstehung maligner Tumoren*. Jena : G. Fischer,. Available at: https://searchworks.stanford.edu/view/10860530 (Accessed: 23 May

2018).

BRANZEI, D. and FOIANI, M. (2007) ‘Interplay of replication checkpoints and repair proteins at stalled replication forks’, *DNA Repair*, 6(7), pp. 994–1003. doi: 10.1016/j.dnarep.2007.02.018.

Brown, K. D. *et al.* (1997) ‘The ataxia-telangiectasia gene product, a constitutively expressed nuclear protein that is not up-regulated following genome damage.’, *Proceedings of the National Academy of Sciences of the United States of America*. National Academy of Sciences, 94(5), pp. 1840–5.

Burden, D. A. and Osheroff, N. (1998) ‘Mechanism of action of eukaryotic topoisomerase II and drugs targeted to the enzyme’, *Biochimica et Biophysica Acta (BBA) - Gene Structure and Expression*, 1400(1–3), pp. 139–154. doi: 10.1016/S0167-4781(98)00132-8.

Burma, S. *et al.* (2001) ‘ATM Phosphorylates Histone H2AX in Response to DNA Double-strand Breaks’, *Journal of Biological Chemistry*, 276(45), pp. 42462–42467. doi: 10.1074/jbc.C100466200.

Bystricky, K. (2015) ‘Chromosome dynamics and folding in eukaryotes: Insights from live cell microscopy.’, *FEBS letters*, 589(20 Pt A), pp. 3014–22. doi: 10.1016/j.febslet.2015.07.012.

Callebaut, I. and Mornon, J. P. (1997) ‘From BRCA1 to RAP1: a widespread BRCT module closely associated with DNA repair.’, *FEBS letters*, 400(1), pp. 25–30.

Callen, E. *et al.* (2013) ‘53BP1 Mediates Productive and Mutagenic DNA Repair through Distinct Phosphoprotein Interactions’, *Cell*. Elsevier, 153(6), pp. 1266–1280. doi: 10.1016/j.cell.2013.05.023.

Calsou, P. *et al.* (2003) ‘Coordinated assembly of Ku and p460 subunits of the DNA-dependent protein kinase on DNA ends is necessary for XRCC4-ligase IV recruitment.’, *Journal of molecular biology*, 326(1), pp. 93–103.

Campos, E. I. and Reinberg, D. (2009) ‘Histones: Annotating Chromatin’, *Annual Review of Genetics*, 43(1), pp. 559–599. doi: 10.1146/annurev.genet.032608.103928.

Caron, P. *et al.* (2015) 'Non-redundant Functions of ATM and DNA-PKcs in Response to DNA Double-Strand Breaks', *Cell Reports*, 13(8), pp. 1598–1609. doi: 10.1016/j.celrep.2015.10.024.

Celeste, A. *et al.* (2002) 'Genomic Instability in Mice Lacking Histone H2AX', *Science*, 296(5569), pp. 922–927. doi: 10.1126/science.1069398.

Celeste, A., Difilippantonio, S., *et al.* (2003) 'H2AX haploinsufficiency modifies genomic stability and tumor susceptibility.', *Cell*, 114(3), pp. 371–383.

Celeste, A., Fernandez-Capetillo, O., *et al.* (2003) 'Histone H2AX phosphorylation is dispensable for the initial recognition of DNA breaks', *Nature Cell Biology*, 5(7), pp. 675–679. doi: 10.1038/ncb1004.

Chan, D. W. and Lees-Miller, S. P. (1996) 'The DNA-dependent protein kinase is inactivated by autophosphorylation of the catalytic subunit.', *The Journal of biological chemistry*, 271(15), pp. 8936–41.

Chapman, J. R. *et al.* (2012) 'BRCA1-associated exclusion of 53BP1 from DNA damage sites underlies temporal control of DNA repair.', *Journal of cell science*, 125(Pt 15), pp. 3529–34. doi: 10.1242/jcs.105353.

Chapman, J. R. and Jackson, S. P. (2008) 'Phospho-dependent interactions between NBS1 and MDC1 mediate chromatin retention of the MRN complex at sites of DNA damage', *EMBO reports*, 9(8), pp. 795–801. doi: 10.1038/embor.2008.103.

Chiolo, I. *et al.* (2011) 'Double-Strand Breaks in Heterochromatin Move Outside of a Dynamic HP1a Domain to Complete Recombinational Repair', *Cell*, 144(5), pp. 732–744. doi: 10.1016/j.cell.2011.02.012.

Cho, N. W. *et al.* (2014) 'Interchromosomal homology searches drive directional ALT telomere movement and synapsis.', *Cell*, 159(1), pp. 108–121. doi: 10.1016/j.cell.2014.08.030.

Choi, S. *et al.* (2010) 'Inhibition of ATM kinase activity does not phenocopy ATM protein disruption: implications for the clinical utility of ATM kinase inhibitors.', *Cell cycle (Georgetown, Tex.)*. Taylor & Francis, 9(20), pp. 4052–7. doi: 10.4161/cc.9.20.13747.

Chou, D. M. *et al.* (2010) 'A chromatin localization screen reveals poly (ADP ribose)-regulated recruitment of the repressive polycomb and NuRD complexes to sites of DNA damage', *Proceedings of the National Academy of Sciences*, 107(43), pp. 18475–18480. doi: 10.1073/pnas.1012946107.

Chubb, J. R. *et al.* (2002) 'Chromatin motion is constrained by association with nuclear compartments in human cells.', *Current biology : CB*, 12(6), pp. 439–45.

Cimprich, K. A. and Cortez, D. (2008) 'ATR: an essential regulator of genome integrity', *Nature Reviews Molecular Cell Biology*, 9(8), pp. 616–627. doi: 10.1038/nrm2450.

CLARK, R. J. and FELSENFELD, G. (1971) 'Structure of Chromatin', *Nature New Biology*. Nature Publishing Group, 229(4), pp. 101–106. doi: 10.1038/newbio229101a0.

Clerici, M. *et al.* (2008) 'The Yku70–Yku80 complex contributes to regulate double-strand break processing and checkpoint activation during the cell cycle', *EMBO reports*, 9(8), pp. 810–818. doi: 10.1038/embor.2008.121.

Cong, L. *et al.* (2013) 'Multiplex genome engineering using CRISPR/Cas systems.', *Science (New York, N.Y.)*. NIH Public Access, 339(6121), pp. 819–23. doi: 10.1126/science.1231143.

Cooper, T. J. *et al.* (2014) 'Homeostatic regulation of meiotic DSB formation by ATM/ATR', *Experimental Cell Research*, 329(1), pp. 124–131. doi: 10.1016/j.yexcr.2014.07.016.

Cooper, T. J., Garcia, V. and Neale, M. J. (2016) 'Meiotic DSB patterning: A multifaceted process', *Cell Cycle*, 15(1), pp. 13–21. doi: 10.1080/15384101.2015.1093709.

Corchero, J. L. and Villaverde, A. (1998) 'Plasmid maintenance in Escherichia coli recombinant cultures is dramatically, steadily, and specifically influenced by features of the encoded proteins.', *Biotechnology and bioengineering*, 58(6), pp. 625–32.

Cowell, I. G., Durkacz, B. W. and Tilby, M. J. (2005) 'Sensitization of breast carcinoma cells to ionizing radiation by small molecule inhibitors of DNA-dependent protein kinase and ataxia telangiectsia mutated.', *Biochemical pharmacology*, 71(1–2), pp. 13–20. doi: 10.1016/j.bcp.2005.09.029.

Daniel, J. A. *et al.* (2012) 'Loss of ATM kinase activity leads to embryonic lethality in mice', *The Journal of Cell Biology*, 198(3).

Decottignies, A. (2013) 'Alternative end-joining mechanisms: a historical perspective', *Frontiers in Genetics*, 4, p. 48. doi: 10.3389/fgene.2013.00048.

Demple, B. and DeMott, M. S. (2002) 'Dynamics and diversions in base excision DNA repair of oxidized abasic lesions', *Oncogene*, 21(58), pp. 8926–8934. doi: 10.1038/sj.onc.1206178.

Dery, U. *et al.* (2008) 'A Glycine-Arginine Domain in Control of the Human MRE11 DNA Repair Protein', *Molecular and Cellular Biology*, 28(9), pp. 3058–3069. doi: 10.1128/MCB.02025-07.

Dimitrova, N. *et al.* (2008) '53BP1 promotes non-homologous end joining of telomeres by increasing chromatin mobility', *Nature*, 456(7221), pp. 524–528. doi: 10.1038/nature07433.

Dion, V. *et al.* (2012) 'Increased mobility of double-strand breaks requires Mec1, Rad9 and the homologous recombination machinery', *Nature Cell Biology*, 14(5), pp. 502–509. doi: 10.1038/ncb2465.

Dion, V. and Gasser, S. M. (2013) 'Chromatin movement in the maintenance of genome stability.', *Cell*. Elsevier, 152(6), pp. 1355–64. doi: 10.1016/j.cell.2013.02.010.

Doil, C. *et al.* (2009a) 'RNF168 binds and amplifies ubiquitin conjugates on damaged chromosomes to allow accumulation of repair proteins.', *Cell*, 136(3), pp. 435–46. doi: 10.1016/j.cell.2008.12.041.

Doil, C. *et al.* (2009b) 'RNF168 Binds and Amplifies Ubiquitin Conjugates on Damaged Chromosomes to Allow Accumulation of Repair Proteins', *Cell*, 136(3), pp. 435–446. doi: 10.1016/j.cell.2008.12.041.

Doksani, Y. and de Lange, T. (2014) 'The Role of Double-Strand Break Repair Pathways at Functional and Dysfunctional Telomeres', *Cold Spring Harbor Perspectives in Biology*, 6(12), pp. a016576–a016576. doi: 10.1101/cshperspect.a016576.

Dou, H. *et al.* (2010) 'Regulation of DNA Repair through DeSUMOylation and

SUMOylation of Replication Protein A Complex', *Molecular Cell*. Cell Press, 39(3), pp. 333–345. doi: 10.1016/J.MOLCEL.2010.07.021.

Du, L.-L., Nakamura, T. M. and Russell, P. (2006) 'Histone modification-dependent and -independent pathways for recruitment of checkpoint protein Crb2 to double-strand breaks.', *Genes & development*. Cold Spring Harbor Laboratory Press, 20(12), pp. 1583–96. doi: 10.1101/gad.1422606.

Eladad, S. *et al.* (2005) 'Intra-nuclear trafficking of the BLM helicase to DNA damage-induced foci is regulated by SUMO modification', *Human Molecular Genetics*, 14(10), pp. 1351–1365. doi: 10.1093/hmg/ddi145.

Elson, A. *et al.* (1996) 'Pleiotropic defects in ataxia-telangiectasia protein-deficient mice.', *Proceedings of the National Academy of Sciences of the United States of America*, 93(23), pp. 13084–9.

Epstein, F. H. *et al.* (1988) 'The Molecular Genetics of Philadelphia Chromosome–Positive Leukemias', *New England Journal of Medicine*, 319(15), pp. 990–998. doi: 10.1056/NEJM198810133191506.

Falk, M. *et al.* (2007) 'Chromatin dynamics during DSB repair', *Biochimica et Biophysica Acta (BBA) - Molecular Cell Research*, 1773(10), pp. 1534–1545. doi: 10.1016/j.bbamcr.2007.07.002.

Falzon, M., Fewell, J. W. and Kuff, E. L. (1993) 'EBP-80, a transcription factor closely resembling the human autoantigen Ku, recognizes single- to double-strand transitions in DNA.', *The Journal of biological chemistry*, 268(14), pp. 10546–52.

Feng, L. and Chen, J. (2012) 'The E3 ligase RNF8 regulates KU80 removal and NHEJ repair', *Nature Structural & Molecular Biology*. Nature Publishing Group, 19(2), pp. 201–206. doi: 10.1038/nsmb.2211.

Fernandez-Capetillo, O. *et al.* (2002) 'DNA damage-induced G2–M checkpoint activation by histone H2AX and 53BP1', *Nature Cell Biology*, 4(12), pp. 993–997. doi: 10.1038/ncb884.

Fernandez-Vidal, A., Vignard, J. and Mirey, G. (2017) 'Around and beyond 53BP1 Nuclear

Bodies', *International Journal of Molecular Sciences*, 18(12), p. 2611. doi: 10.3390/ijms18122611.

Fradet-Turcotte, A. *et al.* (2013) '53BP1 is a reader of the DNA-damage-induced H2A Lys 15 ubiquitin mark', *Nature*, 499(7456), pp. 50–54. doi: 10.1038/nature12318.

Franco, S. *et al.* (2006) 'H2AX Prevents DNA Breaks from Progressing to Chromosome Breaks and Translocations', *Molecular Cell*, 21(2), pp. 201–214. doi: 10.1016/j.molcel.2006.01.005.

Galanty, Y. *et al.* (2009) 'Mammalian SUMO E3-ligases PIAS1 and PIAS4 promote responses to DNA double-strand breaks', *Nature*, 462(7275), pp. 935–939. doi: 10.1038/nature08657.

Gandhi, M. *et al.* (2012) 'Homologous chromosomes make contact at the sites of double-strand breaks in genes in somatic G0/G1-phase human cells.', *Proceedings of the National Academy of Sciences of the United States of America*, 109(24), pp. 9454–9. doi: 10.1073/pnas.1205759109.

Gilbert, N., Gilchrist, S. and Bickmore, W. A. (2004) 'Chromatin Organization in the Mammalian Nucleus', in *International review of cytology*, pp. 283–336. doi: 10.1016/S0074-7696(04)42007-5.

Goodarzi, A. A. *et al.* (2008) 'ATM signaling facilitates repair of DNA double-strand breaks associated with heterochromatin.', *Molecular cell*, 31(2), pp. 167–77. doi: 10.1016/j.molcel.2008.05.017.

Goodarzi, A. A. *et al.* (2008) 'ATM Signaling Facilitates Repair of DNA Double-Strand Breaks Associated with Heterochromatin', *Molecular Cell*, 31(2), pp. 167–177. doi: 10.1016/j.molcel.2008.05.017.

Goodarzi, A. A. and Jeggo, P. A. (2012) 'The heterochromatic barrier to DNA double strand break repair: how to get the entry visa.', *International journal of molecular sciences*. Multidisciplinary Digital Publishing Institute (MDPI), 13(9), pp. 11844–60. doi: 10.3390/ijms130911844.

Goodarzi, A. A., Kurka, T. and Jeggo, P. A. (2011) 'KAP-1 phosphorylation regulates CHD3

nucleosome remodeling during the DNA double-strand break response.', *Nature structural & molecular biology*, 18(7), pp. 831–9. doi: 10.1038/nsmb.2077.

Görisch, S. M., Lichter, P. and Rippe, K. (2005) 'Mobility of multi-subunit complexes in the nucleus: accessibility and dynamics of chromatin subcompartments', *Histochemistry and Cell Biology*, 123(3), pp. 217–228. doi: 10.1007/s00418-005-0752-y.

Grawunder, U. *et al.* (1997) 'Activity of DNA ligase IV stimulated by complex formation with XRCC4 protein in mammalian cells.', *Nature*, 388(6641), pp. 492–5. doi: 10.1038/41358.

Griffin, R. J. *et al.* (2005) 'Selective benzopyranone and pyrimido[2,1-a]isoquinolin-4-one inhibitors of DNA-dependent protein kinase: synthesis, structure-activity studies, and radiosensitization of a human tumor cell line in vitro.', *Journal of medicinal chemistry*, 48(2), pp. 569–85. doi: 10.1021/jm049526a.

Grove, J. I. *et al.* (2008) 'DNA double strand break repair and crossing over mediated by RuvABC resolvase and RecG translocase', *DNA Repair*, 7(9), pp. 1517–1530. doi: 10.1016/j.dnarep.2008.05.010.

Gudjonsson, T. *et al.* (2012) 'TRIP12 and UBR5 suppress spreading of chromatin ubiquitylation at damaged chromosomes.', *Cell*, 150(4), pp. 697–709. doi: 10.1016/j.cell.2012.06.039.

Guigas, G., Kalla, C. and Weiss, M. (2007) 'The degree of macromolecular crowding in the cytoplasm and nucleoplasm of mammalian cells is conserved.', *FEBS letters*, 581(26), pp. 5094–8. doi: 10.1016/j.febslet.2007.09.054.

Guo, Y. *et al.* (2015) 'ATM-dependent Phosphorylation of the Fanconi Anemia Protein PALB2 Promotes the DNA Damage Response.', *The Journal of biological chemistry*, 290(46), pp. 27545–56. doi: 10.1074/jbc.M115.672626.

Haber, J. E. and Leung, W. Y. (1996) 'Lack of chromosome territoriality in yeast: promiscuous rejoining of broken chromosome ends.', *Proceedings of the National Academy of Sciences of the United States of America*, 93(24), pp. 13949–54.

Haince, J.-F. *et al.* (2007) 'Ataxia Telangiectasia Mutated (ATM) Signaling Network Is

Modulated by a Novel Poly(ADP-ribose)-dependent Pathway in the Early Response to DNA-damaging Agents', *Journal of Biological Chemistry*, 282(22), pp. 16441–16453. doi: 10.1074/jbc.M608406200.

Haince, J.-F. *et al.* (2008) 'PARP1-dependent Kinetics of Recruitment of MRE11 and NBS1 Proteins to Multiple DNA Damage Sites', *Journal of Biological Chemistry*, 283(2), pp. 1197–1208. doi: 10.1074/jbc.M706734200.

Harper, J. W. and Elledge, S. J. (2007) 'The DNA Damage Response: Ten Years After', *Molecular Cell*, 28(5), pp. 739–745. doi: 10.1016/j.molcel.2007.11.015.

Harrigan, J. A. *et al.* (2011) 'Replication stress induces 53BP1-containing OPT domains in G1 cells', *The Journal of Cell Biology*, 193(1), pp. 97–108. doi: 10.1083/jcb.201011083.

Hatimy, A. A. *et al.* (2015) 'Histone H2AX Y142 phosphorylation is a low abundance modification', *International Journal of Mass Spectrometry*. Elsevier, 391, pp. 139–145. doi: 10.1016/J.IJMS.2015.07.028.

Hecht, J. L. and Aster, J. C. (2000) 'Molecular Biology of Burkitt's Lymphoma', *Journal of Clinical Oncology*, 18(21), pp. 3707–3721. doi: 10.1200/JCO.2000.18.21.3707.

Heun, P. *et al.* (2001) 'Chromosome Dynamics in the Yeast Interphase Nucleus', *Science*, 294(5549), pp. 2181–2186. doi: 10.1126/science.1065366.

Hickson, I. *et al.* (2004) 'Identification and characterization of a novel and specific inhibitor of the ataxia-telangiectasia mutated kinase ATM.', *Cancer research*, 64(24), pp. 9152–9. doi: 10.1158/0008-5472.CAN-04-2727.

Hopfner, K.-P. *et al.* (2002) 'The Rad50 zinc-hook is a structure joining Mre11 complexes in DNA recombination and repair', *Nature*. Nature Publishing Group, 418(6897), pp. 562–566. doi: 10.1038/nature00922.

Horigome, C. *et al.* (2014) 'SWR1 and INO80 Chromatin Remodelers Contribute to DNA Double-Strand Break Perinuclear Anchorage Site Choice', *Molecular Cell*, 55(4), pp. 626–639. doi: 10.1016/j.molcel.2014.06.027.

Hsieh, P., Camerini-Otero, C. S. and Camerini-Otero, R. D. (1990) 'Pairing of homologous DNA sequences by proteins: evidence for three-stranded DNA.', *Genes & development*,

4(11), pp. 1951–63.

Huen, M. S. Y. *et al.* (2007) 'RNF8 Transduces the DNA-Damage Signal via Histone Ubiquitylation and Checkpoint Protein Assembly', *Cell*, 131(5), pp. 901–914. doi: 10.1016/j.cell.2007.09.041.

Huen, M. S. Y. and Chen, J. (2010) 'Assembly of checkpoint and repair machineries at DNA damage sites', *Trends in Biochemical Sciences*, 35(2), pp. 101–108. doi: 10.1016/j.tibs.2009.09.001.

Huyen, Y. *et al.* (2004) 'Methylated lysine 79 of histone H3 targets 53BP1 to DNA double-strand breaks', *Nature*, 432(7015), pp. 406–411. doi: 10.1038/nature03114.

Iacovoni, J. S. *et al.* (2010) 'High-resolution profiling of γH2AX around DNA double strand breaks in the mammalian genome', *The EMBO Journal*, 29(8), pp. 1446–1457. doi: 10.1038/emboj.2010.38.

Ikura, T. *et al.* (2007) 'DNA Damage-Dependent Acetylation and Ubiquitination of H2AX Enhances Chromatin Dynamics', *Molecular and Cellular Biology*, 27(20), pp. 7028–7040. doi: 10.1128/MCB.00579-07.

Isogai, S. *et al.* (2010) 'Solution structure of a zinc-finger domain that binds to poly-ADP-ribose', *Genes to Cells*, 15(2), pp. 101–110. doi: 10.1111/j.1365-2443.2009.01369.x.

Iwabuchi, K. *et al.* (1994) 'Two cellular proteins that bind to wild-type but not mutant p53.', *Proceedings of the National Academy of Sciences of the United States of America*. National Academy of Sciences, 91(13), pp. 6098–102.

Jackson, S. P. and Bartek, J. (2009) 'The DNA-damage response in human biology and disease.', *Nature*, 461(7267), pp. 1071–8. doi: 10.1038/nature08467.

Jackson, S. P., Downs, J. A. and Lowndes, N. F. (2000a) 'A role for Saccharomyces cerevisiae histone H2A in DNA repair.', *Nature*, 408(6815), pp. 1001–1004. doi: 10.1038/35050000.

Jackson, S. P., Downs, J. A. and Lowndes, N. F. (2000b) 'A role for *Saccharomyces cerevisiae* histone H2A in DNA repair', *Nature*. Nature Publishing Group, 408(6815), pp. 1001–1004. doi: 10.1038/35050000.

Jackson, S. P. and Durocher, D. (2013) 'Regulation of DNA damage responses by ubiquitin and SUMO.', *Molecular cell*, 49(5), pp. 795–807. doi: 10.1016/j.molcel.2013.01.017.

de Jager, M. *et al.* (2001) 'Human Rad50/Mre11 is a flexible complex that can tether DNA ends.', *Molecular cell*, 8(5), pp. 1129–35. Available at: http://www.ncbi.nlm.nih.gov/pubmed/11741547 (Accessed: 15 May 2018).

Jakob, B. *et al.* (2009) 'Live cell microscopy analysis of radiation-induced DNA double-strand break motion.', *Proceedings of the National Academy of Sciences of the United States of America*. National Academy of Sciences, 106(9), pp. 3172–7. doi: 10.1073/pnas.0810987106.

Jakob, B. *et al.* (2011) 'DNA double-strand breaks in heterochromatin elicit fast repair protein recruitment, histone H2AX phosphorylation and relocation to euchromatin', *Nucleic Acids Research*, 39(15), pp. 6489–6499. doi: 10.1093/nar/gkr230.

Jegou, T. *et al.* (2009) 'Dynamics of telomeres and promyelocytic leukemia nuclear bodies in a telomerase-negative human cell line.', *Molecular biology of the cell*, 20(7), pp. 2070–82. doi: 10.1091/mbc.E08-02-0108.

Jiricny, J. (2006) 'The multifaceted mismatch-repair system', *Nature Reviews Molecular Cell Biology*, 7(5), pp. 335–346. doi: 10.1038/nrm1907.

Joo, H.-Y. *et al.* (2007) 'Regulation of cell cycle progression and gene expression by H2A deubiquitination', *Nature*, 449(7165), pp. 1068–1072. doi: 10.1038/nature06256.

Joung, J. K. and Sander, J. D. (2013) 'TALENs: a widely applicable technology for targeted genome editing', *Nature Reviews Molecular Cell Biology*, 14(1), pp. 49–55. doi: 10.1038/nrm3486.

Kanno, S. *et al.* (2007) 'A novel human AP endonuclease with conserved zinc-finger-like motifs involved in DNA strand break responses', *The EMBO Journal*, 26(8), pp. 2094–2103. doi: 10.1038/sj.emboj.7601663.

Karagiannis, T. C. *et al.* (2007) 'Disparity of histone deacetylase inhibition on repair of radiation-induced DNA damage on euchromatin and constitutive heterochromatin compartments', *Oncogene*, 26(27), pp. 3963–3971. doi: 10.1038/sj.onc.1210174.

Karras, G. I. *et al.* (2005) 'The macro domain is an ADP-ribose binding module', *The EMBO Journal*, 24(11), pp. 1911–1920. doi: 10.1038/sj.emboj.7600664.

Kastan, M. B. *et al.* (1992) 'A mammalian cell cycle checkpoint pathway utilizing p53 and GADD45 is defective in ataxia-telangiectasia.', *Cell*, 71(4), pp. 587–97.

Kearney, L. and Horsley, S. W. (2005) 'Molecular cytogenetics in haematological malignancy: current technology and future prospects', *Chromosoma*, 114(4), pp. 286–294. doi: 10.1007/s00412-005-0002-z.

Kim, J.-A. *et al.* (2007) 'Heterochromatin is refractory to γ-H2AX modification in yeast and mammals', *The Journal of Cell Biology*, 178(2), pp. 209–218. doi: 10.1083/jcb.200612031.

Kim, Y.-C. *et al.* (2009) 'Activation of ATM depends on chromatin interactions occurring before induction of DNA damage', *Nature Cell Biology*, 11(1), pp. 92–96. doi: 10.1038/ncb1817.

Kolas, N. K. *et al.* (2007) 'Orchestration of the DNA-Damage Response by the RNF8 Ubiquitin Ligase', *Science*, 318(5856), pp. 1637–1640. doi: 10.1126/science.1150034.

Krawczyk, P. M. *et al.* (2012) 'Chromatin mobility is increased at sites of DNA double-strand breaks', *Journal of Cell Science*, 125(9), pp. 2127–2133. doi: 10.1242/jcs.089847.

Krishnakumar, R. and Kraus, W. L. (2010) 'The PARP Side of the Nucleus: Molecular Actions, Physiological Outcomes, and Clinical Targets', *Molecular Cell*, 39(1), pp. 8–24. doi: 10.1016/j.molcel.2010.06.017.

Krokan, H. E. *et al.* (2000) 'Base excision repair of DNA in mammalian cells.', *FEBS letters*, 476(1–2), pp. 73–7.

Kruhlak, M. *et al.* (2007) 'The ATM repair pathway inhibits RNA polymerase I transcription in response to chromosome breaks', *Nature*, 447(7145), pp. 730–734. doi: 10.1038/nature05842.

Kruhlak, M. J. *et al.* (2006) 'Changes in chromatin structure and mobility in living cells at sites of DNA double-strand breaks.', *The Journal of cell biology*. The Rockefeller University Press, 172(6), pp. 823–34. doi: 10.1083/jcb.200510015.

Kwon, Y.-I. *et al.* (2012) 'Overexpression of OsRecQl4 and/or OsExo1 Enhances DSB-Induced Homologous Recombination in Rice', *Plant and Cell Physiology*, 53(12), pp. 2142–2152. doi: 10.1093/pcp/pcs155.

Lam, I. and Keeney, S. (2015) 'Mechanism and Regulation of Meiotic Recombination Initiation', *Cold Spring Harbor Perspectives in Biology*, 7(1), p. a016634. doi: 10.1101/cshperspect.a016634.

Lau, I. F. *et al.* (2004) 'Spatial and temporal organization of replicating Escherichia coli chromosomes', *Molecular Microbiology*. Blackwell Science Ltd, 49(3), pp. 731–743. doi: 10.1046/j.1365-2958.2003.03640.x.

Lee, C.-S. *et al.* (2014) 'Dynamics of yeast histone H2A and H2B phosphorylation in response to a double-strand break.', *Nature structural & molecular biology*. NIH Public Access, 21(1), pp. 103–9. doi: 10.1038/nsmb.2737.

Lee, J.-H. and Paull, T. T. (2004) 'Direct Activation of the ATM Protein Kinase by the Mre11/Rad50/Nbs1 Complex', *Science*, 304(5667), pp. 93–96. doi: 10.1126/science.1091496.

Lee, J.-H. and Paull, T. T. (2005) 'ATM Activation by DNA Double-Strand Breaks Through the Mre11-Rad50-Nbs1 Complex', *Science*, 308(5721), pp. 551–554. doi: 10.1126/science.1108297.

Lemaître, C. *et al.* (2014) 'Nuclear position dictates DNA repair pathway choice', *Genes & Development*, 28(22), pp. 2450–2463. doi: 10.1101/gad.248369.114.

Lesterlin, C. *et al.* (2014) 'RecA bundles mediate homology pairing between distant sisters during DNA break repair', *Nature*, 506(7487), pp. 249–253. doi: 10.1038/nature12868.

Liao, H. H. (1991) 'Effect of temperature on the expression of wild-type and thermostable mutants of kanamycin nucleotidyltransferase in Escherichia coli.', *Protein expression and purification*, 2(1), pp. 43–50.

Lieber, M. R. *et al.* (2003) 'Mechanism and regulation of human non-homologous DNA end-joining', *Nature Reviews Molecular Cell Biology*, 4(9), pp. 712–720. doi:

10.1038/nrm1202.

Lindahl, T. (1993) ‘Instability and decay of the primary structure of DNA.’, *Nature*, 362(6422), pp. 709–15. doi: 10.1038/362709a0.

LINDAHL, T. and BARNES, D. E. (2000) ‘Repair of Endogenous DNA Damage’, *Cold Spring Harbor Symposia on Quantitative Biology*, 65(0), pp. 127–134. doi: 10.1101/sqb.2000.65.127.

Liu, X., Matsuda, A. and Plunkett, W. (2008) ‘Ataxia-telangiectasia and Rad3-related and DNA-dependent protein kinase cooperate in G2 checkpoint activation by the DNA strand-breaking nucleoside analogue 2’-C-cyano-2’-deoxy-1-beta-D-arabino-pentofuranosylcytosine.’, *Molecular cancer therapeutics*, 7(1), pp. 133–42. doi: 10.1158/1535-7163.MCT-07-0416.

Liu, Y. *et al.* (2007) ‘A Plant Homeodomain in Rag-2 that Binds Hypermethylated Lysine 4 of Histone H3 Is Necessary for Efficient Antigen-Receptor-Gene Rearrangement’, *Immunity*, 27(4), pp. 561–571. doi: 10.1016/j.immuni.2007.09.005.

Lottersberger, F. *et al.* (2015) ‘53BP1 and the LINC Complex Promote Microtubule-Dependent DSB Mobility and DNA Repair.’, *Cell*, 163(4), pp. 880–93. doi: 10.1016/j.cell.2015.09.057.

Luijsterburg, M. S. *et al.* (2016) ‘PARP1 Links CHD2-Mediated Chromatin Expansion and H3.3 Deposition to DNA Repair by Non-homologous End-Joining’, *Molecular Cell*, 61(4), pp. 547–562. doi: 10.1016/j.molcel.2016.01.019.

Lukacs, G. L. *et al.* (2000) ‘Size-dependent DNA mobility in cytoplasm and nucleus.’, *The Journal of biological chemistry*, 275(3), pp. 1625–9.

Lukas, C. *et al.* (2011) ‘53BP1 nuclear bodies form around DNA lesions generated by mitotic transmission of chromosomes under replication stress’, *Nature Cell Biology*, 13(3), pp. 243–253. doi: 10.1038/ncb2201.

Ma, Y. *et al.* (2002) ‘Hairpin opening and overhang processing by an Artemis/DNA-dependent protein kinase complex in nonhomologous end joining and V(D)J recombination.’, *Cell*. Elsevier, 108(6), pp. 781–94. doi: 10.1016/S0092-8674(02)00671-

2.

Malewicz, M. *et al.* (2011) 'Essential role for DNA-PK-mediated phosphorylation of NR4A nuclear orphan receptors in DNA double-strand break repair.', *Genes & development*, 25(19), pp. 2031–40. doi: 10.1101/gad.16872411.

Mari, P.-O. *et al.* (2006) 'Dynamic assembly of end-joining complexes requires interaction between Ku70/80 and XRCC4', *Proceedings of the National Academy of Sciences*, 103(49), pp. 18597–18602. doi: 10.1073/pnas.0609061103.

Marková, E., Schultz, N. and Belyaev, I. Y. (2007) 'Kinetics and dose-response of residual 53BP1/γ-H2AX foci: Co-localization, relationship with DSB repair and clonogenic survival', *International Journal of Radiation Biology*, 83(5), pp. 319–329. doi: 10.1080/09553000601170469.

Marshall, W. F. *et al.* (1997) 'Interphase chromosomes undergo constrained diffusional motion in living cells.', *Current biology : CB*, 7(12), pp. 930–9.

Martin, G. M. *et al.* (1985) 'Increased chromosomal aberrations in first metaphases of cells isolated from the kidneys of aged mice.', *Israel journal of medical sciences*, 21(3), pp. 296–301.

Masuzawa, N. *et al.* (2000) 'Constrained, Random, and Independent Motion of Texas-Red-labeled Chromatin in Living Interphase PtK2 Cells.', *ACTA HISTOCHEMICA ET CYTOCHEMICA*. JAPAN SOCIETY OF HISTOCHEMISTRY AND CYTOCHEMISTRY, 33(6), pp. 419–427. doi: 10.1267/ahc.33.419.

Matsuoka, S. *et al.* (2007) 'ATM and ATR Substrate Analysis Reveals Extensive Protein Networks Responsive to DNA Damage', *Science*, 316(5828), pp. 1160–1166. doi: 10.1126/science.1140321.

Mattiroli, F. *et al.* (2012) 'RNF168 Ubiquitinates K13-15 on H2A/H2AX to Drive DNA Damage Signaling', *Cell*, 150(6), pp. 1182–1195. doi: 10.1016/j.cell.2012.08.005.

Meier, A. *et al.* (2007) 'Spreading of mammalian DNA-damage response factors studied by ChIP-chip at damaged telomeres.', *The EMBO journal*. European Molecular Biology Organization, 26(11), pp. 2707–18. doi: 10.1038/sj.emboj.7601719.

Michaelis, C., Ciosk, R. and Nasmyth, K. (1997) 'Cohesins: chromosomal proteins that prevent premature separation of sister chromatids.', *Cell*, 91(1), pp. 35–45.

Milligan, J. R. *et al.* (1995) 'DNA repair by thiols in air shows two radicals make a double-strand break.', *Radiation research*, 143(3), pp. 273–80.

Mimitou, E. P. and Symington, L. S. (2009) 'Nucleases and helicases take center stage in homologous recombination', *Trends in Biochemical Sciences*, 34(5), pp. 264–272. doi: 10.1016/j.tibs.2009.01.010.

Miné-Hattab, J. and Rothstein, R. (2012) 'Increased chromosome mobility facilitates homology search during recombination', *Nature Cell Biology*, 14(5), pp. 510–517. doi: 10.1038/ncb2472.

Misteli, T. and Soutoglou, E. (2009) 'The emerging role of nuclear architecture in DNA repair and genome maintenance', *Nature Reviews Molecular Cell Biology*, 10(4), pp. 243–254. doi: 10.1038/nrm2651.

Mohammad, D. H. and Yaffe, M. B. (2009) '14-3-3 proteins, FHA domains and BRCT domains in the DNA damage response', *DNA Repair*, 8(9), pp. 1009–1017. doi: 10.1016/j.dnarep.2009.04.004.

Morris, J. R. and Solomon, E. (2004) 'BRCA1 : BARD1 induces the formation of conjugated ubiquitin structures, dependent on K6 of ubiquitin, in cells during DNA replication and repair', *Human Molecular Genetics*, 13(8), pp. 807–817. doi: 10.1093/hmg/ddh095.

Moyal, L. *et al.* (2011) 'Requirement of ATM-dependent monoubiquitylation of histone H2B for timely repair of DNA double-strand breaks.', *Molecular cell*, 41(5), pp. 529–42. doi: 10.1016/j.molcel.2011.02.015.

Moynahan, M. E., Pierce, A. J. and Jasin, M. (2001) 'BRCA2 is required for homology-directed repair of chromosomal breaks.', *Molecular cell*, 7(2), pp. 263–72.

Mund, A. *et al.* (2012) 'SPOC1 modulates DNA repair by regulating key determinants of chromatin compaction and DNA damage response', *Nucleic Acids Research*, 40(22), pp. 11363–11379. doi: 10.1093/nar/gks868.

Murr, R. *et al.* (2006) 'Histone acetylation by Trrap–Tip60 modulates loading of repair proteins and repair of DNA double-strand breaks', *Nature Cell Biology*, 8(1), pp. 91–99. doi: 10.1038/ncb1343.

Nelms, B. E. *et al.* (1998) 'In situ visualization of DNA double-strand break repair in human fibroblasts.', *Science (New York, N.Y.)*, 280(5363), pp. 590–2.

Neumaier, T. *et al.* (2012) 'Evidence for formation of DNA repair centers and dose-response nonlinearity in human cells.', *Proceedings of the National Academy of Sciences of the United States of America*. National Academy of Sciences, 109(2), pp. 443–8. doi: 10.1073/pnas.1117849108.

Neumann, F. R. *et al.* (2012) 'Targeted INO80 enhances subnuclear chromatin movement and ectopic homologous recombination', *Genes & Development*, 26(4), pp. 369–383. doi: 10.1101/gad.176156.111.

NOWELL, P. C. (1962) 'The minute chromosome (Phl) in chronic granulocytic leukemia.', *Blut*, 8, pp. 65–6. Available at: http://www.ncbi.nlm.nih.gov/pubmed/14480647 (Accessed: 23 May 2018).

O'Donovan, A. *et al.* (1994) 'XPG endonuclease makes the 3' incision in human DNA nucleotide excision repair', *Nature*, 371(6496), pp. 432–435. doi: 10.1038/371432a0.

Ochman, H., Gerber, A. S. and Hartl, D. L. (1988) 'Genetic applications of an inverse polymerase chain reaction.', *Genetics*, 120(3), pp. 621–3.

Ohle, C. *et al.* (2016) 'Transient RNA-DNA Hybrids Are Required for Efficient Double-Strand Break Repair', *Cell*, 167(4), p. 1001–1013.e7. doi: 10.1016/j.cell.2016.10.001.

Oza, P. *et al.* (2009) 'Mechanisms that regulate localization of a DNA double-strand break to the nuclear periphery', *Genes & Development*, 23(8), pp. 912–927. doi: 10.1101/gad.1782209.

Oza, P. and Peterson, C. L. (2010) 'Opening the DNA repair toolbox: Localization of DNA double strand breaks to the nuclear periphery', *Cell Cycle*, 9(1), pp. 43–49. doi: 10.4161/cc.9.1.10317.

Panier, S. *et al.* (2012) 'Tandem Protein Interaction Modules Organize the Ubiquitin-

Dependent Response to DNA Double-Strand Breaks', *Molecular Cell*, 47(3), pp. 383–395. doi: 10.1016/j.molcel.2012.05.045.

Panier, S. and Boulton, S. J. (2014) 'Double-strand break repair: 53BP1 comes into focus.', *Nature reviews. Molecular cell biology*. Nature Publishing Group, a division of Macmillan Publishers Limited. All Rights Reserved., 15(1), pp. 7–18. doi: 10.1038/nrm3719.

Pankotai, T. *et al.* (2012) 'DNAPKcs-dependent arrest of RNA polymerase II transcription in the presence of DNA breaks', *Nature Structural & Molecular Biology*. Nature Research, 19(3), pp. 276–282. doi: 10.1038/nsmb.2224.

Pâques, F. and Haber, J. E. (1999) 'Multiple pathways of recombination induced by double-strand breaks in Saccharomyces cerevisiae.', *Microbiology and molecular biology reviews : MMBR*, 63(2), pp. 349–404.

Paull, T. T. *et al.* (no date) 'A critical role for histone H2AX in recruitment of repair factors to nuclear foci after DNA damage.', *Current biology : CB*, 10(15), pp. 886–95.

Pellegrini, L. *et al.* (2002) 'Insights into DNA recombination from the structure of a RAD51–BRCA2 complex', *Nature*, 420(6913), pp. 287–293. doi: 10.1038/nature01230.

Pesavento, J. J. *et al.* (2008) 'Certain and progressive methylation of histone H4 at lysine 20 during the cell cycle.', *Molecular and cellular biology*. American Society for Microbiology (ASM), 28(1), pp. 468–86. doi: 10.1128/MCB.01517-07.

Pickart, C. M. (2001) 'Mechanisms Underlying Ubiquitination', *Annual Review of Biochemistry*, 70(1), pp. 503–533. doi: 10.1146/annurev.biochem.70.1.503.

Pinkel, D. and Albertson, D. G. (2005) 'Array comparative genomic hybridization and its applications in cancer', *Nature Genetics*, 37(6s), pp. S11–S17. doi: 10.1038/ng1569.

Polo, S. E. and Jackson, S. P. (2011) 'Dynamics of DNA damage response proteins at DNA breaks: a focus on protein modifications', *Genes & Development*, 25(5), pp. 409–433. doi: 10.1101/gad.2021311.

Pombo, A. *et al.* (1998) 'Regional and temporal specialization in the nucleus: a transcriptionally-active nuclear domain rich in PTF, Oct1 and PIKA antigens associates

with specific chromosomes early in the cell cycle', *The EMBO Journal*, 17(6), pp. 1768–1778. doi: 10.1093/emboj/17.6.1768.

Pommier, Y. *et al.* (2014) 'Tyrosyl-DNA-phosphodiesterases (TDP1 and TDP2)', *DNA Repair*, 19, pp. 114–129. doi: 10.1016/j.dnarep.2014.03.020.

Prado, F. and Aguilera, A. (2005) 'Impairment of replication fork progression mediates RNA polII transcription-associated recombination', *The EMBO Journal*, 24(6), pp. 1267–1276. doi: 10.1038/sj.emboj.7600602.

Renkawitz, J. *et al.* (2013) 'Monitoring homology search during DNA double-strand break repair in vivo.', *Molecular cell*. Elsevier, 50(2), pp. 261–72. doi: 10.1016/j.molcel.2013.02.020.

Reynolds, P. *et al.* (2012) 'The dynamics of Ku70/80 and DNA-PKcs at DSBs induced by ionizing radiation is dependent on the complexity of damage', *Nucleic Acids Research*, 40(21), pp. 10821–10831. doi: 10.1093/nar/gks879.

Rich, T., Allen, R. L. and Wyllie, A. H. (2000) 'Defying death after DNA damage', *Nature*, 407(6805), pp. 777–783. doi: 10.1038/35037717.

Richardson, C. and Jasin, M. (2000) 'Frequent chromosomal translocations induced by DNA double-strand breaks', *Nature*, 405(6787), pp. 697–700. doi: 10.1038/35015097.

Robinett, C. C. *et al.* (1996) 'In vivo localization of DNA sequences and visualization of large-scale chromatin organization using lac operator/repressor recognition.', *The Journal of cell biology*, 135(6 Pt 2), pp. 1685–700.

Robinson, P. J. J. *et al.* (2008) '30 nm Chromatin Fibre Decompaction Requires both H4-K16 Acetylation and Linker Histone Eviction', *Journal of Molecular Biology*, 381(4), pp. 816–825. doi: 10.1016/j.jmb.2008.04.050.

Rogakou, E. P. *et al.* (1998) 'DNA double-stranded breaks induce histone H2AX phosphorylation on serine 139.', *The Journal of biological chemistry*, 273(10), pp. 5858–68.

Rogakou, E. P. (1999) 'Megabase Chromatin Domains Involved in DNA Double-Strand Breaks In Vivo', *The Journal of Cell Biology*, 146(5), pp. 905–916. doi:

10.1083/jcb.146.5.905.

Rooney, S., Chaudhuri, J. and Alt, F. W. (2004) 'The role of the non-homologous end-joining pathway in lymphocyte development', *Immunological Reviews*, 200(1), pp. 115–131. doi: 10.1111/j.0105-2896.2004.00165.x.

Roukos, V. *et al.* (2013) 'Spatial dynamics of chromosome translocations in living cells.', *Science (New York, N.Y.)*, 341(6146), pp. 660–4. doi: 10.1126/science.1237150.

Roukos, V. *et al.* (2013) 'Spatial Dynamics of Chromosome Translocations in Living Cells', *Science*, 341(6146), pp. 660–664. doi: 10.1126/science.1237150.

Rowley, J. D. (2001) 'Chromosome translocations: dangerous liaisons revisited', *Nature Reviews Cancer*. Nature Publishing Group, 1(3), pp. 245–250. doi: 10.1038/35106108.

Sachs, R. K., Chen, A. M. and Brenner, D. J. (1997) 'Review: proximity effects in the production of chromosome aberrations by ionizing radiation.', *International journal of radiation biology*, 71(1), pp. 1–19.

Sanders, S. L. *et al.* (2004) 'Methylation of Histone H4 Lysine 20 Controls Recruitment of Crb2 to Sites of DNA Damage', *Cell*, 119(5), pp. 603–614. doi: 10.1016/j.cell.2004.11.009.

Sanders, S. L., Arida, A. R. and Phan, F. P. (2010) 'Requirement for the Phospho-H2AX Binding Module of Crb2 in Double-Strand Break Targeting and Checkpoint Activation', *Molecular and Cellular Biology*. American Society for Microbiology (ASM), 30(19), p. 4722. doi: 10.1128/MCB.00404-10.

Sartori, A. A. *et al.* (2007) 'Human CtIP promotes DNA end resection', *Nature*. Nature Publishing Group, 450(7169), pp. 509–514. doi: 10.1038/nature06337.

Savic, V. *et al.* (2009) 'Formation of dynamic gamma-H2AX domains along broken DNA strands is distinctly regulated by ATM and MDC1 and dependent upon H2AX densities in chromatin.', *Molecular cell*, 34(3), pp. 298–310. doi: 10.1016/j.molcel.2009.04.012.

Savic, V. (2013) 'Do chromatin changes around a nascent double strand DNA break spread spherically into linearly non-adjacent chromatin?', *Frontiers in genetics*, 4, p. 139. doi: 10.3389/fgene.2013.00139.

Saxton, M. J. (2007) 'Modeling 2D and 3D Diffusion', in *Methods in molecular biology*

(Clifton, N.J.), pp. 295–321. doi: 10.1007/978-1-59745-519-0_20.

Schatz, D. G. and Swanson, P. C. (2011) 'V(D)J Recombination: Mechanisms of Initiation', *Annual Review of Genetics*, 45(1), pp. 167–202. doi: 10.1146/annurev-genet-110410-132552.

Schultz, L. B. *et al.* (2000) 'p53 binding protein 1 (53BP1) is an early participant in the cellular response to DNA double-strand breaks.', *The Journal of cell biology*, 151(7), pp. 1381–90.

Scully, R. *et al.* (1997) 'Dynamic changes of BRCA1 subnuclear location and phosphorylation state are initiated by DNA damage.', *Cell*, 90(3), pp. 425–35.

Seeber, A., Dion, V. and Gasser, S. M. (2013) 'Checkpoint kinases and the INO80 nucleosome remodeling complex enhance global chromatin mobility in response to DNA damage', *Genes & Development*, 27(18), pp. 1999–2008. doi: 10.1101/gad.222992.113.

Shanbhag, N. M. *et al.* (2010) 'ATM-Dependent Chromatin Changes Silence Transcription In cis to DNA Double-Strand Breaks', *Cell*, 141(6), pp. 970–981. doi: 10.1016/j.cell.2010.04.038.

Sharan, S. K. *et al.* (1997) 'Embryonic lethality and radiation hypersensitivity mediated by Rad51 in mice lacking Brca2', *Nature*, 386(6627), pp. 804–810. doi: 10.1038/386804a0.

Shi, L. and Oberdoerffer, P. (2012) 'Chromatin dynamics in DNA double-strand break repair', *Biochimica et Biophysica Acta (BBA) - Gene Regulatory Mechanisms*, 1819(7), pp. 811–819. doi: 10.1016/j.bbagrm.2012.01.002.

Shiloh, Y. (2003) 'ATM and related protein kinases: safeguarding genome integrity', *Nature Reviews Cancer*, 3(3), pp. 155–168. doi: 10.1038/nrc1011.

Shroff, R. *et al.* (2004) 'Distribution and Dynamics of Chromatin Modification Induced by a Defined DNA Double-Strand Break', *Current Biology*, 14(19), pp. 1703–1711. doi: 10.1016/j.cub.2004.09.047.

Sirbu, B. M. and Cortez, D. (2013) 'DNA Damage Response: Three Levels of DNA Repair Regulation', *Cold Spring Harbor Perspectives in Biology*, 5(8), pp. a012724–a012724. doi:

10.1101/cshperspect.a012724.

Sobhian, B. *et al.* (2007) 'RAP80 targets BRCA1 to specific ubiquitin structures at DNA damage sites.', *Science (New York, N.Y.)*, 316(5828), pp. 1198–202. doi: 10.1126/science.1139516.

Sofueva, S. *et al.* (2010) 'BRCT Domain Interactions with Phospho-Histone H2A Target Crb2 to Chromatin at Double-Strand Breaks and Maintain the DNA Damage Checkpoint', *Molecular and Cellular Biology*, 30(19), pp. 4732–4743. doi: 10.1128/MCB.00413-10.

Sollier, J. and Cimprich, K. A. (2015) 'Breaking bad: R-loops and genome integrity', *Trends in Cell Biology*, 25(9), pp. 514–522. doi: 10.1016/j.tcb.2015.05.003.

Soutoglou, E., Dorn, J. F., *et al.* (2007) 'Positional stability of single double-strand breaks in mammalian cells.', *Nature cell biology*, 9(6), pp. 675–82. doi: 10.1038/ncb1591.

Soutoglou, E., Dorn, J. F., *et al.* (2007) 'Positional stability of single double-strand breaks in mammalian cells', *Nature Cell Biology*, 9(6), pp. 675–682. doi: 10.1038/ncb1591.

Stewart, G. S. *et al.* (2003) 'MDC1 is a mediator of the mammalian DNA damage checkpoint', *Nature*. Nature Publishing Group, 421(6926), pp. 961–966. doi: 10.1038/nature01446.

Stewart, G. S. *et al.* (2009) 'The RIDDLE syndrome protein mediates a ubiquitin-dependent signaling cascade at sites of DNA damage.', *Cell*, 136(3), pp. 420–34. doi: 10.1016/j.cell.2008.12.042.

Stiff, T. *et al.* (2004) 'ATM and DNA-PK function redundantly to phosphorylate H2AX after exposure to ionizing radiation.', *Cancer research*, 64(7), pp. 2390–6.

Stucki, M. *et al.* (2005) 'MDC1 Directly Binds Phosphorylated Histone H2AX to Regulate Cellular Responses to DNA Double-Strand Breaks', *Cell*, 123(7), pp. 1213–1226. doi: 10.1016/j.cell.2005.09.038.

Stucki, M. and Jackson, S. P. (2006) 'γH2AX and MDC1: Anchoring the DNA-damage-response machinery to broken chromosomes', *DNA Repair*, 5(5), pp. 534–543. doi: 10.1016/j.dnarep.2006.01.012.

Sun, Y., Jiang, X. and Price, B. D. (2010) 'Tip60: connecting chromatin to DNA damage

signaling.', *Cell cycle (Georgetown, Tex.)*, 9(5), pp. 930–6. doi: 10.4161/cc.9.5.10931.

Sung, P. and Klein, H. (2006) 'Mechanism of homologous recombination: mediators and helicases take on regulatory functions', *Nature Reviews Molecular Cell Biology*, 7(10), pp. 739–750. doi: 10.1038/nrm2008.

Taddei, A. *et al.* (2006) 'Nuclear pore association confers optimal expression levels for an inducible yeast gene', *Nature*, 441(7094), pp. 774–778. doi: 10.1038/nature04845.

Takata, M. *et al.* (1998) 'Homologous recombination and non-homologous end-joining pathways of DNA double-strand break repair have overlapping roles in the maintenance of chromosomal integrity in vertebrate cells.', *The EMBO journal*. European Molecular Biology Organization, 17(18), pp. 5497–508. doi: 10.1093/emboj/17.18.5497.

Talbert, P. B. and Henikoff, S. (2010) 'Histone variants — ancient wrap artists of the epigenome', *Nature Reviews Molecular Cell Biology*, 11(4), pp. 264–275. doi: 10.1038/nrm2861.

Tang, J. *et al.* (2013) 'Acetylation limits 53BP1 association with damaged chromatin to promote homologous recombination', *Nature Structural & Molecular Biology*, 20(3), pp. 317–325. doi: 10.1038/nsmb.2499.

Therizols, P. *et al.* (2006) 'Telomere tethering at the nuclear periphery is essential for efficient DNA double strand break repair in subtelomeric region', *The Journal of Cell Biology*, 172(2), pp. 189–199. doi: 10.1083/jcb.200505159.

Thevenaz, P., Ruttimann, U. E. and Unser, M. (1998) 'A pyramid approach to subpixel registration based on intensity', *IEEE Transactions on Image Processing*, 7(1), pp. 27–41. doi: 10.1109/83.650848.

Thompson, L. H. (2012) 'Recognition, signaling, and repair of DNA double-strand breaks produced by ionizing radiation in mammalian cells: The molecular choreography', *Mutation Research/Reviews in Mutation Research*. Elsevier, 751(2), pp. 158–246. doi: 10.1016/J.MRREV.2012.06.002.

Tinevez, J.-Y. *et al.* (2017) 'TrackMate: An open and extensible platform for single-particle tracking', *Methods*. Academic Press, 115, pp. 80–90. doi:

10.1016/J.YMETH.2016.09.016.

Tomimatsu, N., Mukherjee, B. and Burma, S. (2009) 'Distinct roles of ATR and DNA-PKcs in triggering DNA damage responses in ATM-deficient cells.', *EMBO reports*, 10(6), pp. 629–35. doi: 10.1038/embor.2009.60.

Uematsu, N. *et al.* (2007) 'Autophosphorylation of DNA-PK $_{CS}$ regulates its dynamics at DNA double-strand breaks', *The Journal of Cell Biology*, 177(2), pp. 219–229. doi: 10.1083/jcb.200608077.

Ui, A., Nagaura, Y. and Yasui, A. (2015) 'Transcriptional elongation factor ENL phosphorylated by ATM recruits polycomb and switches off transcription for DSB repair.', *Molecular cell*. Elsevier, 58(3), pp. 468–82. doi: 10.1016/j.molcel.2015.03.023.

Uziel, T. *et al.* (2003) 'Requirement of the MRN complex for ATM activation by DNA damage.', *The EMBO journal*. European Molecular Biology Organization, 22(20), pp. 5612–21. doi: 10.1093/emboj/cdg541.

Velic, D. *et al.* (2015) 'DNA Damage Signalling and Repair Inhibitors: The Long-Sought-After Achilles' Heel of Cancer', *Biomolecules*, 5(4), pp. 3204–3259. doi: 10.3390/biom5043204.

Veuger, S. J. *et al.* (2003) 'Radiosensitization and DNA repair inhibition by the combined use of novel inhibitors of DNA-dependent protein kinase and poly(ADP-ribose) polymerase-1.', *Cancer research*, 63(18), pp. 6008–15.

de Vries, E. *et al.* (1989) 'HeLa nuclear protein recognizing DNA termini and translocating on DNA forming a regular DNA-multimeric protein complex.', *Journal of molecular biology*, 208(1), pp. 65–78.

Walker, J. R., Corpina, R. A. and Goldberg, J. (2001) 'Structure of the Ku heterodimer bound to DNA and its implications for double-strand break repair.', *Nature*, 412(6847), pp. 607–614. doi: 10.1038/35088000.

Wang, S. *et al.* (2000) 'The catalytic subunit of DNA-dependent protein kinase selectively regulates p53-dependent apoptosis but not cell-cycle arrest.', *Proceedings of the National Academy of Sciences of the United States of America*, 97(4), pp. 1584–8.

Watanabe, K. *et al.* (2009) 'RAD18 promotes DNA double-strand break repair during G1 phase through chromatin retention of 53BP1', *Nucleic Acids Research*, 37(7), pp. 2176–2193. doi: 10.1093/nar/gkp082.

Weinfeld, M. and Soderlind, K. J. (1991) '32P-postlabeling detection of radiation-induced DNA damage: identification and estimation of thymine glycols and phosphoglycolate termini.', *Biochemistry*, 30(4), pp. 1091–7.

Weinstock, D. M., Brunet, E. and Jasin, M. (2007) 'Formation of NHEJ-derived reciprocal chromosomal translocations does not require Ku70.', *Nature cell biology*, 9(8), pp. 978–81. doi: 10.1038/ncb1624.

Weterings, E. *et al.* (2003) 'The role of DNA dependent protein kinase in synapsis of DNA ends.', *Nucleic acids research*. Oxford University Press, 31(24), pp. 7238–46. doi: 10.1093/NAR/GKG889.

Williams, R. S. *et al.* (2008) 'Mre11 dimers coordinate DNA end bridging and nuclease processing in double-strand-break repair.', *Cell*. Elsevier, 135(1), pp. 97–109. doi: 10.1016/j.cell.2008.08.017.

Woo, R. A. *et al.* (2002) 'DNA damage-induced apoptosis requires the DNA-dependent protein kinase, and is mediated by the latent population of p53.', *The EMBO journal*, 21(12), pp. 3000–8. doi: 10.1093/emboj/cdf307.

Wu, L. and Hickson, I. D. (2003) 'The Bloom's syndrome helicase suppresses crossing over during homologous recombination', *Nature*, 426(6968), pp. 870–874. doi: 10.1038/nature02253.

Wurtele, H. and Verreault, A. (2006) 'Histone post-translational modifications and the response to DNA double-strand breaks', *Current Opinion in Cell Biology*, 18(2), pp. 137–144. doi: 10.1016/j.ceb.2006.02.008.

Xiao, A. *et al.* (2009) 'WSTF regulates the H2A.X DNA damage response via a novel tyrosine kinase activity', *Nature*, 457(7225), pp. 57–62. doi: 10.1038/nature07668.

Xu, Y. *et al.* (1996) 'Targeted disruption of ATM leads to growth retardation, chromosomal fragmentation during meiosis, immune defects, and thymic lymphoma.',

Genes & development. Cold Spring Harbor Laboratory Press, 10(19), pp. 2411–22. doi: 10.1101/GAD.10.19.2411.

Xu, Y. and Price, B. D. (2011) 'Chromatin dynamics and the repair of DNA double strand breaks', *Cell Cycle*, 10(2), pp. 261–267. doi: 10.4161/cc.10.2.14543.

Yamamoto, K. *et al.* (2012) 'Kinase-dead ATM protein causes genomic instability and early embryonic lethality in mice.', *The Journal of cell biology*, 198(3), pp. 305–13. doi: 10.1083/jcb.201204098.

Yamauchi, M. *et al.* (2017) 'Regulation of pairing between broken DNA-containing chromatin regions by Ku80, DNA-PKcs, ATM, and 53BP1.', *Scientific reports*, 7, p. 41812. doi: 10.1038/srep41812.

Yano, K. and Chen, D. J. (2008) 'Live cell imaging of XLF and XRCC4 reveals a novel view of protein assembly in the non-homologous end-joining pathway', *Cell Cycle*, 7(10), pp. 1321–1325. doi: 10.4161/cc.7.10.5898.

Yurchenko, V., Xue, Z. and Sadofsky, M. J. (2006) 'SUMO Modification of Human XRCC4 Regulates Its Localization and Function in DNA Double-Strand Break Repair', *Molecular and Cellular Biology*, 26(5), pp. 1786–1794. doi: 10.1128/MCB.26.5.1786-1794.2006.

Zgheib, O. *et al.* (2009) 'An Oligomerized 53BP1 Tudor Domain Suffices for Recognition of DNA Double-Strand Breaks', *Molecular and Cellular Biology*, 29(4), pp. 1050–1058. doi: 10.1128/MCB.01011-08.

Zhang, Y. and Heermann, D. W. (2014) 'DNA double-strand breaks: linking gene expression to chromosome morphology and mobility', *Chromosoma*, 123(1–2), pp. 103–115. doi: 10.1007/s00412-013-0432-y.

Zhao, Y. *et al.* (2006) 'Preclinical evaluation of a potent novel DNA-dependent protein kinase inhibitor NU7441.', *Cancer research*, 66(10), pp. 5354–62. doi: 10.1158/0008-5472.CAN-05-4275.

Zink, D. *et al.* (1999) 'Organization of Early and Late Replicating DNA in Human Chromosome Territories', *Experimental Cell Research*, 247(1), pp. 176–188. doi: 10.1006/excr.1998.4311.

Ziv, Y. *et al.* (2006) 'Chromatin relaxation in response to DNA double-strand breaks is modulated by a novel ATM- and KAP-1 dependent pathway', *Nature Cell Biology*, 8(8), pp. 870–876. doi: 10.1038/ncb1446.